SAFETY CASE 2015

Tihange 2

Reactor Pressure Vessel Assessment

Version 1

28 10 2015

e.r. Electrabel SA, Boulevard Simon Bolivar 34, 1000 Bruxelles

Electrabel

GDF SUEZ

Contents

1 Summary

1.1 Executive Summary

In 2012, indications were found inside the shell material of the Doel 3 and Tihange 2 reactor pressure vessels (RPVs). These gave rise to a series of examinations, tests and inspections with a clear outcome. It was demonstrated that these indications are hydrogen flakes and that they do not affect the structural integrity of the RPVs (Doel 3 and Tihange 2), regardless of the operating mode, transient or accident condition. An independent review team of national and international experts and academics confirmed the outcome.

The results of the investigations were synthesized in comprehensive Safety Case Reports, and submitted to the Federal Agency for Nuclear Control (FANC) in December 2012.

Midterm requirements

On 30 January 2013, the FANC provided Electrabel with a Provisional Evaluation Report identifying a number of remaining issues. Some had to be addressed before a potential restart in 2013 (short-term requirements), others could be treated after restart (midterm requirements). In response to these short-term requirements, Electrabel submitted an action plan that was approved by the FANC. Two addenda to the Safety Cases Reports were submitted in April 2013.

Based on the addenda, the FANC issued its Final Evaluation Report and authorized the restart of both units on 17 May 2013. Operation of the two units was resumed in June 2013. An action plan was set up and deployed to address the midterm requirements. The actions addressed three main topics:

- Ultrasonic (UT) inspection
- Material properties investigation
- Structural Integrity Assessment (SIA)

Unexpected test results

One of the midterm requirements is related to an irradiation programme on specimens containing hydrogen flakes. It aimed at confirming the conservativeness of the additional shift in RT_{NDT} of 50°C on irradiated materials used in the Safety Case Reports for structural analyses.

In March 2014, preliminary results of the tests on irradiated specimens extracted from the AREVA VB395 shell (which was rejected during the manufacturing process) showed unexpected results regarding the shift in RT_{NDT}. In other words, the conservativeness of the 50°C value considered in the Safety Case Reports could not be confirmed. As a precautionary measure, Electrabel decided to immediately stop operations at the Doel 3 and Tihange 2 nuclear power plants (NPP).

Action plan extended

In order to fully address this concern, the initial action plan was gradually extended taking full benefit of the available materials (i.e. Doel 3 and Tihange 2 RPV forgings, VB395 and KS 02):

- New irradiation campaigns were performed and microstructural material investigations were launched in order to assess the atypical embrittlement of the flake-affected material VB395.
- Investigation on another reference material (KS 02) was resumed, after discovery of the existence of a remaining block of this vessel material known to contain defects.

In addition, the extension of qualification process of the applied MIS-B UT inspection procedure led to an update of the sizing methodology and to the choice of new inspection settings, in order to achieve a high confidence level in detection and sizing. This led to a complete characterization of the hydrogen flakes (inclination and faceting) and an updated cartography of the flakes as well as a decision to reassess the structural integrity of the RPV.

Safety Case completed

The present document gives a structured and complete answer to each of the FANC's midterm requirements for the Tihange 2 RPV. It also provides the results and conclusions of additional analyses, tests, and inspections that were performed to complement the Safety Case. The results of these complementary tests and analyses lead to the following conclusions:

- Hydrogen flakes are fully characterized and have a laminar orientation.
- Qualified UT inspection procedure achieves high performance in detection and sizing.
- Re-inspection of the vessel shells delivers a complete cartography of the indications and confirms that the flakes are stable.
- Conservative material properties are derived for use in the SIA.
- Structural integrity of the RPV is demonstrated with large safety margins, and has never been a concern during the whole operation of the plant since commissioning.

Based on all of these inspections, additional tests and detailed analyses, Electrabel is convinced that the structural integrity of the Tihange 2 RPV has been demonstrated and that all safety requirements are met. Therefore, Electrabel considers that the Tihange 2 NPP can be safely restarted with no need for further action.

At the end of the next fuel cycle a follow-up inspection of the RPV will be performed with the qualified UT inspection procedure.

1.2 Context

During the 2012 outage at the Doel 3 nuclear power plant (NPP), specific ultrasonic (UT) in-service inspections were performed to check for underclad cracking in the reactor pressure vessel (RPV). No underclad defects were found. However, a large number of nearly laminar indications were detected, mainly in the lower and upper core shells. A second inspection was performed with UT probes to inspect the entire thickness of the vessel. This inspection identified the same type of nearly laminar indications deeper in the material. A similar inspection performed in September 2012 at the Tihange 2 NPP showed similar indications, but to a lesser extent.

As a consequence, the Doel 3 and Tihange 2 NPPs remained core unloaded until proven that they can be safely operated.

Based on the findings of the in-service inspections, the manufacturing documentation review, and their vast experience with heavy forging manufacturing, the AREVA metallurgy experts came to the preliminary conclusion that hydrogen flaking in the macro-segregation zone of the shells was the most likely cause of the indications and that they had originated during the manufacturing of the reactor shells. Hydrogen flaking is a known metallurgical phenomenon that may occur during the casting and forging process and causes flaws in steel under specific circumstances. This diagnosis triggered the development of a roadmap to confirm hydrogen flaking as the most likely cause and assess the structural integrity of the Doel 3 and Tihange 2 RPVs.

Therefore a Safety Case (a case per unit) for requesting their restart has been prepared by the operator, Electrabel, and submitted to the Federal Agency for Nuclear Control (FANC) on 5 December 2012.

The FANC issued in January 2013 a Provisional Evaluation Report on the Safety Cases, identifying some remaining open issues. Some had to be addressed before a potential restart in 2013 (short-term requirements), the others could be treated after restart (midterm requirements). In response to these requirements, Electrabel submitted an Action Plan that was approved by the FANC.

In answer to the short-term requirements of the FANC, two Addenda to the Safety Cases Reports were submitted in April 2013. Based on both Addenda, the FANC issued its Final Evaluation Report and authorized the restart of both units on 17 May 2013. Operation of the two units was resumed in June 2013.

1.3 Main Conclusions of the 2012 Safety Case Reports and their Addenda

The diagnosis of hydrogen flaking, initiated during manufacturing in macro-segregated areas (in particular in ghost lines at manganese sulphide inclusions) was confirmed after thorough investigation, based on a root cause analysis of all potential causes. It was also concluded that the identified indications were stable.

Not all forged components of the Doel 3 and Tihange 2 RPVs contain the same amount of hydrogen flakes. They were obtained from different sizes of ingots and with different combinations of sulphur and hydrogen content. Analysis of these characteristics revealed a good correlation with the amount of flakes found in each forged component.

A close review of all of the original manufacturing data and documentation confirmed that both the Doel 3 and Tihange 2 RPVs were manufactured in accordance with the prevailing international codes and standards, in particular the ASME Boiler & Pressure Vessel Code.

In 2012, the Doel 3 and Tihange 2 RPVs were subjected to ultrasonic inspection using the automated MIS-B (Machine d'Inspection en Service Belge) equipment, which has been used for over thirty years to inspect the RPVs of all Belgian units. The testing programme demonstrated that the applied inspection technique is valid and appropriate for characterizing the quasi-laminar indications found in the Doel 3 and Tihange 2 RPVs.

A comprehensive testing programme was launched in addition to a material-related literature survey. Many mechanical and metallurgical tests were performed on archived non-irradiated materials, including a piece of 1.2m diameter originating from the Doel 3 vessel itself (D3H1 nozzle shell cut-out), and on the rejected AREVA shell VB395 known to contain hydrogen flakes. These tests showed that there is no significant effect of orientation or macro-segregation on fracture toughness. All results confirmed that the curves required by the ASME code in the assessment are conservative. The destructive tests performed on steel samples containing hydrogen flakes also showed that the material between and around the flaws is sound and has a similar microstructure as in absence of flaws.

Complementary tests performed on the D3H1 nozzle shell cut-out showed that the ghost lines have no significant effect on the Charpy impact test results or fracture toughness properties.

Additional tests on the VB395 material containing hydrogen flakes confirmed the limited effect of hydrogen flaking on the material properties. The ductility of the material in the ligaments between flakes is similar to the ductility of the material that is free of flakes. Large-scale tests on material containing flakes confirmed the good ductility and load bearing capacity. The fracture toughness of the ligaments between flakes is only slightly lower as compared to the flake-free material. This is confirmed through tests on specimens with a flake as crack tip.

Detailed methodologies were developed and validated for assessing the structural behaviour of each flaw that is detected in the vessel shells, in all possible operational modes and transients, as well as to assess general stresses in the vessel. Based on these methodologies, calculations were made using state-of-the-art modelling and computing techniques, in order to verify the applicable structural integrity requirements. The calculations confirmed that the acceptance criteria of the deterministic studies are met with a significant safety margin. The suitability and conservativeness of the SIA was validated through large-scale tensile and bending tests on material containing flakes.

Finally, a load test performed at a pressure slightly above the design pressure of the RPV did not reveal any unexpected condition nor induce any flaw evolution.

1.4 Further Developments since the 2013 Restart – Action Plan

An action plan was set up and deployed to address the FANC's midterm requirements. Actions 1, 4, 5, 6, and 14 were already satisfied in 2013. The following actions answer the midterm requirements issued by the FANC:

Topic	Requirement	Action
Ultrasonic (UT) inspection	Non-inspectable areas	2b
	Potentially unreported higher tilted flaws	3b
	Extension of MIS qualification	7
	Follow-up inspection for Doel 3 and Tihange 2	8
Material properties investigation	Additional tensile tests of specimens with a ghost line	9b
	Residual hydrogen content	10b
	Material properties of flaked material under irradiated conditions	11
	Local (micro-scale) properties of specimens with macro-segregations, ghost lines and hydrogen flakes	12
	Effect of thermal ageing of the zone of macro-segregation	13
Structural Integrity Assessment (SIA)	Large-scale tensile testing on flaked material	15b
Post-load test	Additional questions on load test	16b

Table 1.1: Overview of actions.

Preliminary results of the tests on irradiated specimens extracted from the AREVA shell VB395 showed unexpected results regarding the shift in RT_{NDT} and could not confirm the conservativeness of the 50°C value considered in the Safety Cases.

Therefore, Electrabel decided to immediately stop operations at the Doel 3 and Tihange 2 NPPs in March 2014 as a precautionary measure while further tests and verifications were performed to analyse in more detail the preliminary results. Consequently, the initial action plan launched to answer the midterm requirements was extended, as detailed below.

- New irradiation campaigns were performed and microstructural material investigations were launched in order to assess the atypical embrittlement of the flake-affected material VB395.
- Investigation on another reference material (KS 02) was resumed, after discovery of the existence of a remaining block of this vessel material that is known to contain defects.

Also, the extension of qualification process of the applied MIS-B UT inspection procedure led to an update of the sizing methodology and to the choice of new inspection settings, in order to achieve a high confidence level in detection and sizing. This led to a complete characterization of the hydrogen flakes (inclination and faceting) and an updated cartography of the flakes as well as a decision to reassess the structural integrity of the RPVs.

In September 2014, the FANC set up a group of Belgian and foreign scientists, the International Review Board (IRB), in order to consolidate the regulatory body's analysis of the results of the mechanical resistance tests and the finding on materials performed within the framework of this extended action plan. The IRB held a Workshop in November 2014 and formulated a set of comments and questions that were included in a set of Recommendations and Suggestions that the FANC addressed to Electrabel in December 2014.The action plan was updated accordingly, to address these recommendations and suggestions.

The action plan is now completed and an answer was given to all of the requirements and suggestions formulated by the FANC with the goal to confirm the structural integrity of the reactor pressure vessels (RPVs).

1.5 Conclusions

Electrabel is convinced of having demonstrated that the structural integrity of the Tihange 2 RPV is fully maintained, under all operating and accidental conditions. The SIA has provided evidence of the harmless character of all detected flaws in the RPV. This allows for a safe restart and operation of the Tihange 2 NPP with no need for further action.

The Safety Case roadmap with its extensive phase of studies and material tests has led to the following results and conclusions (see Chapter 8 for more details):

- Phenomenology of flaking is independent of the level of segregation in the material
- Hydrogen flakes are fully characterized and have a laminar orientation.
- Qualified UT inspection procedure achieves high performance in detection and sizing.
- Re-inspection of the vessel shells delivers a complete cartography of the indications and confirms that the flakes are stable.
- Conservative material properties are derived for use in the SIA.
- Structural integrity of the RPV is demonstrated with large safety margins, and has never been a concern during the whole operation of the plant since commissioning.

To ensure a high confidence in its conclusions, each step of the Safety Case has been taken from a very conservative approach. This conservativeness leads to the existence of additional margins between the assessments and reality.

At the end of the next fuel cycle a follow-up inspection of the RPV will be performed with the qualified UT inspection procedure.

1.6 External and Independent Review

Due to the complexity of the issue, the licence holder Electrabel decided to install a multidisciplinary project team. This team consisted of experts from:

- Electrabel: the license holder with expertise in nuclear operations and safety
- Laborelec: knowhow in non-destructive testing techniques and material properties
- Tractebel Engineering: specialized knowledge of nuclear engineering and design as well as structural integrity, materials, and safety

External organizations and experts

In building up the Safety Case, the project team could rely on different external organizations and laboratories, each with its particular domain of expertise:

Organization	Domain of expertise
SCK•CEN (Belgium)	Material testing and fracture mechanics
AREVA (France)	Material testing and metallurgy
University of Ghent (Belgium)	
CRM (Belgium)	
Tohoku University (Japan)	Material testing
CEA (France)	Materials examination and metallurgy
VTT (Finland)	Materials examination

Table 1.2: External organizations.

In view of ensuring the quality, completeness and reliability of the Safety Case, the project team mobilized a team of external experts, to review its work. Consulting experts with specialized knowhow in the field of material properties were involved throughout the root cause analysis of VB395's atypical embrittlement.

Name	Organization	Domain of expertise
Dr. Rachid Chaouadi	SCK•CEN (Belgium)	Material properties
Dr. Bernard Marini	CEA (France)	
Prof. George Robert Odette	UCSB Department of Mechanical Engineering (USA)	
Prof. Grace Burke	Manchester University (UK)	
Prof. Hannu Hänninen	Aalto University (Finland)	
Prof. Yasuyoshi Nagai	Tohoku University (Japan)	
Prof. Kim Verbeken	University of Ghent (Belgium)	
Prof. Emeritus Dr. Gerard Lesoult	Independent consultant (France)	Metallurgy
Dr. Alain Schmitz	CRM (Belgium)	
Dr. Clarisse Poidevin	CEA (France)	Non-destructive testing
Philippe Benoît	M2M (France)	
Dr. Kunio Hasegawa	Hasegawa consulting (Japan)	Structural integrity
Dr. Greg Wilkowski	Emc² (USA)	
Bud Burst	Emc² (USA)	
Russel Cipolla	Intertek (USA)	

Table 1.3: External experts.

Independent Analysis and Review

One of the requests formulated by the FANC involves an independent analysis and review by Electrabel's Service de Contrôle Physique (SCP). They relied upon a panel of external international academics and experts such as Sandia National Laboratories (US Department of Energy) as well as its own resources (both on corporate and site level).

Although it will be issued in a separate report, this independent review is part of the Safety Case File and will be presented to the Belgian Safety Authorities.

2 Roadmap for the Midterm Action Plan

The Final Evaluation Report issued by the FANC on May 2013 contains a set of midterm requirements to be fulfilled before restart after the next scheduled outage. During the deployment of the corresponding action plan, several events led to the re-orientation and extension of this roadmap, as the initial conditions (flaw population and material properties) were no longer valid. The roadmap was consequently completed through an updated SIA, primarily based on the methodologies that were developed and validated for the initial Safety Cases. The roadmap incorporated the actions subsequent to the International Review Board (IRB) workshop that specifically addressed materials issues.

Roadmap Structure

The roadmap (Figure 2.1) identifies the steps and actions that were developed in order to assess the structural integrity of the Tihange 2 RPV. It also gives the links between the different steps and actions.

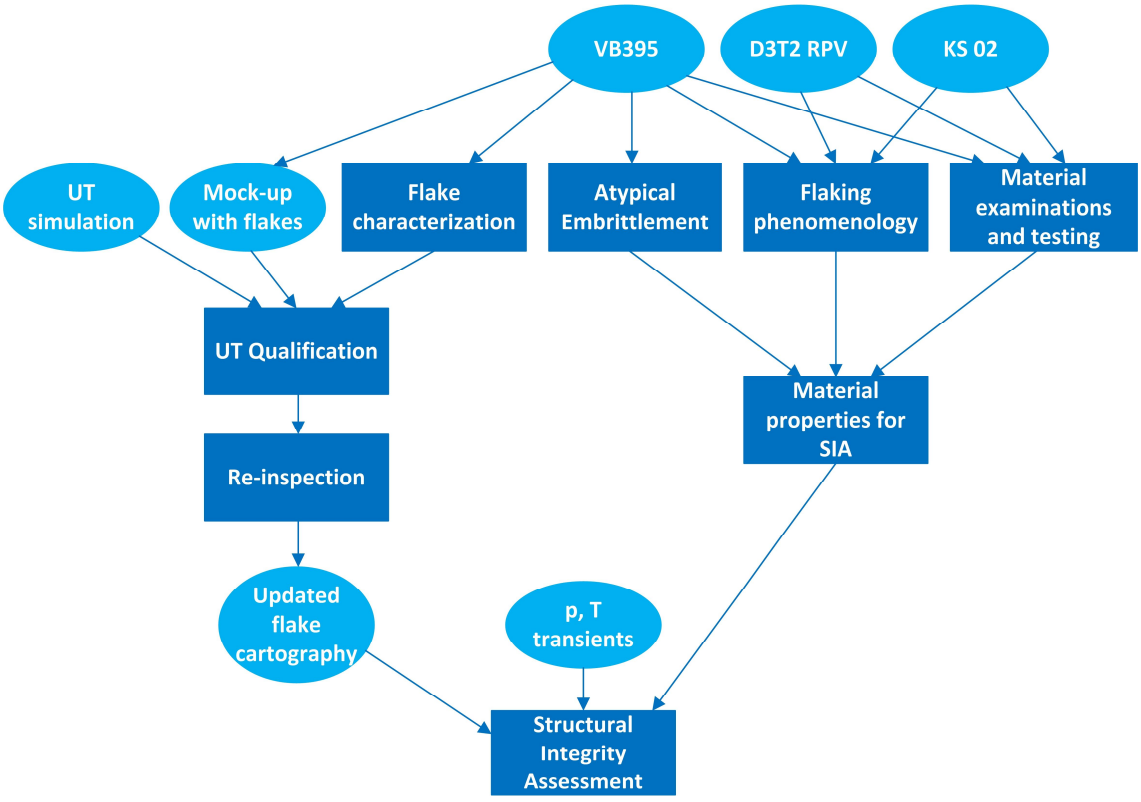

Figure 2.1: Roadmap of the midterm action plan.

The left-hand side of this roadmap includes the following successive steps:

- Characterization of the hydrogen flakes (orientation and faceting)
- Qualification of the applied UT inspection methodology in order to achieve a very high level of confidence regarding the detection and characterization of the indications
- Inspection of the RPV using the qualified procedure in order to assess the possible evolution of the indications between successive inspections and the determination of the indications' cartography in the RPV shell

The right-hand side of the roadmap concerns the materials aspects and includes the following steps:

- Investigations of the different materials (VB395, Doel 3 and Tihange 2 RPV forgings and KS 02) used in the test programme, with evaluation of their basic properties and suitability, for determination of material properties of the Tihange 2 RPV.
- Material tests, with presentation and discussion of the test results in non-irradiated and irradiated conditions.
- Assessment of the atypical embrittlement of the VB395 material.
- Characterization of the flaking phenomenology
- Determination of material properties to be used for SIA.

The roadmap ends with the performance of the SIA, based on the findings from the two sides in the roadmap, as well as on the RPV's geometric data and the pressure/temperature (p, T) loadings on the RPV wall. The structural integrity of the Tihange 2 RPV is proven based on the satisfaction of the acceptance criteria, the conservativeness of the methodology and the assumptions, and the existing safety margins.

3 Hydrogen Flaking

3.1 Phenomenology of flaking

The concern was raised that the high number of flakes found in some areas of the RPV shells could be correlated with a high level of chemical enrichment inside the macro-segregation in those areas. A complementary evaluation of the level of segregation of the Doel 3 and Tihange 2 RPV forgings showed that no such correlation exists.

Context

The Safety Case Report and the Addendum confirm that the indications in the RPV shell can be associated with a zone of macro-segregations that is the result of complex mechanisms occurring during solidification of the ingot during fabrication. Moreover, the flaws are situated in very specific locations: the so-called 'ghost lines', which correspond to the residual features of the ingot after forging.
In addition, the Addendum explains why not all forged components of the Doel 3 and Tihange 2 RPVs contain the same amount of hydrogen flakes. Based on an analysis of the ingot size and the combined sulphur and hydrogen content, the forgings were ranked according to their susceptibility to hydrogen flaking. This revealed a good correlation with the amount of flakes found in each forged component.
During the discussion of the Safety Case Report, the concern was raised that the high density of flakes found in some macro-segregated areas of the RPV shells could be correlated with a high level of chemical enrichment inside those areas. If so, this would have to be considered when assuming initial fracture toughness values for those zones.

Approach

The level of segregation of the Doel 3 and Tihange 2 RPV forgings was evaluated through an empirical formula developed on the bases of examinations performed on a large number of conventional ingots. This formula gives the level of carbon enrichment in the final forging as a function of its average chemical composition. Since enrichment in other alloying elements is proportional to the carbon enrichment, the latter is thus a good indicator for the enrichment level of segregations. In order to validate the formula, the predicted enrichment for the nozzle shells of Doel 3 and Tihange 2 was compared to carbon enrichments levels measured on the respective D3H1 and T2H2 cut-outs from those shells. And for all forgings, the predicted segregation levels were compared to the observed numbers of hydrogen flakes.

Results

The predicted carbon enrichment levels for the Doel 3 and Tihange 2 RPV forgings are given in Table 3.1. The enrichment is expressed as the ratio between the difference between the maximum and minimum carbon content encountered in the final forging, and the average carbon content of the ladle.

RPV forging	Carbon enrichment [%]	Number of indications (2012)
Doel 3 Lower Core Shell	43.3	7205
Tihange 2 Upper Core Shell	49.2	1931
Tihange 2 Lower Core Shell	47.6	80
Doel3 Upper Core Shell	50.2	857
Doel 3 Nozzle Shell	45.6	11
Tihange 2 Nozzle Shell	50.8	0

Table 3.1: Comparison of carbon enrichment level and number of hydrogen flakes

The carbon enrichments measured on the Doel 3 and Tihange 2 nozzle cut-outs correspond well to the predicted values illustrating the applicability of the correlation to the Doel 3/Tihange 2 RPV forgings. As shown in Table 3.1, the forging with the highest number of flakes (Doel 3 Lower Core Shell) is the less segregated one, and the forging without any flake (Tihange 2 Nozzle Shell) is the most segregated one.

Conclusions

The evaluation shows there is no correlation between the number of hydrogen flakes encountered in the forging and the chemical enrichment of the macro-segregation that contains the flakes.

3.2 Characterization of hydrogen flakes

As part of the midterm action plan related to the Tihange 2 RPV Safety Case, detailed metallurgical investigations were conducted focusing on the inclination and faceting of the hydrogen flakes. These investigations confirmed that the flakes are located in ghost lines only, primarily in those with the highest level of segregation. The flakes also have a quasi-laminar character (with an average inclination of 4° and a maximum of 15°) and a faceted appearance, influencing their reflectivity to ultrasonic waves.

Context

In order to achieve a high confidence level in detection and sizing, it was decided to further evaluate the flakes' metallurgical characteristics, focusing on the factors that might influence their detectability, i.e. their inclination and faceting. It was important to do so in the context of the extension of qualification (Chapter 4.1 Ultrasonic Testing Qualification) as well as for the SIA (Chapter 6 Structural Integrity Assessment).

Approach

Previous investigations had revealed that the flakes are situated systematically within the local segregations (ghost lines) of macro-segregated zones. Because of the close association between flakes and ghost lines, the measurement of the maximum possible inclination was performed on ghost lines of a cut-out from the Doel 3 nozzle shell (D3H1), both in axial and circumferential directions and correlated to ghost lines and flake inclination in VB395.

The inclination and faceting of the flakes was evaluated by examination of the profile of several flakes on metallographic samples from two test blocks from the AREVA VB395 shell (VB395/1 and VB395/2), both in axial and circumferential directions. The inclination of ghost lines was investigated using the same specimens as well as the cut-out D3H1. To get a statistically valid evaluation, the measurements were performed on more than 30 ghost lines per test block. The test matrix is presented in Table 3.2.

Test block	Flake inclination		Detailed profile of flakes		Ghost line inclination	
	Axial direction	Circumferential direction	Axial direction	Circumferential direction	Axial direction	Circumferential direction
VB395/1	46	25	18	11	192	34
VB395/2	43	38	5	/	156	113
D3H1	N.A.	N.A.	N.A.	N.A.	62	58

Table 3.2: Test matrix with the number of measurements per test block, for each type of analysis.

The purpose of the examination was to measure the angle of the ghost lines that are the most susceptible to flaking (in macro-segregated areas, the darkest zones) and have the greatest inclination. Therefore, the test procedure consisted of identifying the areas with the most inclined ghost lines, taking micrographs of the selected areas (magnified by a factor 50), selecting the worst ghost lines on the micrographs and measuring the angles in axial and circumferential directions (Figure 3.3).

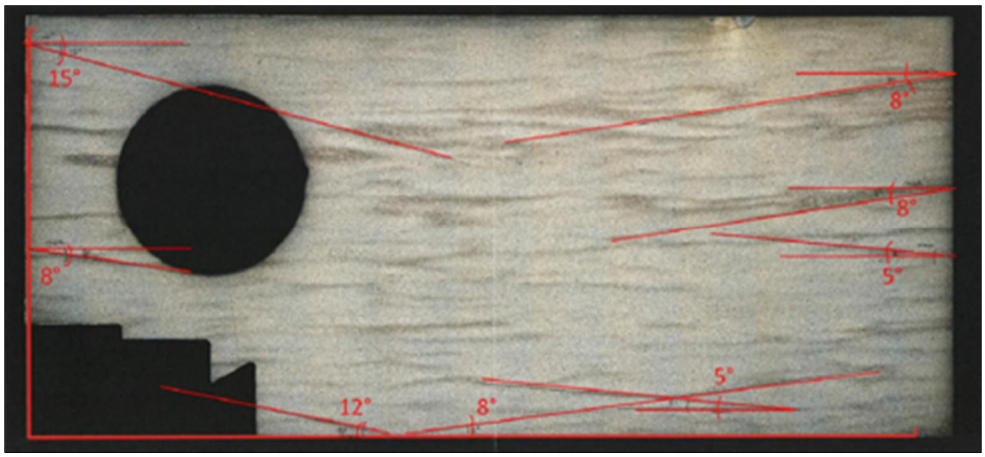

Figure 3.3: Example of inclination measurement (D3H1, axial direction).

The global inclination of the flakes was measured by drawing the line that connects the two end points (Figure 3.4).

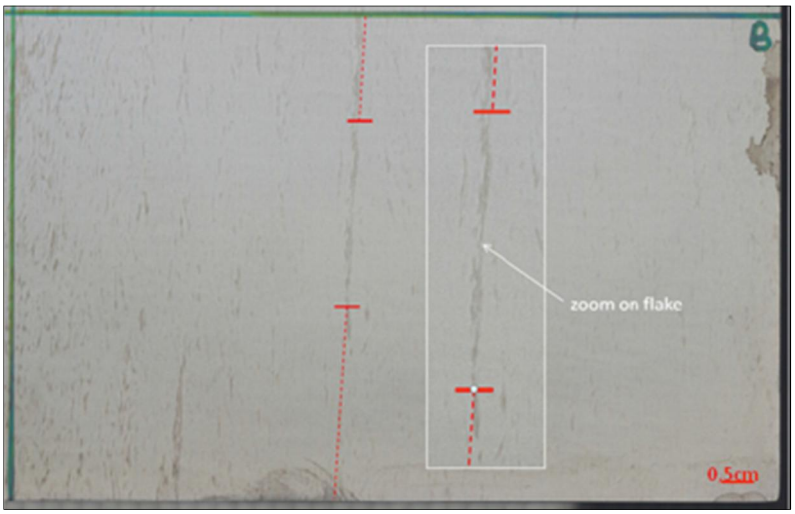

Figure 3.4: Detail of inclination measurement (VB395/1, axial direction).

To get an accurate picture of the flakes' faceting (Figure 3.5), successive cross sections of the flakes were made, resulting in a series of crack profiles. These profiles were then superimposed and projected onto a single plane. This made it possible to estimate the degree of faceting. Finally, 3D profiling was applied.

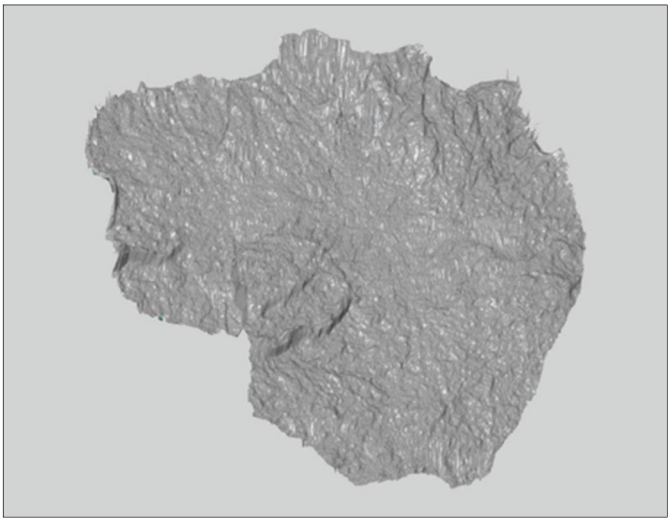

Figure 3.5: Typical flake appearance.

Complementary characterization investigations were also performed on KS 02 material.

Results

- The observations confirmed that the flakes are located in ghost lines, primarily in those with the highest level of segregation.
- The flakes tend to remain in the laminar direction even when the hosting ghost line deviates.
- The correlation between ghost line inclination and flake inclination was evaluated on several flakes. The average flake inclination is approximately 4° while the average ghost line inclination is approximately 7°. The investigation revealed that the flakes are systematically less inclined than the maximum ghost line inclination (Figure 3.6).

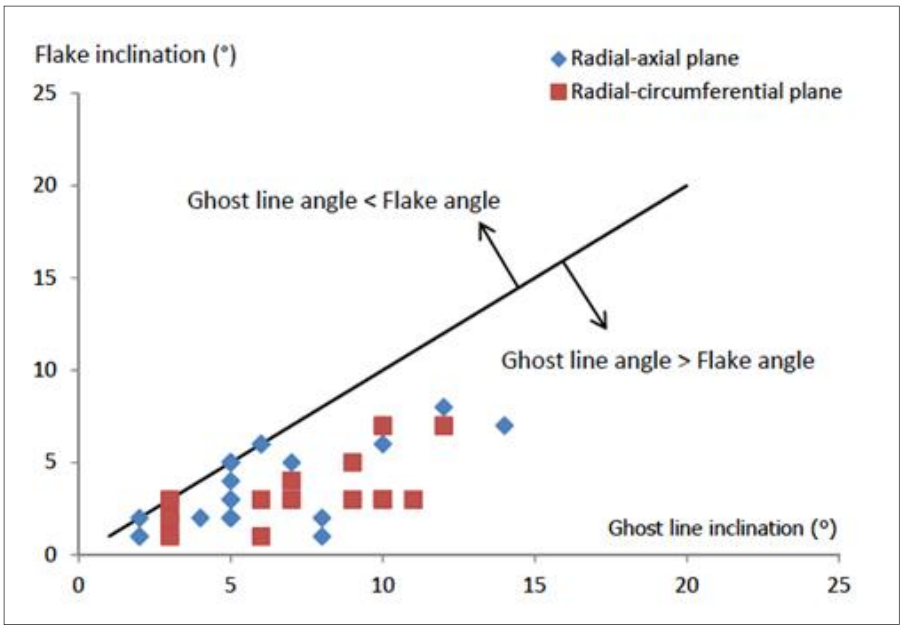

Figure 3.6: The flakes are systematically less inclined than the ghost lines (representative sample).

- The histograms of the maximum inclination measurements (worst ghost line angle distribution) are very similar for the three test blocks VB395/1, VB395/2 and D3H1.
- Among the 152 flake inclinations considered, only 5 flakes showed an inclination above 10° (3 with 11°, 1 with 12° and 1 with 15°). The mean value was approximately 4°.
- This value resulted from observations on a significant number of samples: 120 ghost line angles in D3H1, 495 ghost line angles and 152 flake angles in the two VB395 test blocks.

Conclusions

- The observations confirmed that the flakes are located in ghost lines, primarily in those with the highest level of segregation.
- The flakes show multiple facets, both in the micro range (10 to 100 μm) and in the macro range (100 to 500 μm). No significant difference was found between the axial and circumferential directions.
- The characteristics of the KS 02 flakes are comparable to the characteristics of the VB395 flakes.
- The flakes were globally less inclined than the maximum angle of the ghost lines. They tend to remain laminar due to the influence of the forging's residual stresses.
- The maximum inclination of the ghost lines susceptible for flaking did not exceed 16° in both axial and circumferential directions.
- 15° is the maximum value expected for the flake inclination.

4 Ultrasonic Inspection

The hydrogen flakes in the reactor pressure vessels (RPVs) were detected, located and sized using the MIS-B equipment (Figure 4.1). This inspection tool is qualified and has been used for more than 30 years to inspect the reactor pressure vessel (RPV) welds.

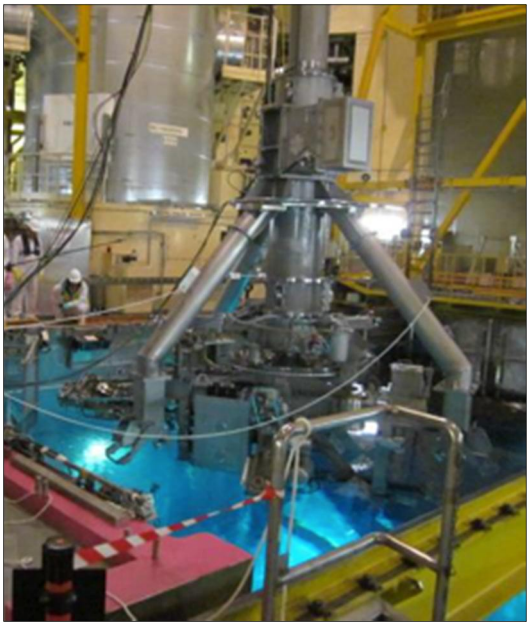

Figure 4.1: UT inspection is performed with the MIS-B equipment.

The MIS-B equipment uses the acoustic beam focusing technique, concentrating sound energy in a restricted volume. It applies a set of ultrasonic transducers to examine the complete thickness of the vessel wall (Table 4.2).

Transducer identification	Beam angle	Frequency	Minimum beam size
OL 0° MER or EAR	0°	4 MHz	3 mm
OL 0° T1	0°	1.5 MHz	8 mm
OL 0° T2	0°	1 MHz	12 mm
OT 45° T1 *	45°	1 MHz	8 mm
OT 45° T2 *	45°	1 MHz	10 mm

* 4 transducers orthogonally oriented

Table 4.2: Ultrasonic transducers used for RPV shell inspection.

In 2012, the MIS-B equipment was qualified and used for the first time to check for cracks underneath the vessel's internal cladding. This inspection revealed no underclad cracking, but it did detect the presence of a significant population of indications that were subsequently confirmed to be hydrogen flakes.

4.1 Ultrasonic Testing Qualification

One of the midterm actions (Action 7) to be performed after the plant's restart in 2013 focused on the formal extension of qualification of the MIS-B UT inspection procedure for the detection and sizing of hydrogen flakes. This qualification process has demonstrated that the UT inspection procedure is capable of achieving a very high confidence level. All necessary parameters have been identified for performing a robust and reliable detection, localization and characterization of hydrogen flakes in RPVs.

The validation of the MIS-B technique was explained in detail in the 2012 RPV Safety Case Reportg.

Requirements

Regarding this validation, the AIA (Authorized Inspection Agency) requested additional validation of the UT simulations. The main action regarding UT inspection aimed to achieve the formal extension of qualification of the MIS-B technique for detection, localization and characterization of hydrogen flakes. The FANC expressed the qualification requirement as follows (Action 7):

> *The licensee shall achieve a full qualification program to demonstrate the suitability of the in-service inspection technique for the present case. The qualification shall give sufficient confidence in the accuracy of the results with respect to the number and features (location, size, orientation...) of the flaw indications. Where appropriate, the process shall be substantiated by appropriate experimental data using representative specimens. The full qualification program shall be achieved before the next planned outage for refuelling.*

The objective of the extension of qualification is to ensure that the inspection procedure correctly and accurately detects, locates and sizes hydrogen flakes. The objective was to reach a very high confidence level, even for flakes inclined up to 16°, what is more than the maximum predicted inclination of the flakes, as demonstrated in Chapter 3.

In addition to this midterm Action 7, the FANC also asked to investigate the potentially unreported higher tilted flaws (Action 3b):

> *The licensee shall demonstrate that the applied ultrasonic testing procedure allows the detection of the higher tilt defects in the Doel 3/Tihange 2 data (2012 inspections) with a high level of confidence.*

4.1.1 UT Qualification Process

A qualification programme was established, based on the methodology of the European Network for Inspection and Qualification (ENIQ). The entire programme was supervised by the AIA and consisted of three main parts:

- Practical trials
- UT modelling (computer simulations)
- Reconciliation of trials and modelling

4.1.1.1 Practical trials

A primary aspect of the inspection qualification process is the execution of practical trials on test blocks extracted from the VB395 shell, containing hydrogen flakes (Figure 4.3).

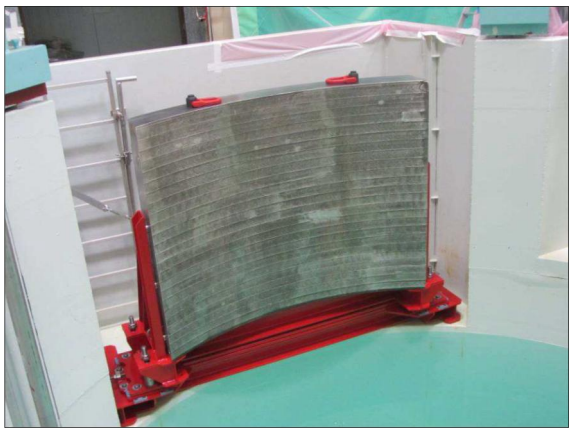

Figure 4.3: Block VB395/2.

Block VB395/2 was subjected to heat treatment and an austenitic stainless steel cladding was applied on the inner surface in order to meet the acoustic characteristics of the RPV shells. Analysis of the inspection data revealed numerous indications.

Three smaller test blocks were cut out of block VB395/2 for more detailed examinations (Figure 4.4).

- Test block 2A: in original condition, with stainless steel cladding.
- Test block 2B: the inner surface was machined at an angle of 15° (including removal of the stainless steel cladding) to check whether the UT inspection technique is capable of correctly detecting and characterizing highly inclined flakes.
- Test block 2C: the inner surface was machined (including removal of the stainless steel cladding), in order to bring the present hydrogen flakes closer to the inspection surface to assess the inspection capability for flakes located close to the vessel's inner wall.

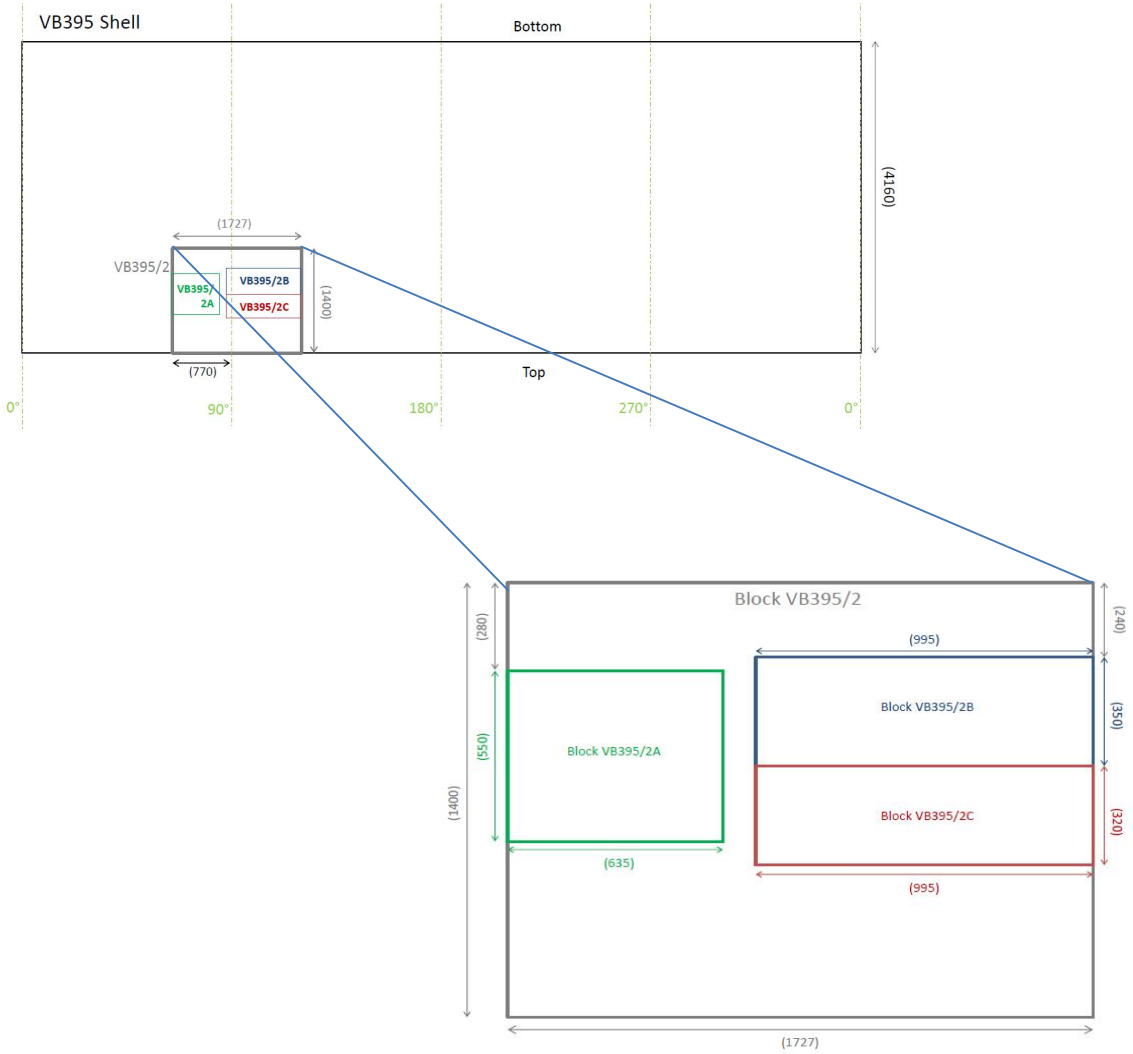

Figure 4.4: Position of test blocks in VB395 shell (dimensions in mm).

A total of approximately 100 indications were selected from the UT inspection data on these three blocks, covering a wide range of positions, sizes and ultrasonic reflectivity. The corresponding flakes were extracted and subjected to detailed destructive analysis: they were sliced into individual sections of 1 mm. The information from all slices was then combined to give the full 3D information for the selected hydrogen flake (position, size, inclination). This information could then be compared with the results of the ultrasonic investigation of the considered flake.

4.1.1.2 UT modelling (computer simulations)

There are an important number of parameters, which can potentially influence the performance of the inspection (e.g. equipment, UT method, components and flakes). The influence of each essential parameter, as well as their combinations, was investigated using computer simulations with the CIVA software of CEA (Commissariat à l'Energie Atomique et aux Energies Alternatives).

The variation of the ultrasonic response with all relevant parameters is calculated. The combination of the most penalizing parameters is identified to determine the sensitivity settings that meet the high detection capability under all circumstances.

4.1.1.3 Reconciliation of trials and modelling

In spite of the very high number of flaws cut during the practical trials, it is not possible to consider all possible values—and combinations—of the various parameters that influence inspection capability. These parameters are considered in the CIVA simulations, with the exception of the morphological characteristics of the flakes (as the software can only model perfectly flat and smooth flaws). Reconciling the results of the practical trials and modelling enables the combination of the outcomes – and strengths – of both exercises.

The actual flake characteristics (position, dimensions, orientation) as obtained through destructive testing have been inserted in the CIVA software to calculate their ultrasonic responses. These were then compared to the practical trial data.

The gap between the measured and computed signal amplitudes quantifies the influence of the flaw morphology that could not be modelled. The gap was compensated for by an adequate correction of the inspection procedure sensitivity settings. In this way, all equipment, method, component and flaw parameters (as well as all possible combinations) are taken into consideration in the qualification process to ensure its robustness.

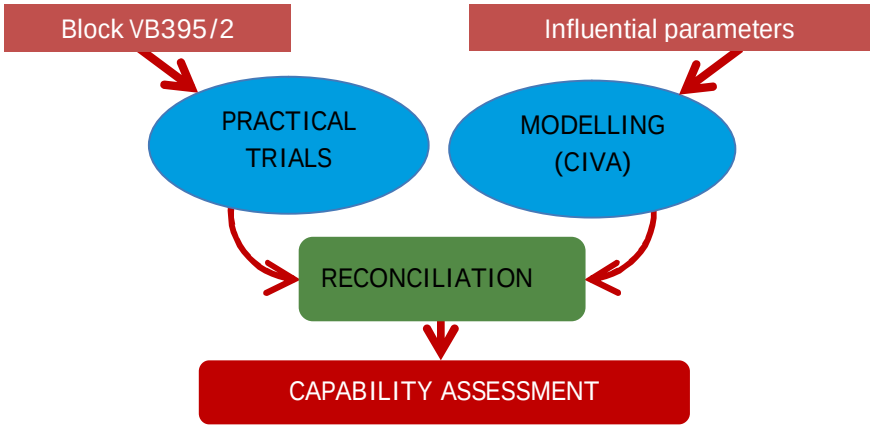

Figure 4.5: Schematic representation of the qualification structure.

4.1.2 Outcome of the UT Qualification Process

Flaw detection capability

In order to ensure the detection of all relevant flakes, even under the most unfavourable conditions, some modifications were introduced in the inspection procedure:

- The detection capability in the nearest depth range was enhanced by the introduction of the MER transducer instead of the EAR.
- The depth range distribution between the various 0° transducers was adapted.
- UT signal reporting thresholds of 0° transducers were lowered to ensure the detection of flakes inclined up to 16°.
- 45° transducer data were exploited to detect hypothetical radial connections between flakes.

Transducer identification	Depth range *	Reporting level **
OL 0° MER	8-35 mm	-24 dB
	35-50 mm	-30 dB
OL 0° T1	50-110 mm	-24 dB
OL 0° T2	110-200 mm	-24 dB
OT 45° T1	8-60 mm	0 dB
OT 45° T2	60-140 mm	0 dB

* 0-8 mm is the depth range of the stainless steel clad
** With reference to 2 mm diameter side-drilled hole

Table 4.6: Transducer settings of the qualified UT inspection procedure.

Flaw localization capability

The qualification programme confirmed that the UT inspection procedure achieves the required precision in locating the hydrogen flakes.

Flaw sizing capability

The practical trials conducted on block VB395/2A showed that some flaws were undersized in the axial and azimuthal directions by the original (2012) analysis procedure. The sizing procedure has been optimized to remove such occurrences. The optimized flaw sizing procedure results in conservative reporting of the main dimensions of the flakes:

- The vast majority of the UT indications is larger than the associated flakes.
- Sound metal distances separating neighbouring flaws are generally underestimated, and may even be overlooked in case of very close flaws. In such cases, only one larger indication is reported instead of two—or several—individual indications.

The original procedure used in 2012 to size flaws in the through-wall direction remained unchanged: practical trials and destructive testing confirmed its conservativeness on real flakes.

4.1.3 Conclusions

The qualification process led to an inspection procedure that achieves a very high level of confidence for the detection, localization and sizing of the flakes:

- A robust qualification methodology was applied:
  - Practical trials were executed on test blocks containing real flakes.
  - Destructive tests were performed on approximately 100 flakes.
  - Simulations were performed to calculate the influence of a multitude of parameters on inspection capability.
  - Comparisons were made between UT and destructive testing results.
- The qualification process resulted in upgrading the inspection procedure to ensure its compliance with inspection objectives in terms of flaw detection and characterization. A very high confidence level is achieved for detecting flakes. Flake sizing was shown to be conservative.
- The straight beam technique used in 2012 and 2013 is adequate to detect the presence, if any, of hydrogen flaking in the RPV shells.

4.2 Re-inspection

In accordance with the action plan (Action 8), the Tihange 2 RPV core shells were re-inspected during the plant's outage of May 2014. The goal was to check for any possible evolution of the flakes since the 2012 UT inspection. No evolution was revealed. In addition, the qualified UT procedure was applied to the 2014 data. Due to the lower threshold, this resulted in a higher number of reported flakes as compared to 2012, and pointed out an increased indication density without an extension of the affected volume. It also indicated that all flakes are reported.

Requirements

The action plan called for a follow-up UT inspection of both Tihange 2 RPV core shells to be carried out during the next outage. This in-service inspection was meant to detect any possible evolution of the previously reported flakes during operation. The FANC expressed the requirement as follows (Action 8):

> *The licensee shall perform follow-up in-service inspections during the next planned outage for refuelling to ensure that no evolution of the flaw indications has occurred during operation.*

Approach

During the 2014 outage, a follow-up UT inspection of the RPVs was performed. The objectives were to investigate the in-service growth of the flakes and establish an update of the flake cartography.

4.2.1 Verification of the In-Service Stability of the Flakes

The hypothetical in-service growth of the flakes between the restart in 2013 and the shutdown in 2014 was investigated. For this purpose, the data collected during the 2014 UT inspection were analysed in accordance with the 2012 inspection procedure, applying the same parameters and reporting thresholds. The optimized sizing procedure resulting from the qualification was implemented on both data sets.

The ultrasonic amplitude and dimensions associated to each indication of both the 2012 and 2014 datasets were compared (using criteria derived from the French RSE-M code) to verify any hypothetical occurrence of in-service growth of the flakes between 2012 and 2014. This comparison revealed no evolution. None of the indications showed any sign of modification between the two inspections.

4.2.2 Updated Flake Cartography

The updated flake cartography was established using the qualified UT inspection procedure.

4.2.2.1 Number of indications

The inspection with the 0° transducers using the updated parameters of the qualified inspection procedure reported in the upper core shell approximately 60% more indications compared to the 2012 data (Table 4.7). This is a consequence of the enhanced sensitivity of the inspection procedure and not of the emergence of new flaws or the growth of pre-existing flaws.

Number of indications	Tihange 2 Upper Core Shell	Tihange 2 Lower Core Shell
2012 inspection	1931	80
2014 inspection	3064	85

Table 4.7: Number of indications reported in the Tihange 2 core shells.

Additional investigations were conducted to verify whether the number of flakes reported in 2014 is exhaustive:

- The data recorded by the eight 45° transducers were analysed in order to detect any hypothetical radial connections between flakes of slightly different depths.
- An additional transducer, refracting ultrasonic waves under a 15° angle, was mounted on the MIS-B inspection tool in order to detect any highly inclined flakes.

These investigations revealed no additional information, confirming the quasi-laminar character of the flakes.

The full detection capability is further demonstrated by the vanishing left end of the amplitude distribution of each transducer at its reporting threshold (Figure 4.8).

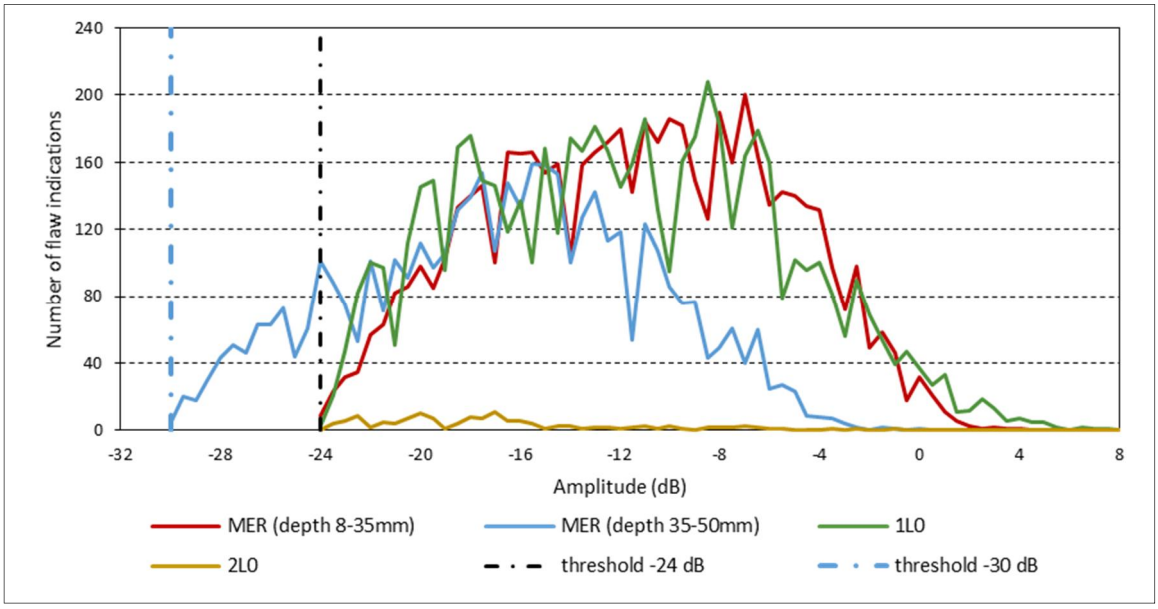

Figure 4.8: Indication amplitude distribution (4 shells).

4.2.2.2 Spatial distribution of the indications

The 2012 inspection showed that the indications are not spread over the entire volume of the RPV shells. The 2014 re-inspection confirmed that the indications are located in those parts of the shells that were already known to contain flakes during the 2012 inspection (Figure 4.9).

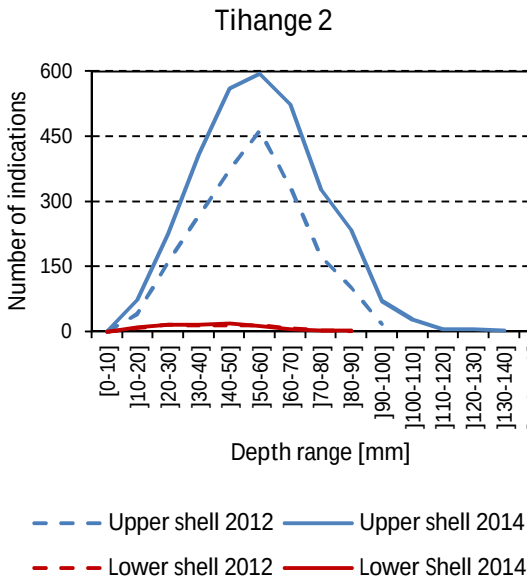

Figure 4.9: Depth distribution of the indications in the RPV shells.

As more indications have been reported in the same zones of the RPV shells, the indication density has increased and the distance between the indications has decreased as compared to 2012. The conservativeness of the optimized sizing process tending to report indications larger than the actual flake size, even further decreases the measured distance between the indications.

4.2.2.3 Dimensions of the indications

The average dimensions of the indications are larger than what was originally reported during the 2012 UT inspection (Table 4.10). This is the result of:

- The conservativeness introduced by the optimized flaw sizing procedure (UT qualification).
- The merger of small neighbouring indications. They are now considered as one larger indication as a consequence of the evolution of the inspection procedure.

Dimensions (mm)	Tihange 2 Upper Core Shell		Tihange 2 Lower Core Shell	
Examination*	2012	2014	2012	2014
Average X-Y dimensions	9.8-7.9	14.8-13.8	10.2-9.3	15.5-15.4
Maximum X-Y dimensions	38.0-25.4	154.5-70.9	27.4-19.1	33.1-27.6

Table 4.10: Dimensions of indications reported in the Tihange 2 core shells.

The maximum reported dimensions are much larger than what was reported in 2012. These large indications result from the non-discrimination of smaller clustered flakes using the optimized sizing procedure.

The re-inspection of the RPV shells revealed that the size distribution of the indications remained practically unchanged from 2012 to 2014 (Figure 4.11).

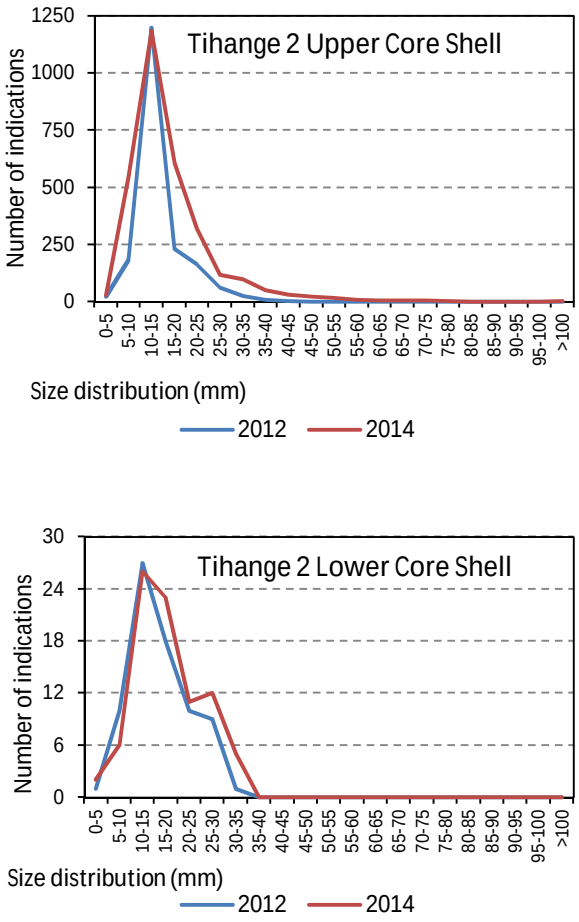

Figure 4.11: Indication size distribution in the Tihange 2 RPV shells.

4.2.3 Clad interface imperfections

As mentioned in the Doel 3 Safety Case report Addendum, the RPV UT inspections also revealed, in addition to the hydrogen flakes, indications located at the interface between cladding and base metal, that have been classified as clad interface imperfections (French: *défauts technologiques de revêtement* or DTR). In Tihange 2, 4 such indications were found: 1 in the lower core shell and 3 in the upper core shell.

Since for a number of those indications the distinction between DTR and hydrogen flake could not be made for 100% sure, it was decided to conservatively consider all of them as additional hydrogen flakes in the SIA.

A DTR is any flaw located at the cladding-base metal interface, that does not penetrate the base metal itself. A DTR should not be confused with underclad cracks (French: défauts sous revêtement or DSR), which are planar flaws at the cladding-base metal interface, located in the base metal, oriented perpendicular to the RPV surface and generated by cold cracking. No underclad cracks were discovered during the 2012 inspections.

4.2.4 Conclusions

- No in-service growth of the hydrogen flakes was observed between 2012 and 2014.
- An update of the flake cartography is issued, based on the application of the qualified inspection procedure. As a consequence of the inspection procedure evolution, the number of reported indications is significantly higher than in 2012.
- The newly reported indications are located in the same shell volumes as the indications that were reported in 2012. The indication density in those volumes therefore increases significantly, whereas the other shell parts are confirmed to be unaffected by flaking.
- The conservativeness introduced by the updated flaw sizing procedure and the tendency to report clusters of indications as large individual flakes leads to the reporting of larger average dimensions and much larger maximum dimensions in 2014.
- The re-inspection of the RPV shells revealed that the size distribution of the indications remained practically unchanged from 2012 to 2014.
- The re-inspection also revealed a few additional indications that have been classified as clad interface imperfections. However, in the SIA, these indications are conservatively considered as hydrogen flakes. In addition, these indications will be included in future inspections of Tihange 2 RPV and will be treated as hydrogen flakes in evolution checks.
- Additional inspections aimed at detecting non-laminar flaws reported no extra indications, confirming the quasi-laminar character of the hydrogen flakes.
- The results confirm the adequacy of the qualified UT inspection technique for the detection, localization and sizing of hydrogen flakes.

4.3 Acoustic Emission Measurements

Under Action 16b additional questions were asked on the load tests performed on the Tihange 2 RPV in 2013. All questions have been successfully addressed, confirming the validity of the Acoustic Emission (AE) measurements performed during the load tests.

Requirements

In 2013 the Tihange 2 RPV was subjected to a load test, as required under Action 16. Simultaneously, AE measurements were performed in order to demonstrate that no unexpected condition was present in the RPV.

The goal of the AE test was to detect the propagation of flaws in the RPV core shells, if any. In order to reach this objective, the RPV was equipped with fifteen sensors positioned on the RPV head, on the RPV inlet and outlet nozzles, and on the in-core instrumentation connected to the bottom of the RPV. The AE measurements performed on the Tihange 2 RPV did not reveal any critical sources and/or areas for which supplementary investigations are mandatory.

However, the Safety Authorities had some additional questions on the AE test (Action 16b). Besides asking for detailed information related to the test results and the equipment used, they requested to demonstrate that the method was correctly applied and that it would have allowed detecting cracks anywhere in the RPV, as well as to verify whether sensors positioned in the in-core instrumentation room can provide useful information regarding the acoustic activity in the RPV core shells.

Approach

As an answer to these questions, detailed information related to the test equipment and test results were provided. In addition, tests were successfully performed on a mock-up in order to demonstrate the effectiveness of the method used for measuring the sensitivity of AE sensors in comparison with the method prescribed in the guide to good practices.

In order to demonstrate that any location of the RPV is covered by the AE test, signal attenuation values from an AE test performed in a French NPP were presented to the Safety Authorities. It proves that a signal coming from anywhere in the RPV can be detected by at least one of the sensor placed on the RPV during the load test.

Sensors that are placed in the in-core instrumentation room are not used for the AE diagnosis but it was confirmed by analysis that AE sources that were recorded by these sensors did not come from the RPV core shells.

5 Material Properties

Tests performed on flaked material from KS 02 and VB395 confirmed that the presence of hydrogen flakes does not have any effect on the evolution of fracture toughness under irradiation. In a similar way, the evaluation of possible root causes for the atypical embrittlement of the rejected VB395 shell excludes any role of hydrogen or hydrogen flakes. The tests also showed that the D3T2 RPV forgings and the KS 02 flange behave as expected under irradiated conditions. On the contrary, VB395 does not behave as expected under irradiated conditions, and is to be considered as an outlier.

Although it is very unlikely that the D3T2 RPV core shells would be more sensitive to irradiation due to the presence of hydrogen flakes, it is however conservatively postulated they are. The RT_{NDT} trend curves considered in the SIA therefore include the atypical embrittlement observed on VB395, more specifically in the material between hydrogen flakes.

Context

In view of the Structural Integrity Assessment (SIA) of the D3T2 RPV core shells, it was of utmost importance to determine the material properties in the most comprehensive and complete way. Central to this material properties investigation is the evolution of the fracture toughness properties under irradiation.

As presented in the roadmap (Figure 2.1), three segregated material types containing high numbers of hydrogen flakes were considered: the D3T2 RPV forgings, the VB395 shell and the KS 02 flange.

Requirements

This Chapter reports on the comprehensive material investigation and testing programme. As such, it also covers all the midterm actions related to the properties of segregated materials affected by hydrogen flaking.

These midterm actions were formulated by the FANC (see each of the following sections in this Chapter) and can be listed as in Table 5.1.

Midterm Action	Topic	Section
Action 11	Material properties of flaked material under irradiated conditions	5.2 Material Tests for SIA
Action 9b	Additional tensile tests of specimens with a ghost line	5.2 Material Tests for SIA
Action 10b	Residual hydrogen content	5.4 Assessment of Atypical Embrittlement of VB395
Action 12	Local (micro-scale) properties of specimens with macro-segregations, ghost lines and hydrogen flakes	5.1.3 Characterization of the Microstructures
Action 13	Effect of thermal ageing of the zone of macro-segregation	5.3.1 Effect of Thermal Ageing on Zones of Macro-segregation
Action 15b	Large-scale tensile testing on flaked material	5.3.2 Large-Scale Tests

Table 5.1: Midterm actions related to material properties.

Approach

Unexpected results obtained during the initial tests performed on irradiated VB395 material (Action 11) gave rise to a gradual re-orientation and extension of the material test matrix finally covering more than 1,500 tests on the three materials (D3T2 RPV forgings, VB395 shell and KS 02 flange), both in non-irradiated and irradiated condition. A series of investigations were started in order to assess the embrittlement mechanism and root causes.

Additional tensile tests (Action 9b) were performed at room temperature on Doel 3 RPV specimens containing a ghost line. Additional measurements (Action 10b) were performed to check the residual hydrogen content in specimens with hydrogen flakes. Microstructural investigations (Action 12) were performed on the three materials looking for similarities and differences. Accelerated ageing tests (Action 13) were performed to check for possible thermal ageing effects in the D3T2 RPV materials. Large-scale tensile tests (Action 15b) were performed on specimens with either inclined hydrogen flakes or with inclined machined notches to confirm the load bearing capacity of flaked components.

5.1 Tested Materials

In the context of the RPV Safety Case three types of materials were tested: samples coming from the D3T2 RPV forgings, VB395 shell and KS 02 flange, all belonging to two well-known RPV steel type families. Although their manufacturing process was different, they are all similar materials with segregated areas containing large numbers of hydrogen flakes.

The macro- and microstructures of the examined D3T2 forgings are globally identical. The VB395 shell can be considered as similar to the D3T2 forgings but with more tempered martensite in the dark zones (ghost lines) and globally harder. The KS 02 forging has a similar microstructure as the D3T2 forgings but with a slightly different chemical composition.

5.1.1 Material Types

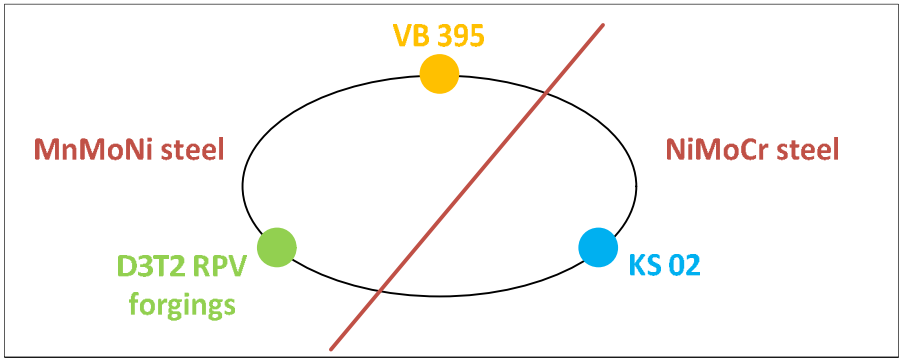

Figure 5.2: The forgings of interest and their steel type family.

The D3T2 RPV forgings are made according to the US standard SA508 Cl.3, and VB395 is made of French steel type 18MND5. Both steels belong to the same family of MnMoNi RPV steel. On the other hand, KS 02 is made of German 22NiMoCr37 steel belonging to the family of NiMoCr RPV steel (Figure 5.2).

The main difference between the two steel type families as shown in Table 5.3 is the fact that the MnMoNi steels contain considerably less chromium and more manganese than the NiMoCr steels. Chromium is known to increase the susceptibility for reheat cracking (e.g. underclad cracking) while manganese is known to increase the steel's hardenability.

In Germany, a steel type 20MnMoNi55 was developed that is very similar to SA508 Cl.3. Extensive studies performed in Germany show that 20MnMoNi55 and 22NiMoCr37, although belonging to two different families of RPV steels, are really equivalent regarding mechanical properties.

The table below gives the ladle chemical analysis and the Carbon Equivalent (CE) for the considered forgings. VB395 is close to the D3T2 RPV forgings but has more chromium and less sulphurous and phosphorous impurities. KS 02 has less manganese, more chromium and in addition more nickel.

Element	Doel 3	Tihange 2	VB395	KS 02
C	0.21-0.23	0.20-0.23	0.18	0.19
Si	0.21-0.27	0.20-0.26	0.17	0.20
Mn	1.30-1.45	1.30-1.41	1.46	0.93
P	0.008-0.012	0.010-0.015	0.006	0.008
S	0.007-0.011	0.009-0.010	0.002	0.006
Cr	0.04-0.18	0.05-0.11	0.254	0.50
Mo	0.48-0.50	0.46-0.52	0.50	0.56
Ni	0.71-0.77	0.65-0.73	0.72	1.29
V	0.01	0.01	0.005	Unknown
Cu	0.04-0.06	0.04-0.06	0.05	0.10
CE	0.58-0.62	0.60-0.64	0.63	0.65

Table 5.3: Ladle chemical analysis of D3T2, VB395 and KS 02 forgings.

5.1.2 Manufacturing Process

Investigation made clear that the manufacturing process of the materials D3T2, VB395 and KS 02 was different (Figure 5.4). But despite the differences, there is one similarity: all materials have segregated zones with high amounts of flakes.

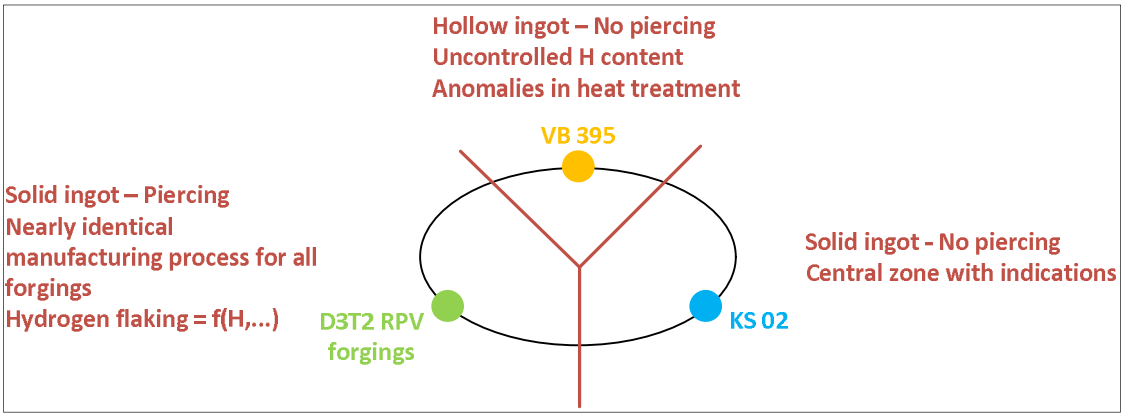

Figure 5.4: Manufacturing process of the tested materials D3T2, VB395 and KS 02.

D3T2 RPV forgings

All D3T2 RPV forgings went through a nearly identical manufacturing process: starting from a (vacuum-cast, top poured) solid ingot, followed by cropping the head and foot of the ingot, then removal of the central segregated part of the ingot (piercing), and finally forging. The forgings contain remains of the segregated areas that may be very close to the inner surface. All forgings were then subjected to a similar preliminary heat treatment and quenching and tempering.

As shown in Table 5.3, the chemical composition of all D3T2 RPV forgings is very similar. Moreover, they are nearly as susceptible to the formation of segregations during solidification of the ingot. The latter is confirmed by metallographic observations and carbon-mapping on nozzle cut-outs from the D3T2 nozzle shells.

Although the D3T2 RPV forgings were manufactured in a very similar way, they are not equally affected by hydrogen flakes. Their number of detected flakes ranges from zero to more than 11,000. However, this difference is perfectly understandable and primarily governed by the difference in hydrogen content of the ingots in combination with the sulphurous content.

The remnants of the D3T2 RPV forgings available for testing come from both upper core shells (belonging to the RPV Surveillance Programme) and from the nozzle shell cut-outs D3H1 (Doel 3) and T2H2 (Tihange 2). The latter both contain segregations but are free of hydrogen flakes.

VB395 shell

In contrast to the D3T2 RPV forgings, the VB395 shell was manufactured from a (air-cast, bottom poured) hollow ingot – so no piercing was needed to get a ring shaped forging. As a result of this manufacturing method, the (less enriched) segregations are not removed from the ingot and are located in the central part of the wall thickness.

VB395 shell suffered some manufacturing issues:

- Unreliable measurement of hydrogen content followed by an inadequate de-hydrogenation heat treatment and resulting flaking
- Cr contamination leading to upper bound Cr content
- Anomalies with heat treatments

Since thousands of hydrogen flakes were found in the VB395, different test blocks were taken out from this shell to be used for the qualification procedure of the UT inspection (Chapter 4.1.1), for microstructural examinations and for mechanical testing.

KS 02 flange

The KS 02 flange is a half ring of which the forging started from a solid ingot without applying any piercing. This explains why the segregated area is situated in the central part of the half ring, i.e. both in height and in thickness. Examination of this segregated area showed thousands of indications that turned out to be hydrogen flakes.

The KS 02 was examined in the 1980s as part of a comprehensive German research project with large forgings. Various samples were taken from the segregated and non-segregated areas in segment KS 02 B (Figure 5.5) and were tested in non-irradiated and irradiated conditions. Some irradiated samples from the segregated area are still available in AREVA Erlangen.

Another small block – from segment KS 02 M – was still available at MPA in Stuttgart. Part of this block, containing a few tens of flakes, was used for further testing in the framework of the Safety Case.

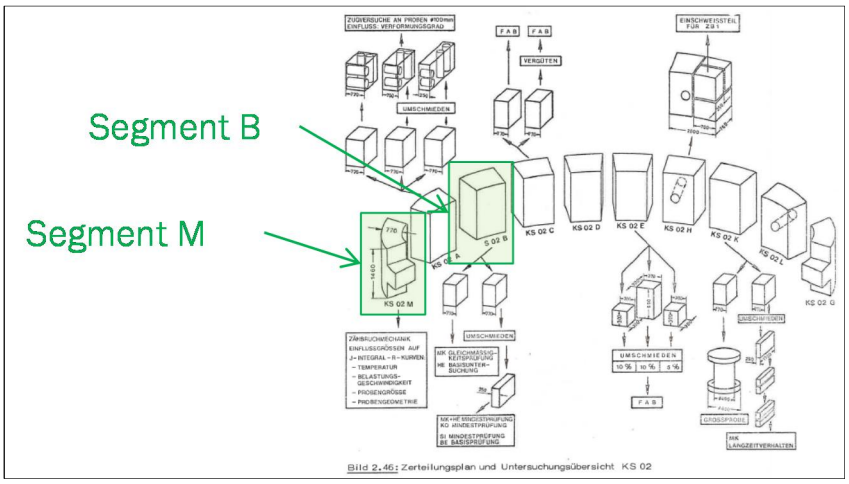

Figure 5.5: Samples taken from the KS 02 material for tests under non-irradiated and irradiated conditions.

5.1.3 Characterization of the Microstructures

Requirement

One of the FANC midterm requirements (Action 12) stated:

> *The licensee shall further investigate experimentally the local (micro-scale) material properties of specimens with macro-segregations, ghost lines and hydrogen flakes (for example local chemical composition). Depending on these results, the effect of composition on the local mechanical properties (i.e. fracture toughness) shall be quantified.*

This requirement was further completed with KS 02 investigations and by complementary detailed investigations, performed in the context of the assessment of the root cause of the atypical VB395 embrittlement under irradiation (Chapter 5.4 Assessment of Atypical Embrittlement of VB395).

Approach

The global characterization of the different materials was based on the following test programme:

- Macro-structural characterization
- Metallographic examinations by means of Light Optical Microscopy
- Micro-hardness measurements
- Local chemical enrichment assessment by Electron Probe Micro Analysis

5.1.3.1 Macro-structural examinations

In spite of the different manufacturing of the three tested materials, all materials present non-segregated areas and macro-segregated areas with locations and shapes corresponding to their manufacturing process.

D3T2 RPV forgings

Because of their similar chemical composition and manufacturing history, all D3T2 RPV forgings are similarly susceptible to the formation of segregations. This is confirmed by the observed macro-segregations in the D3T2 nozzle shell cut-outs, D3H1 and T2H2 evidenced by carbon mapping and macro-etching, which show comparable characteristics (location, shape) and enrichment. Both cut-outs contain also ghost lines with the same maximum inclination of 16° (measured for D3H1).

Ghost lines are residues, after forging, of localized segregations formed in ingots during their solidification. They appear as dark zones after etching.

Residues of A-segregates are residues, after forging-induced flattening and fragmentation, of positive macro-segregated cylindrical channels, distributed along a cone pointing towards the top of the ingot (A-segregates). They can be present in the macro-segregated as well as in the non-segregated zones. The residues of A-segregates can be considered as a specific type of ghost line.

VB395 shell

Due to a different manufacturing history (in particular, VB395 is forged from a hollow ingot), the shape and the location of the macro-segregation, identified by carbon mapping and macro-etching, are different than in the D3T2 forgings. Despite the absence of a piercing operation removing segregated areas, the local C-enrichment of VB395 is slightly lower than in the D3T2 forgings. The ghost lines observed in the macro-segregations of VB395 have the same maximum inclination of 16° and the hydrogen flakes are all located inside the ghost lines.

KS 02 flange

No detailed information is available on the macro-structural characteristics of the KS 02 material: a macro-segregated zone was reported in the middle of the forging but not confirmed by chemical analyses. It is also worth to remind that no piercing of the ingot was performed.

5.1.3.2 Microstructural examinations

D3T2 RPV forgings

As previously mentioned, both D3 and T2 forgings contain non-segregated and segregated areas, all presenting ghost lines. The ghost lines are mainly enriched in Mo and P. A significant amount of MnS is also present.

Similar microstructures are found in the dark and light zones of the different samples, respectively: tempered lower bainite with some tempered martensite and/or tempered upper bainite in the dark zones of the macro-segregated area (Figure 5.6) and upper bainite in the light zones (Figure 5.7). The average grain size observed in the different zones and materials is about 30µm.

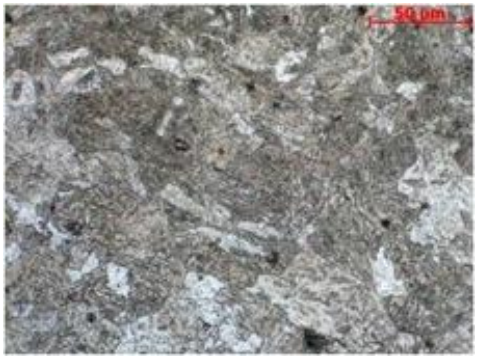

Figure 5.6: D3H1: dark zone microstructure: mostly lower bainite (red scale 50 µm).

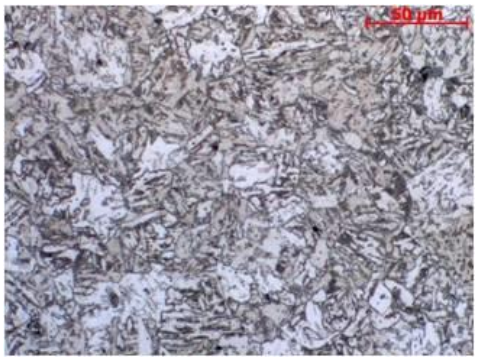

Figure 5.7: D3H1: light zone microstructure: upper bainite (red scale 50 µm).

For all the tested materials, similar hardness values are measured in similar zones; hardness values are somewhat higher in the ghost lines.

VB395 shell

As previously stated, VB395 contains non-segregated and segregated areas, all presenting ghost lines (micro-segregations and residues of A-segregates appearing as dark zones after etching). The ghost lines of VB395 have the same maximum inclination of 16° as the D3T2 ghost lines and are mainly enriched in Mo and P. The hydrogen flakes are all located inside the ghost lines. Despite a high scatter in the data, the enrichment is lower than in the D3H1 ghost lines.

VB395 has globally a similar microstructure in the dark and light zones (Figure 5.8) as D3T2 RPVs, with similar grain sizes, although a bit smaller than observed in D3H1. However, VB395 presents more tempered martensite in the dark zones (Figure 5.9), compared to D3T2, as well as less coarse precipitates. The dark zones form a marked segregation network. This trend is more pronounced for VB395/6BF (material between flakes – BF) than for VB395/5 and VB395/6OF (material outside of flakes – OF).

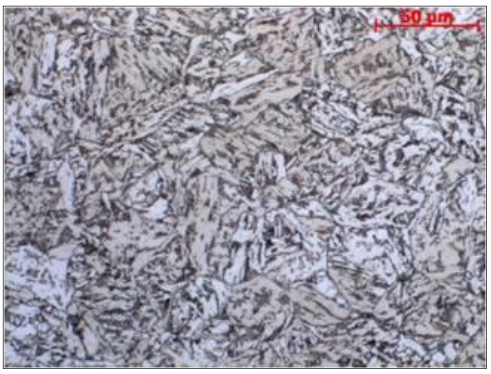

Figure 5.8: VB395/6BF: light zone microstructure: upper bainite (red scale 50 µm).

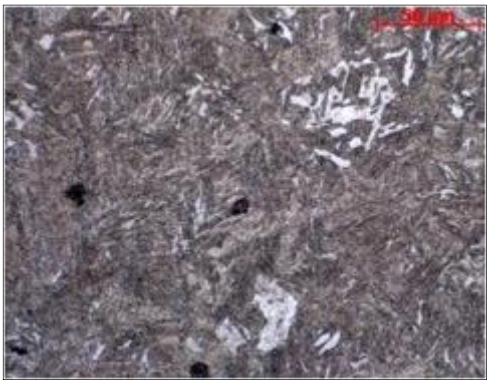

Figure 5.9: VB395/6BF: dark zone microstructure: tempered martensite (red scale 50 µm).

The hardness of VB395 is globally higher than the hardness of D3T2 materials.

KS 02 flange

KS 02 contains non-segregated and segregated areas, all presenting light zones and dark zones (ghost lines) (Figure 5.10 and Figure 5.11). No investigation on the inclination of the local segregation has been performed.

The microstructure of KS 02 is close to the microstructure of the D3T2 materials, i.e. a mix of tempered bainite with some tempered martensite in the ghost lines and upper bainite with some lower bainite between the ghost lines. No marked segregation network, such as in VB395, is observed.

The hardness of KS 02 is globally comparable to the hardness of D3H1.

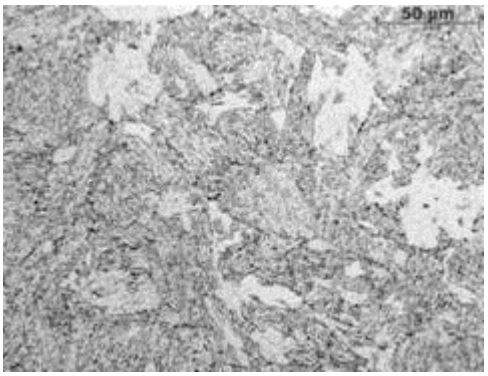

Figure 5.10: KS 02: dark zone microstructure: mostly tempered bainite (black scale 50 µm).

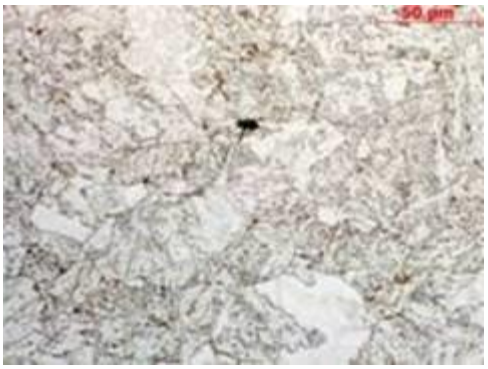

Figure 5.11: KS 02: light zone microstructure: mostly upper bainite (red scale 50 µm).

5.2 Material Tests for SIA

Unexpected results obtained during the initial tests performed on irradiated VB395 material (Action 11) led to a gradual extension of the material test matrix covering finally more than 1,500 tests on the three materials, both in non-irradiated and irradiated condition.

Tests performed on flaked material from KS 02 and VB395 confirmed that the presence of hydrogen flakes does not have any effect on the evolution of fracture toughness under irradiation.

The tests also showed that the D3T2 RPV forgings and the KS 02 flange behave as expected under irradiated conditions. On the contrary, VB395 does not behave as expected under irradiated conditions, and is to be considered as an outlier.

Requirement

One of the midterm actions (Action 11) to be performed by Electrabel refers to an extensive mechanical test programme. The requirement is formulated as follows:

> *A further experimental program to study the material properties of irradiated specimens containing hydrogen flakes shall be elaborated by the licensee.*

The initial Action 11 tests were limited to irradiated VB395 material. The test matrix has been gradually extended covering different material zones in the D3T2 RPV forgings, VB395 and KS 02, and non-irradiated as well as irradiated conditions. The following paragraphs address the full material test programme performed in the framework of Action 11.

Paragraph 5.2.2 on test results under non-irradiated conditions also covers the midterm requirement (Action 9b) to perform additional tensile testing on specimens containing ghost lines:

> *The licensee shall provide data about the tensile properties at ambient temperature of specimens with T orientation and taken in ghost lines (ghost line along the specimen axis).*

5.2.1 Material Test Matrix

In the framework of the RPV Safety Case, extensive mechanical tests were performed on the three materials D3T2, VB395 and KS 02, both in non-irradiated and irradiated condition.

5.2.1.1 Mechanical tests

In general, the mechanical tests cover:

- Instrumented Charpy-V impact testing to determine the shift in RT_{NDT} under irradiation
- Fracture toughness testing based on PCCV and/or Compact Tension (CT) specimens to determine the shift in Master Curve Reference Temperature T_0
- Tensile testing

5.2.1.2 Material Test Matrix

The material test matrix (Table 5.12) gives an overview of the tested materials and their tested zones. For the tests performed in irradiated conditions, the table indicates the fluence levels (x 10^{19} n/cm^2) at which the irradiation tests were performed. Fluence levels corresponding to 40 years of operation are typically 6 10^{19} n/cm^2. The test matrix is briefly addressed below.

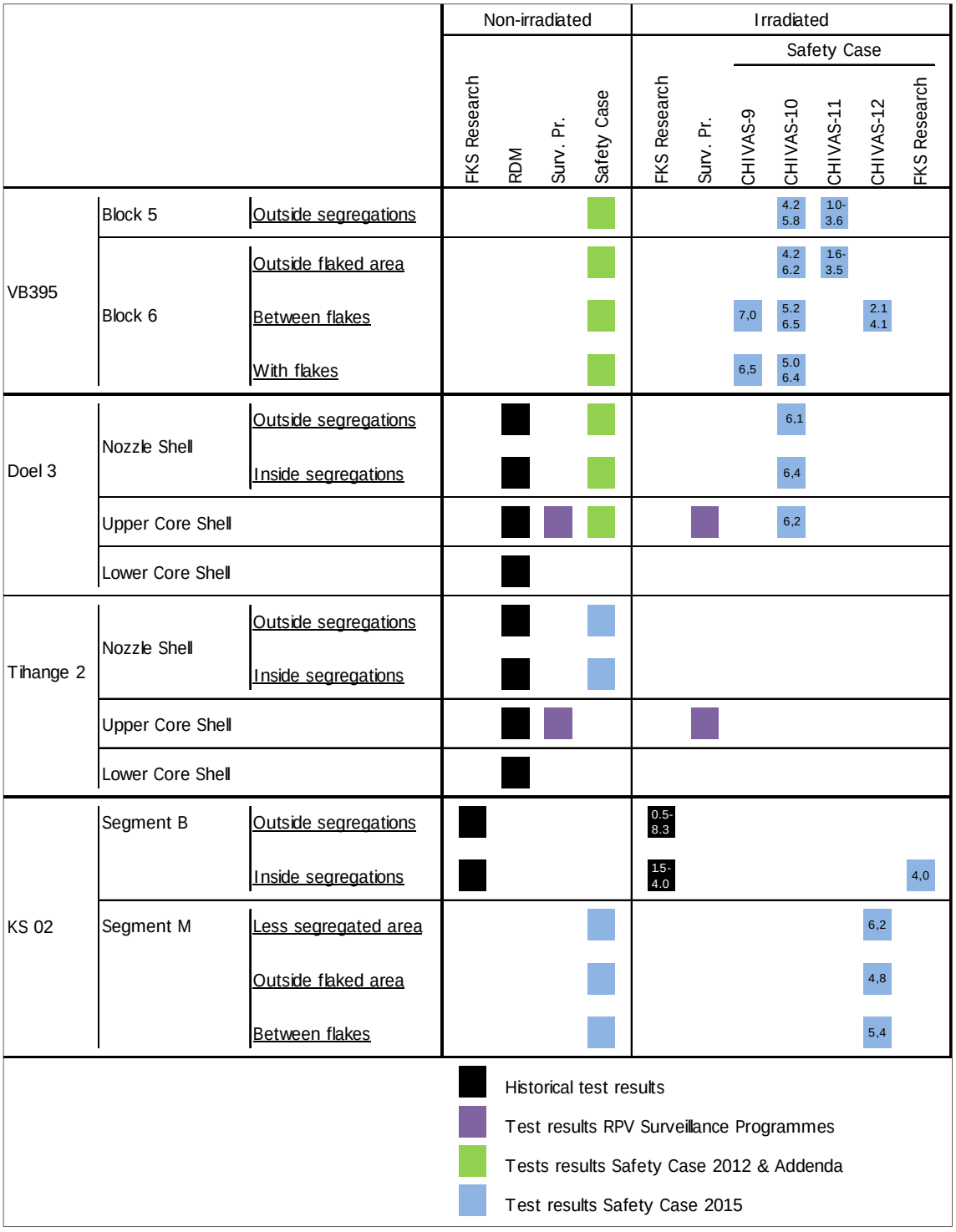

Table 5.12: Material test matrix.

VB395 shell

From shell VB395 specimens were taken from the areas indicated in Figure 5.13:

- Block 5: outside segregations and far away from the area with hydrogen flakes
- Block 6: outside the area with hydrogen flakes but adjacent to that area (OF)
- Block 6: between hydrogen flakes (BF)
- From Block 6 specimens with flakes inside were also extracted (F)

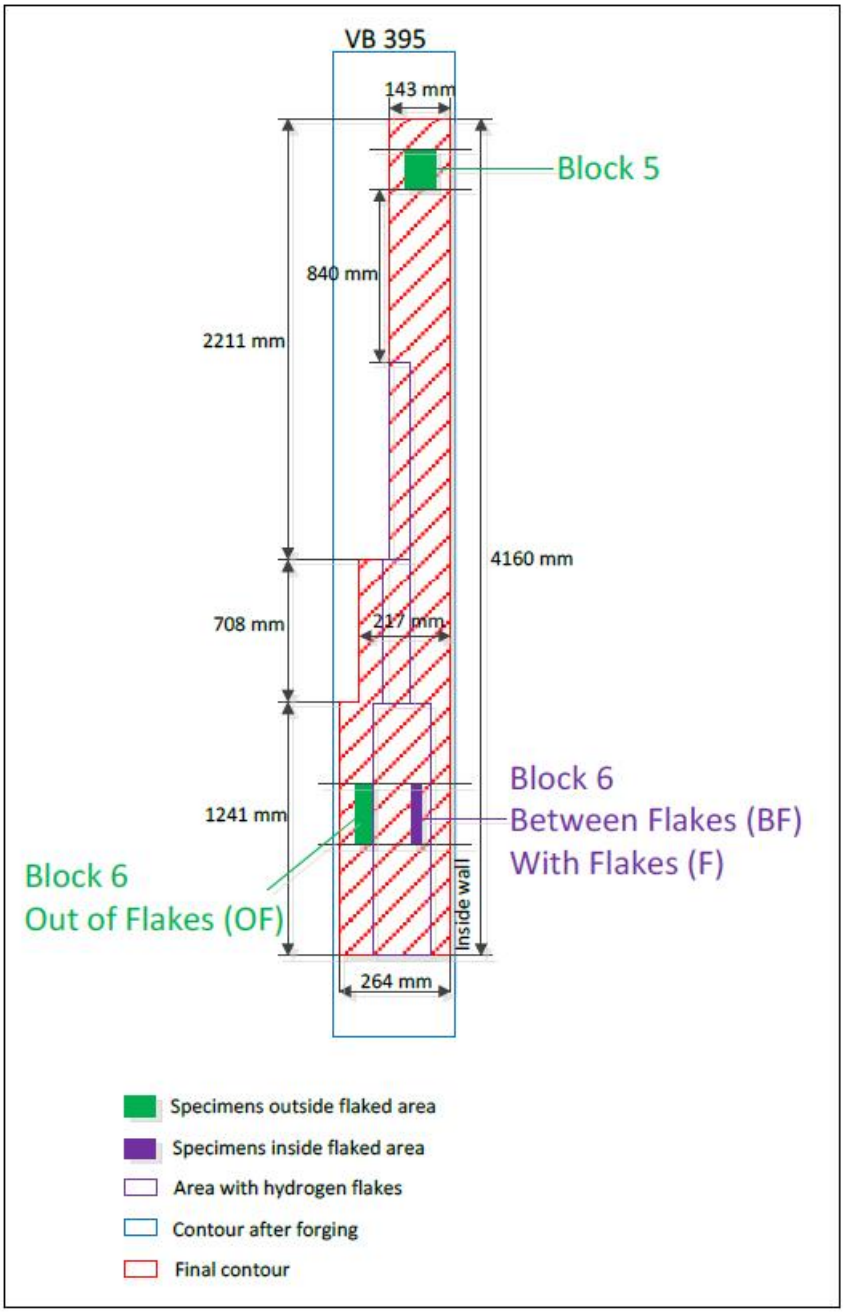

Figure 5.13: Position of sampled areas in VB395 shell with respect to areas affected by hydrogen flakes.

D3T2 RPV forgings

- The baseline mechanical properties of the D3T2 RPV forgings were determined through the acceptance tests performed by RDM at the time of manufacturing.
- The core shells of both RPVs were further covered by the RPV Surveillance Programme. This programme includes only material from the non-segregated area of the upper core shells of both RPV's and allows assessing the evolution of the mechanical properties as a function of fluence. In the framework of the Safety Case, some additional testing was performed on specimens taken from remaining material from the Doel 3 RPV Surveillance Programme.
- Additional testing was also performed on specimens taken from the nozzle shell cut-outs D3H1 (Doel 3) and T2H2 (Tihange 2) corresponding to the central parts of the nozzle shells. In both cases, specimens were taken in the segregated and non-segregated areas. Only Doel 3 specimens were irradiated (Chivas-10) and tested.

KS 02 flange

- Both in non-irradiated and irradiated conditions, the majority of tests on specimens from the segregated and non-segregated areas of segment KS 02 B, were performed in the 1980s in the framework of the German FKS (Forschungsvorhaben Komponenten Sicherheit) research programme.
- The specimens from the segregated area were irradiated and tested by Siemens/KWU – part of them is still at AREVA Erlangen. In the framework of the Safety Case, it was demonstrated that the specimens tested in the framework of FKS were actually taken between the hydrogen flakes. In order to get a valid T_0 value under irradiated condition (to be compared to the corresponding RT_{NDT}), PCCV specimens were reconstituted from irradiated broken Charpy-halves and tested at AREVA Erlangen.
- In addition, testing and examinations were performed on specimens taken from the remaining segment KS 02 M containing a few tens of hydrogen flakes. The tests were performed under non-irradiated and irradiated conditions (Chivas-12).

Conclusions

A comprehensive mechanical test programme was performed on the three materials: D3T2 RPV forgings, VB395 shell and KS 02 flange, covering more than 1500 specimens. The specimens were taken from segregated and non-segregated areas, between hydrogen flakes and outside the flaked area, and some specimens even contained flakes inside. In addition, specimens were taken in different orientations within the forgings. Testing under irradiated conditions was performed at different fluence levels up to the expected fluence of the RPVs at 40 years of operation.

5.2.2 Results under Non-Irradiated Conditions

Basically, mechanical properties under non-irradiated conditions must be determined in order to have a reference point for addressing the effect of irradiation. As such, for all available materials the initial values of RT_{NDT} and Master Curve T_0 have been determined.

However, in the framework of the 2012 Safety Case and its Addenda, numerous tests were performed on non-irradiated specimens from the different zones of VB395 and from the D3 nozzle shell cut-out in order to investigate the potential effect of specimen orientation, presence of macro-segregations and the presence of flakes on the mechanical properties. Initially, mainly fracture toughness tests were performed (T_0 approach), either on PCCV or CT12.5 specimens, but in 2014 additional Charpy impact testing was performed in order to determine the different materials reference RT_{NDT} values.

The mechanical testing on different materials under non-irradiated conditions showed that in the transition region there is no significant effect of the specimen orientation or segregation level on the fracture toughness. More specifically, the following may be highlighted.

D3T2 RPV forgings

- Tests performed during manufacturing showed there is only a very small difference between the initial RT_{NDT} values for nozzle shells and core shells (15°C) and this difference is even smaller for the four core shells (5°C only).
- Additional testing in the framework of the Safety Case confirmed the limited effect of segregations on the initial Charpy curve: the difference in T_{41J} between segregated and non-segregated zone is 22°C and 6°C for the T2H2 and D3H1 nozzle shell cut-outs respectively. In a similar way, fracture toughness tests showed that the effect of segregations on the initial T_0 was less than 10°C for both cut-outs.
- In addition, tests on the D3H1 nozzle shell cut-out showed that ghost lines have practically no effect on Charpy properties and on fracture toughness. Three additional tensile tests on specimens with a ghost line along the specimen axis were performed at room temperature at the request of the AIA (Action 9b). They confirmed the results obtained previously on similar specimens at operating temperature, thereby confirming the good ductility of the material.
- Tests performed on the spare surveillance material from the Doel 3 Upper Core Shell showed there is little influence of specimen orientation on fracture toughness.

KS 02 flange

- Tests performed on Pellini drop weight and Charpy-V specimens taken from the segregated and non-segregated areas showed that there is only a very small difference in initial RT_{NDT} value between both areas (3°C).
- The difference in T_{41J} observed on the Charpy impact energy transition curves between segregated and non-segregated areas varies between 31°C and 47°C. However, this difference can at least partly be attributed to the sampling position of the non-segregated specimens. They were taken close to the surface and hence take profit from the beneficial effect of quenching on their mechanical properties. Also, the difference between both areas is smaller when considering other transition curve parameters such as lateral expansion. Consequently, the observed difference in T_{41J} is not representative for the difference in initial RT_{NDT}.
- The difference in T_0 between both areas is 25°C, i.e. much smaller than the difference in T_{41J}. This is probably also due to the fact that the larger CT specimens (50 and 100 mm thick) were sampled farther away from the surface and hence were less subjected to the quenching effect. The difference in T_0 is larger than in the D3T2 forgings, but similar to VB395.
- Specimens taken between hydrogen flakes or outside the flaked area yield very similar T_{41J} values which illustrates again that the presence of hydrogen flakes has no effect on the material properties.

VB395 shell

- The difference in Master Curve T_0 encountered in different material zones in Block 6 (specimens with flakes, taken between flakes or adjacent to the flaked area) is less than 25°C. In terms of RT_{NDT}, this difference is less than 20°C.
- In particular no significant difference in T_0 is observed between CT12.5 specimens taken between flakes and CT12.5 specimens with a real flake as pre-crack demonstrating that the presence of hydrogen flakes has no effect on the material properties.
- The maximum difference between Block 5 and Block 6 is only slightly larger than inside Block 6, i.e. 30°C in terms of T_0 and 24°C in terms of RT_{NDT}.

- The difference between fracture toughness results obtained through PCCV and CT12.5 specimen testing is not always in agreement with the known bias of 10 to 15°C. In particular, this is true for Block 5 where $T_{0,PCCV}$ is 7°C higher than $T_{0,CT12.5}$ instead of being 10 to 15°C lower. This illustrates the large scatter encountered on the VB395 material.
- VB395 is characterized by very low initial T_0 temperatures, ranging between -126.5°C and -116.1°C.

Conclusions

- The tests demonstrate there is a similar limited effect of segregation on the initial $RT_{NDT,41J}$ and T_0 for the D3T2 forgings and VB395 under non-irradiated conditions. For KS 02 the observed differences in T_{41J} and T_0 are clearly influenced by the sampling location of the non-segregated specimens. The actual effect of segregations on the initial properties should be less important than the observed T_{41J} difference, as illustrated by the difference in initial RT_{NDT} determined through Pellini drop weight/Charpy-V impact testing.
- Tests performed on flaked material (VB395 and KS 02) show that the presence of flakes has no impact on the mechanical properties as very similar results are obtained for specimens with flakes, for specimens taken between flakes and for specimens taken outside the flaked area.

5.2.3 Results under Irradiated Conditions

As shown in the material test matrix (Table 5.12), the following materials were tested under irradiated conditions:

- Doel 3 Nozzle Shell cut-out D3H1
- Doel 3 Upper Core Shell
- Tihange 2 Upper Core Shell (tested only in the framework of the RPV Surveillance Programme)
- KS 02 flange
- VB395 shell

5.2.3.1 Mechanical tests

The objective of the initial test programme on irradiated specimens (Chivas-9) was to demonstrate the conservativeness of the 50°C margin on RT_{NDT} shift considered in the 2012 Safety Case & Addendum. Since the flaked VB395 material exhibited an unexpectedly high embrittlement, additional testing was performed (Chivas-10/11/12). The additional testing also included specimens from the Doel 3 Upper Core Shell, the Doel 3 Nozzle Shell cut-out D3H1 and the German KS 02 material.

The findings resulting from the test programme on irradiated specimens are summarized in the table below (Table 5.14). The table focuses on the consistency between the different test results addressed through:

- Comparison of RT_{NDT} and T_0 shift versus prediction formula.
- Comparison between measured shifts in RT_{NDT} and Master Curve T_0: typically, for this type of RPV forgings the generally accepted ratio between ΔT_0 and ΔRT_{NDT} is around 1.16.
- Comparison between the observed shifts in RT_{NDT} and tensile strength: typically, transition temperature shift and yield stress are proportional. The proportionality factor may vary between 0.5 and 1.0, with a generally accepted average value of 0.63°C of RT_{NDT} shift per MPa of yield stress increase.

- Advanced interpretation of the instrumented Charpy load diagrams recorded during Charpy impact testing, as developed by SCK•CEN. This analysis allows assessing the evolution of the micro-cleavage fracture stress with fluence. Typically, the micro-cleavage fracture stress of RPV steels only show small variations with fluence.

			ΔRT_{NDT} versus prediction	ΔT_0 versus prediction	Ratio $\Delta T_0/\Delta RT_{NDT}$	Ratio $\Delta RT_{NDT}/\Delta\sigma$	µ–cleavage fracture stress drop	Atypical Embrittlement
Reference value			RSE-M (Ed.2010) or ASTM E-900	1.16 x RSE-M (Ed.2010)	1.16 [Nanstad-Sokolov]	0.63°C/MPa		
VB395	Block 5	Outside segregations	OK	OK	OK	OK	Yes	No
	Block 6	Outside flaked area	OK	> prediction	NOK	OK	Yes	Yes
		Between flakes	> prediction	> prediction	OK	NOK	Yes	Yes
		With flakes	-	> prediction	-	-	-	-
Doel 3	Nozzle Shell	Outside segregations	OK	OK	OK	OK	No	No
		Inside segregations	OK	OK	OK	OK	No	No
	Upper Core Shell		OK	OK	OK	OK	No	No
Tihange 2	Upper Core Shell		OK	OK	OK	OK	-	No
KS 02	Segment B	Outside segregations	OK	OK	OK	OK	No	No
		Inside segregations	OK	OK	OK	OK	No	No
	Segment M	Less segregated area	OK	-	-	OK	No	No
		Outside flaked area	OK	-	-	OK	No	No
		Between flakes	OK	-	-	OK	No	No

Test results in **red** are atypical.

Table 5.14: Evaluation of mechanical tests performed on irradiated specimens.

5.2.3.2 Results D3T2 RPV forgings

For the Doel 3 Upper Core Shell – one of the core shells affected by flaking – spare surveillance material taken from the extremity of the shell was irradiated in Chivas-10. In addition, specimens from the Doel 3 Nozzle Shell cut-out D3H1, from segregated and non-segregated zones, were also included in Chivas-10.

For the Tihange 2 Upper Core Shell – also affected by flaking – test results are available from the RPV Surveillance Programme. The following conclusions can be drawn.

Shift in RT_{NDT}

For the Doel 3 Upper Core Shell, the obtained RT_{NDT} shift is perfectly in line with the results from the RPV Surveillance Programme (Figure 5.15), thereby also confirming the absence of any measurable effect of the higher flux in BR2 on the irradiation of this material at this fluence level. The trend line depicted in Figure 5.15 is the RSE-M trend curve for the chemical composition of the Upper Core Shells.

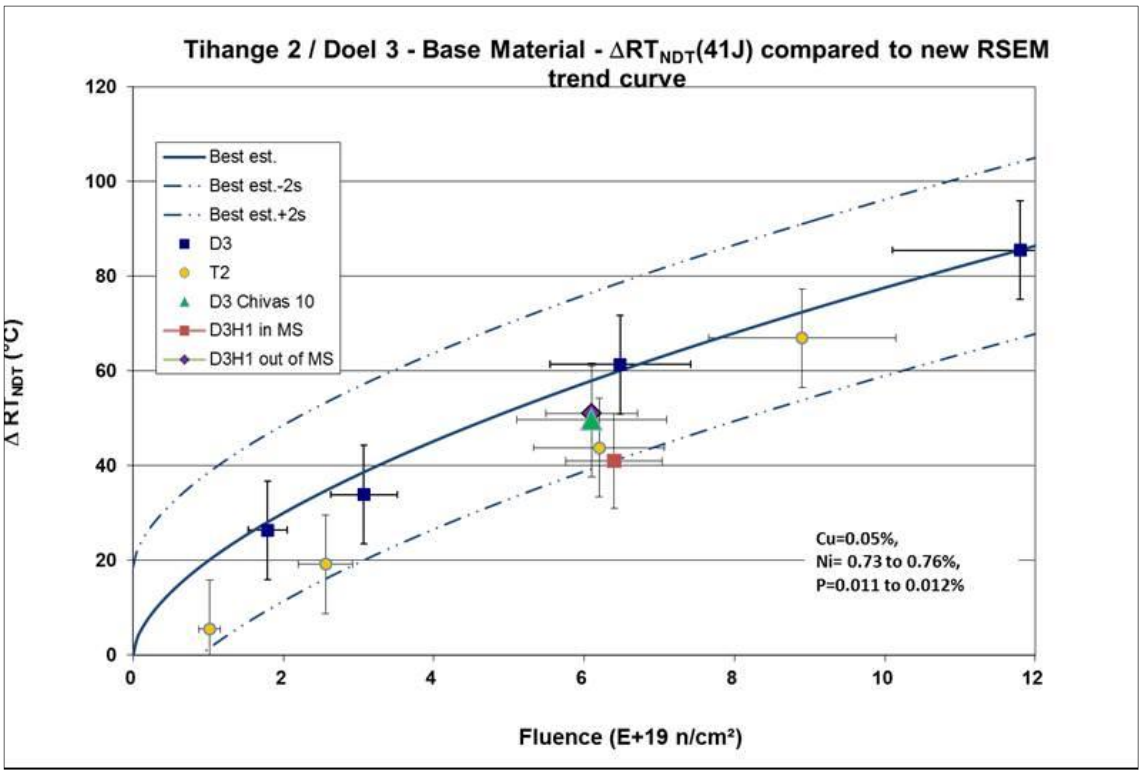

Figure 5.15: CHIVAS-10 results for D3 UCS and D3H1 compared to RPV Surveillance results and to RSE-M prediction.

For the Doel 3 Nozzle Shell cut-out D3H1, the measured RT_{NDT} shifts for segregated and non-segregated zones are very similar, and they are in excellent agreement with the core shell results. Both points have been added to Figure 5.15 but one should keep in mind that the RSE-M trend curve for the chemical composition of the nozzle shell is actually a few degrees below the trend curve for the upper core shells. As for the core shells, there is no visible effect of the BR2 flux on the RT_{NDT} shift of the nozzle shell material.

Shift in T_0

The material from the Doel 3 Upper Core Shell and Nozzle Shell included in Chivas-10 show shifts in T_0 that are in agreement with the RPV Surveillance Programme, which on turn are in very good agreement with the prediction of the RSE-M trend curves for RT_{NDT} shift, multiplied by 1.16. Comparison with the T_0 shift evaluated by the SINTAP method shows that there is even a better consistency with the RSE-M predictions than for the standard Master Curve.

Ratio between RT_{NDT} and T_0 shift

For the D3T2 RPV materials, the ratio between individual ΔT_0 and ΔRT_{NDT} values is between 0.7 and 1.6, being a range that can be considered as normal. Based on fitted T_0 curves the ratio is 1.09.

Ratio between RT_{NDT} shift and yield stress increase

The ratio between the RT_{NDT} shift and yield stress increase under irradiation is in the expected range. This confirms that this material is only affected by the expected hardening embrittlement. Again, the yield stress increase is in very good agreement with the results from the RPV Surveillance Programme.

Micro-cleavage fracture stress

None of the D3T2 RPV materials show a significant drop in micro-cleavage fracture stress when fluence increases.

Conclusions on D3T2 RPV forgings

- All tested D3T2 RPV materials from the upper core shells and nozzle shell show very similar shifts in RT_{NDT} and T_0, without any significant difference between segregated and non-segregated zones.
- The shifts are in excellent agreement with the predictive curves and correspond to the expected hardening embrittlement.
- There is no measurable effect of the high BR2 flux on the measured shifts in RT_{NDT} and T_0.

5.2.3.3 Results KS 02 flange

In the 1980s, in the framework of the German FKS research programme, specimens from the non-segregated and segregated area of segment KS 02 B were tested under irradiated conditions. Examinations of remnants of irradiated Charpy and Pellini specimens taken from the segregated zone revealed laminar indications that were confirmed to be hydrogen flakes. This proves that KS 02 B specimens taken from the segregated zone have actually been taken between hydrogen flakes.

Since almost no fracture toughness values were available for the segregated zone under irradiated conditions, fracture toughness specimens were reconstituted in 2015 from remnants of Charpy-V specimens irradiated at the highest fluence ($4\ 10^{19}$ n/cm^2), and tested.

In the CHIVAS-12 irradiation campaign specimens taken from a remaining segregated block from segment KS 02 M were included. Specimens were taken between flakes (BF), outside the flaked area (OF) and in a less segregated zone.

For the different tested specimens of KS 02 the following results can be given (Figure 5.16 and Figure 5.17):

- The shifts of RT_{NDT} for specimens taken from non-segregated and segregated areas, and from both segments, fall practically on the same upper bound RSE-M trend curve (Figure 5.16) (although not strictly applicable to this material due to its high Ni content).
- The CHIVAS-12 results are in line with the historical German results. This confirms the absence of significant flux effect for this material, the BR2 flux being an order of magnitude higher than in the German irradiations.
- As can be seen in Figure 5.17, the T_0 shift for specimens from the segregated zone is on the power law curve fitted through the existing results for the non-segregated area.
- The ratios between ΔT_0 and ΔRT_{NDT} are between 1.12 and 1.29, i.e. within the scatter band around the generally accepted value of 1.16.
- The ratios between ΔRT_{NDT} and $\Delta\sigma_y$ obtained in the FKS research programme and in CHIVAS-12 are similar and confirm there is no sign of Atypical Embrittlement of KS 02 under irradiation.
- There is practically no evolution of the micro-cleavage fracture stress with fluence, which again confirms the expected embrittlement behaviour of the KS 02 material.
- The KS 02 results confirm that there is no specific sensitivity of this material to irradiation embrittlement due to the presence of hydrogen flakes.

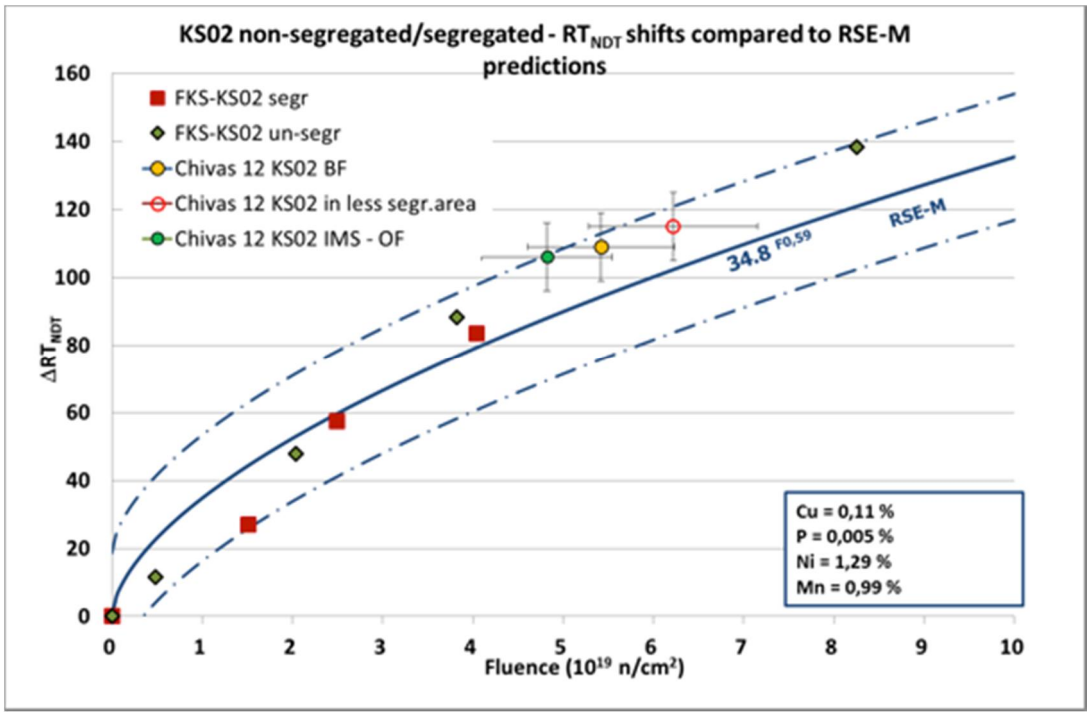

Figure 5.16: Measured shifts of RT_{NDT} for KS 02.

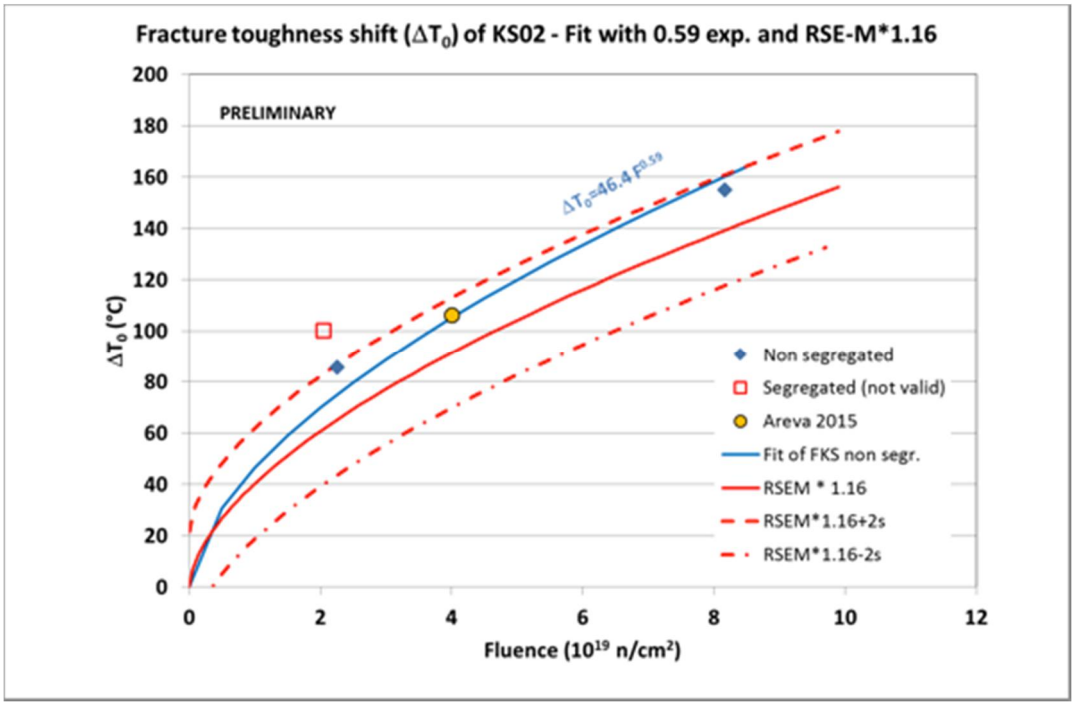

Figure 5.17: Measured shifts of T_0 for KS 02.

Conclusions for KS 02

- The historical FKS test results on specimens from segment KS 02 B are confirmed by recent tests performed on specimens from segment KS 02 M under non-irradiated and irradiated (CHIVAS-12) conditions.
- Non-destructive and destructive examinations confirm that the segregated zones of KS 02 are affected by hydrogen flaking, and that specimens taken from this zone were actually taken between hydrogen flakes.
- There is no difference of shift in transition temperature with irradiation between non-segregated and segregated zone, the shift is in agreement with predictions and corresponds to the expected hardening embrittlement.
- There is no measurable effect of the high BR2 flux on the test results.
- The results confirm that there is no specific sensitivity of KS 02 for irradiation embrittlement due to the presence of hydrogen flakes.

5.2.3.4 Results VB395 shell

For the different tested specimens (Block 5 and Block 6) of the VB395 shell the following results can be given (Figures 5.18 and 5.19).

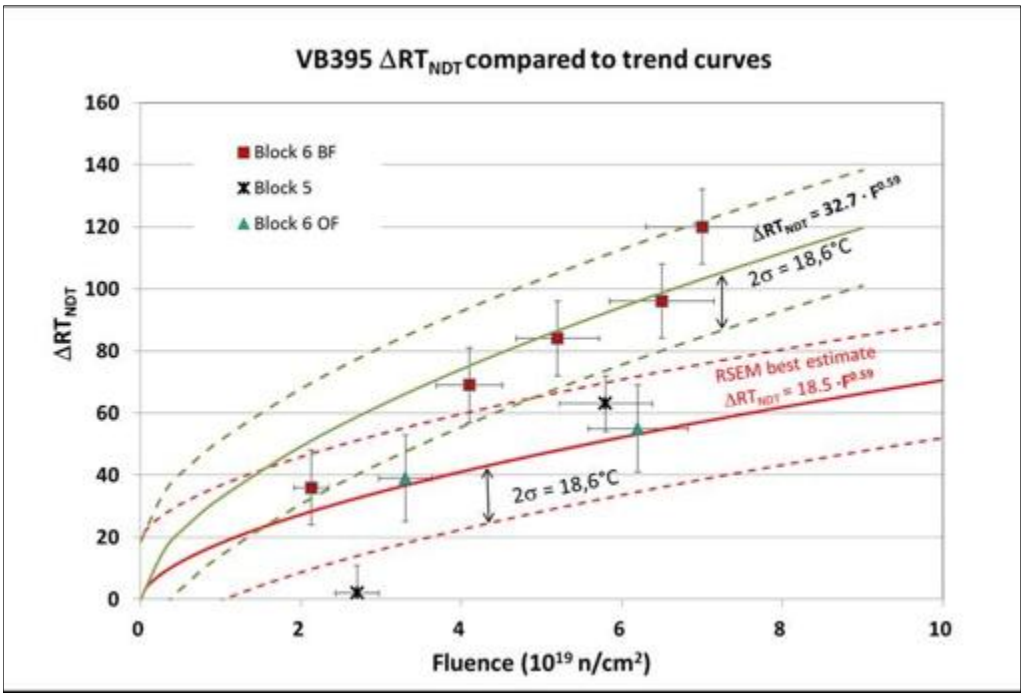

Figure 5.18: Measured shifts in RT_{NDT} for VB395.

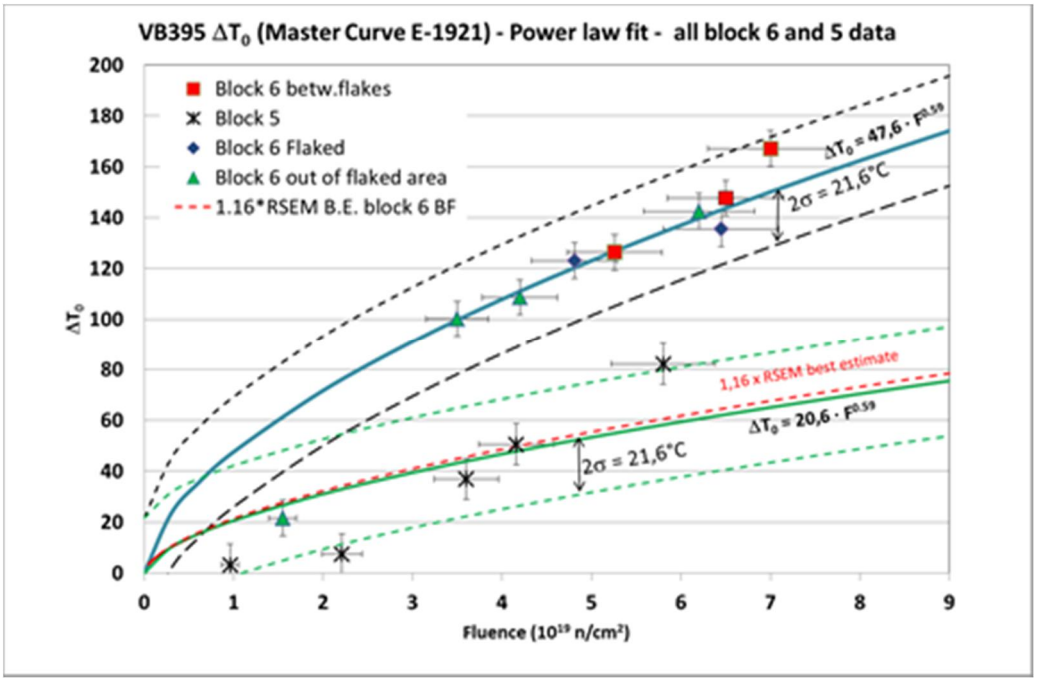

Figure 5.19: Measured shifts in T_0 for VB395.

Block 6: specimens between flakes and with flakes

- As shown in Figure 5.19, specimens between flakes and with flakes follow the same T_0 trend curve confirming the finding under non-irradiated conditions that the presence of hydrogen flakes does not cause a specific sensitivity to irradiation embrittlement.
  This observation is further confirmed through ductile fracture resistance tests performed on specimens taken between flakes and with flakes as crack initiator.
- The T_0 shift is largely above predictions.
- The RT_{NDT} shift in specimens taken between flakes is above the trend curve predictions but to a lesser extent than the fracture toughness (Figure 5.18).
- The ratio between ΔT_0 and ΔRT_{NDT} for specimens between flakes is of the order of 1.4, i.e. above the generally accepted value of 1.16 (typical ratio determined by Nanstad-Sokolov), but still in a range considered as normal.
- The observed shift in RT_{NDT} is much larger than the shift that may be expected based on the observed increase in tensile strength.
- The specimens between flakes also show a substantial drop in micro-cleavage fracture stress.
- This reveals an atypical embrittlement.

Block 6: specimens outside zone with flakes but adjacent to it

- The T_0 shift is largely above predictions and follows the same trend curve as for the specimens between flakes and with flakes.
- The observed RT_{NDT} shift falls almost exactly on the RSE-M best estimate trend curve.
- The ratio between ΔT_0 and ΔRT_{NDT} is of the order of 2.5, i.e. largely above the generally accepted value of 1.16 and clearly out of the generally accepted range of variation.
- The observed shift in RT_{NDT} is in line with the increase in tensile strength.
- The large T_0 shift and the substantial micro-cleavage fracture stress drop lead to the conclusion that this zone is also affected by an atypical embrittlement.

Block 5: specimens taken outside macro-segregations

- The observed T_0 shift falls in the scatter band of the prediction, i.e. the RSE-M trend curve multiplied by 1.16. However, the evolution with fluence does apparently not follow the power law with a 0.59 exponent as in the RSE-M trend curve. In particular, a very low embrittlement is measured at low fluence.
- At high fluence the RT_{NDT} shift falls close to the prediction but the lowest fluence point shows practically no embrittlement, as confirmed by a low shift in T_0 in the low fluence range.
- The ratio between ΔT_0 and ΔRT_{NDT} is of the order of 1.4, i.e. above the average value of 1.16 but still in a range that can be considered as normal.
- The observed shift in RT_{NDT} is in line with the increase in tensile strength.
- Although the T_0 and RT_{NDT} shifts do not reveal the behaviour of an outlier, Block 5 shows an atypical drop in micro-cleavage fracture stress.

SINTAP approach

Since the VB395 material properties are very different from one zone to another, an alternative interpretation of the fracture toughness data according to the SINTAP lower tail approach was made.

- The T_0 values obtained by this approach for the VB395 materials are in most cases only slightly higher than the T_0 of the standard Master Curve approach, and the effect is more pronounced in non-irradiated conditions (where the scatter is higher) than in irradiated condition. In terms of T_0 shift under irradiation, the standard master curve is therefore more conservative.
- The slightly higher initial T_0 obtained by the SINTAP method is compensated by a slightly lower shift under irradiation, leading to similar final values in irradiated condition.

Conclusions for VB395

- Results obtained under irradiated conditions confirm that the presence of hydrogen flakes does not induce a specific sensitivity of the material to irradiation embrittlement: specimens with flakes, specimens taken between flakes, and specimens taken outside the flaked area follow the same T_0 trend curve.
- The test results for VB395 are very different from one zone to another. This is particularly true for Block 6 out of the flaked area where the observed RT_{NDT} shift is within the prediction and in line with the observed increase in tensile strength, but where the shift in fracture toughness is largely above the predicted value.
- Block 6 is clearly affected by an atypical embrittlement characterized by an embrittlement higher than expected on the basis of the current scientific knowledge, while the material hardening remains in line with expectations. A decrease of the micro-cleavage fracture stress is also observed. This is generally associated with grain boundary segregation of phosphorus and other species, and with a change of fracture mode from transgranular to intergranular. However, the latter is not observed in VB395.
- In comparison with the D3T2 RPV forgings and the KS 02, it can thus be concluded that the VB395 demonstrates the behaviour of an outlier. Its embrittlement under irradiation is characterized by a substantial decrease in micro-cleavage fracture stress in Blocks 5 and 6, and a shift in fracture toughness T_0 that is considerably higher than predicted in all zones of Block 6. This outlier behaviour only affects the irradiation embrittlement, while the non-irradiated properties are representative for this type of material.
- Nevertheless, all fracture toughness results for VB395 remain enveloped by the RSE-M (Ed. 2010) and ASME K_{Ic} curves indexed to $T\text{-}RT_{NDT}$, as shown in Figure 5.20.
- Although there is a high shift of the fracture toughness curve under irradiation, there is no indication of a decrease of the lower shelf of the fracture toughness curves.

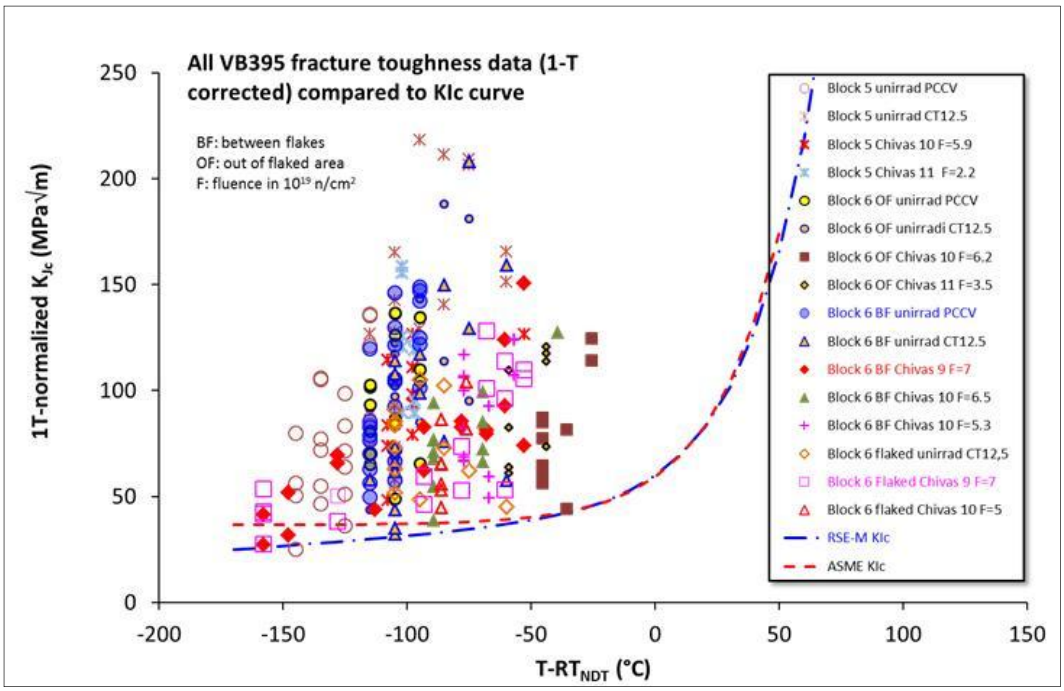

Figure 5.20: All fracture toughness results for VB395 materials compared to RSE-M and ASME K_{Ic} curves.

5.2.3.5 Overall conclusions

Tests performed under non-irradiated and irradiated conditions on flaked material from VB395 and KS 02 confirm that the presence of hydrogen flakes does not have any effect on the evolution of fracture toughness under irradiation.

The D3T2 RPV forgings and the German KS 02 flange behave as expected under irradiation conditions, as shown by:

- Very similar material properties in their different zones
- An embrittlement that is in line with the predictions
- The expected hardening embrittlement
- Almost no variation of micro-cleavage fracture stress when fluence increases

Contrary to the D3T2 RPV forgings and KS 02, the VB395 shell does not behave as expected under irradiation, and is to be considered as an outlier because of:

- Very different properties in different zones
- An embrittlement that is far beyond predictions as evidenced by detailed comparison to embrittlement data from the ASTM E-900 database and to the French database used to develop the RSE-M trend curve
- Atypical embrittlement characterized by a high shift of the fracture toughness curve while the hardening is as expected for this type of material
- A substantial decrease in micro-cleavage fracture stress with fluence in all zones and a shift in fracture toughness that is considerably higher than predicted, especially in one zone (Block 6)

The overall conclusions for the material tests for SIA are as follows (Figure 5.21):

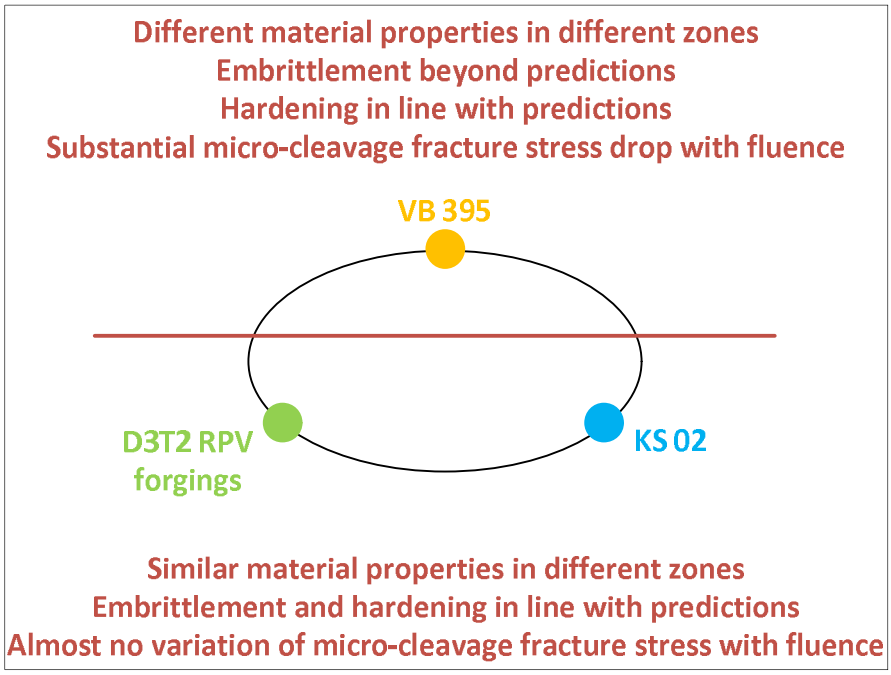

Figure 5.21: Overall conclusions on mechanical test results.

5.3 Additional Material Investigations

5.3.1 Effect of Thermal Ageing on Zones of Macro-segregation

A literature survey showed that thermal ageing is not to be expected for the Tihange 2 RPV forgings. The limited evolution of the mechanical properties and the small proportion of inter-granular fracture after irradiation and/or accelerated ageing tests confirmed that thermal ageing has no significant effect in the D3T2 RPV materials.

Requirement

The FANC expressed the following additional requirement (Action 13):

The licensee shall further evaluate the effect of thermal ageing of the zone of macro-segregation.

Thermal Ageing is a temperature diffusion-induced embrittlement, typically characterized by segregation at the grain boundaries inducing an inter-granular fracture mode.

Approach

The following steps were taken to fulfil this requirement:

- A literature survey was conducted on the effects of long-term thermal ageing and related accelerated ageing tests.
- Thermal ageing was investigated through a qualitative evaluation of the sensitivity by means of an accelerated ageing test (step cooling heat treatment), not representative of real service conditions but known to maximize thermal ageing effect. The mechanical tests were conducted on the Doel 3 nozzle shell cut-out, on the VB395 materials, and for comparison with JRQ (IAEA material widely used for international benchmarking). Fractographic examination of the fracture surfaces of the D3H1 and VB395 materials were also performed by means of a Scanning Electron Microscope (SEM) for evaluation of the intergranular character of the fracture surfaces.
- The fracture surfaces of (irradiated) specimens from the Doel 3 and Tihange 2 RPV Surveillance Programmes were examined by means of a SEM. The specimens had spent approximately 25 equivalent full power years in the reactor at 285°C. The objective of the SEM examination was to look for intergranular fracture areas that could indicate phosphorus segregation on grain boundaries. Phosphorus migration towards the grain boundaries can induce embrittlement.

Conclusions

- The literature survey revealed that no thermal ageing effect is to be expected for the Tihange 2 RPV forgings, because of their fine grain size and relatively low phosphorus content.
- The accelerated ageing test (step cooling) showed only a very limited effect on the Tihange 2 material in terms of Charpy properties. This effect was significantly smaller than the effect on the JRQ material. The VB395 was slightly more sensitive than the Doel 3 material but the effect remained limited.

- The fracture toughness test results on D3H1 and JRQ showed an improvement of the fracture toughness (decrease of the T_0 temperature) after step cooling. This illustrates that the occurrence of partially intergranular fracture is not synonymous of embrittlement.
- SEM examination of the fracture surfaces of Charpy and fracture toughness specimens from the Doel 3 and Tihange 2 RPV Surveillance Programme showed that the fracture mode is essentially transgranular cleavage, despite traces of local intergranular fracture.

5.3.2 Large-Scale Tests

Fracture mechanics tests were performed at different temperatures by tensioning 25 mm diameter tensile type specimens with flakes or machined notches inclined at 20° with respect to the specimen axis.

The tests confirmed the load bearing capacity of the flaked and notched specimens.

The fracture modes of the different types of specimens were as expected and were well predicted by the simulations using the Extended Finite Element Method.

Requirement

The FANC asked to consider two additional Bel V requirements (Action 15b):

> *Bel V considers that it would have been a significant contribution to the demonstration to perform tensile testing of large-scale specimen(s) taken from the AREVA shell VB395 in the ligament between the flakes and provided with a notch made by electro-erosion and representative of a flake with a 20° tilt angle. Comparing the results of these tests with the results of the tests performed on specimens with tilted flakes would allow to discriminate between the effects of a flake configuration and the effects of a notch configuration on the fracture behaviour.*
>
> *Without putting into question this conclusion, Bel V reminds his reservations about the fracture process of the large scale tensile specimens tested at 20°C. These reservations would be withdrawn if tensile testing at a temperature of about 100°C of a specimen with 20° tilted flakes showed mostly ductile fracture.*

Approach

The following steps were taken to fulfil this requirement:

- Two VB395 specimens with real flakes, artificially tilted at 20°, were tested at 100°C (in the initial Safety Case similar specimens were tested at 20°C).
- Four tests were performed on 25 mm tensile VB395 specimens taken adjacent to the flaked area and provided with an electro-eroded notch at a 20° tilt angle. Two specimens were tested at 20° and two at 100°C.
- The tests performed on the two types of specimens were compared.
- Simulations were performed using the Extended Finite Element Method in linear-elastic and elasto-plastic conditions in order to predict the fracture mode and fracture load.

It should be pointed out that due to the presence of the inclined flake or notch, the test is actually a fracture mechanics test on a flawed component, not a traditional tensile test. As such, the fracture is governed by the rules of fracture mechanics, not by the tensile properties.

Results and Discussion

- Specimens with real flakes tested at 100°C show a typical ductile dimple fracture as confirmed by SEM examinations of the fracture surface. In similar tests performed earlier at 20°C some specimens had failed partly by cleavage rather than in a fully ductile manner. This is however not typical for flaked components, but it is generally observed for most RPV steels with sharp crack tips, tested well above the Master Curve transition temperature T0.
- Specimens with tilted electro-eroded notches:
  - At 100°C, those specimens show the same type of dimple fracture as the specimens with real flakes.
  - At 20°C, the tested specimens show a fully ductile fracture mode without cleavage initiation. The difference with respect to the specimens with real flakes tested at 20°C is due to the presence of a rounded notch (radius 0.15 mm) instead of a sharp crack tip in the case of real flakes. The load-displacement curve is nevertheless comparable to those of the specimens with flakes.

Conclusions

- The tests confirm the load bearing capacity of specimens with real tilted hydrogen flakes or machined tilted notches.
- The fracture mode of all tested specimens was well predicted by the Extended Finite Element Method analyses.

5.3.3 Assessment of the Impact of H Uptake from the primary side

Based on an extensive study, it can be concluded that the hydrogen uptake during operation is too low to induce propagation of the existing hydrogen flakes in the D3T2 RPVs by a hydrogen-related mechanism.

As described in the 2012 Safety Cases and their addenda (Action 10), the potential influence of hydrogen uptake from the primary side on the propagation of the hydrogen flakes has been extensively investigated based on literature research, calculations, finite element modelling simulations and hydrogen measurements, as well as consultation with international experts. The assessment has been re-validated in 2015, with an update of the literature review, with newly published results.

The assessment approach consisted of the following steps:

- Identification of the possible hydrogen sources from the primary side (corrosion, water treatment, radiolysis).
- Quantification of the hydrogen sources (the principal source is the primary H_2 water treatment; the total amount is very low).
- Calculation of hydrogen accumulation and pressure evolution in the flakes during normal operation and cooldown transients using finite element and analytical modelling.
- Evaluation of the risk of propagation due to hydrogen-related mechanisms (hydrogen-induced cracking and blistering) based on the calculated hydrogen content and pressure in the flakes.

As the hydrogen content and pressure in the flakes is too low, no primary side hydrogen impact is expected on the material properties and no hydrogen-related propagation mechanism is possible.

The approach and calculation hypotheses have been validated by measurements of residual H content in flakes (showing no significant H content), through literature review and advice from international experts.

The absence of H-induced flake propagation is also confirmed by the absence of evolution of the flakes after one complete cycle and shutdown.

5.4 Assessment of Atypical Embrittlement of VB395

Unexpected embrittlement results obtained on VB395 material triggered the implementation of a comprehensive root cause analysis approach. It included a literature study and a comprehensive programme of additional material investigations. A panel of international experts participated actively in the whole process.

The analysis concludes that all hydrogen-related mechanisms may be excluded as root cause, showing that the hydrogen flakes are not responsible for the atypical embrittlement of VB395. This conclusion is in line with the results on the flaked KS 02 material, which behaves as expected under irradiation.

Two possible mechanisms at the basis of the atypical embrittlement of VB395 have been identified. These mechanisms might be linked to the specific manufacturing history of the rejected VB395 shell (different from the D3T2 RPV forgings in many aspects).

Consequently, the D3T2 RPV forgings are not expected to show an atypical embrittlement under irradiation such as observed on VB395.

Requirement

Following the unexpected embrittlement results obtained on the first set of irradiated VB395 specimens (Action 11), additional tests were performed under different environmental conditions and including additional reference materials. These tests allowed to exclude any testing anomaly and confirmed the atypical embrittlement of VB395. As a consequence, a systematic root cause analysis approach was set up aiming at clarifying the unexpected behaviour of VB395.

This chapter addresses the implemented comprehensive root cause analysis approach. As such, it also covers Action 10b regarding the residual hydrogen content in flaked material. This item is closely linked to the root cause analysis and was formulated as follows by the FANC:

> *The licensee shall perform additional measurements of the current residual hydrogen content in specimens with hydrogen flakes, in order to confirm the results of the limited number of tests achieved so far. For example, the licensee has estimated an upper bound on the amount of residual hydrogen that might still be present in the flaws. The licensee should demonstrate that the chosen material properties are still valid, even if the upper bound quantity of hydrogen would still be present in critical flaws.*

Approach

The implemented approach is double:

- A mechanistic approach aiming at identifying the microstructural mechanisms at the basis of the atypical embrittlement of VB395. All possible embrittlement mechanisms were listed, a programme for additional material investigations was set-up (specific heat treatments, mechanical tests, chemical analyses, fractography, metallographic examinations, etc.). Based on literature data, test results and experts' opinions, each mechanism was evaluated and classified according to its plausibility: excluded, unlikely, possible or likely.
- A manufacturing history based approach looking for the possible relationship between the specific manufacturing history of the rejected VB395 shell and its mechanical behaviour under irradiation. Therefore, the specific aspects of the manufacturing history of VB395 as compared to the D3T2 RPVs were identified, evaluated and classified according to the same plausibility scale.

At the end, the combination of the findings of both approaches aims to identify the remaining possible mechanisms at the origin of the atypical VB395 embrittlement and to determine whether they can affect the D3T2 RPV forgings.

Results of the Mechanistic Approach

All considered mechanisms have been qualified as excluded, unlikely or possible. The results are the following (Figure 5.22):

♦ Most of the mechanisms are excluded

H-induced embrittlement

Such mechanisms rely on diffusion of residual hydrogen present in the RPV material. As shown by the investigations performed under Action 10b, only a very low amount of hydrogen is measured, and most of it is trapped at high-energy traps. Hence, all H-induced mechanisms can be excluded.

Irradiation induced precipitates

- Cu-enriched precipitates and Mn-Ni-Si nanoscale clusters are too small to initiate cleavage and are associated with embrittlement that goes with hardening. This mechanism cannot be responsible for the observed embrittlement that is not proportional to the observed hardening.
- Scanning Electron Microscope (SEM) and Transmission Electron Microscope (TEM) investigations have not revealed any large precipitates (other than expected carbides) that could initiate cleavage fracture.

Irradiation induced voids or bubbles

- Positron Annihilation Spectroscopy (PAS) examinations on VB395 material yields similar results as for other RPV materials. PAS results are in line with classical hardening embrittlement, which suggests that the atypical embrittlement is not associated with irradiation induced vacancy-type defects.
- Bubbles of helium may be generated only at much higher fluence values.

Localised hardening due to ferrite or upper bainite phases

Metallographic analysis shows that VB395 has similar amounts of ferrite and upper bainite as the D3H1 nozzle cut-out that behaves as expected under irradiation. Localised hardening embrittlement resulting in a decrease of overall toughness without increase of overall hardness is therefore excluded.

Unstable matrix defects (UMD)

UMDs could appear during the accelerated irradiation at rather high flux in BR2, and embrittle the material. However, applying a thermal treatment that is known to anneal UMDs did not result in an improvement of the mechanical properties of the VB395 material, which means that this mechanism can be excluded.

♦ Some mechanisms are considered as unlikely

Unlikely means that they have a low probability of being the main mechanism, but that there is no hard evidence to exclude they played some role.

Segregation of impurities to primary austenite grain and lath boundaries

Although thermal treatment test results could indicate some susceptibility of VB395 to segregation of impurities such as P, potentially associated with the atypical embrittlement, the P-content is low and the total intergranular fracture remains low after irradiation.

Coarsening of carbides

This has never been observed at irradiation temperatures lower than 400°C and has neither been observed by the performed TEM analyses. Nevertheless, the number of TEM investigations is not high enough to totally exclude the mechanism.

Loss of strength of segregation network due to relaxation of internal stresses

Although VB395 has a specific segregation network, an annealing treatment which is not supposed to re-introduce internal stresses, induces a quasi-complete recovery of the atypical embrittlement.

♦ Two mechanisms remain considered as possible

Possible means that there is no dominant evidence to demonstrate the occurrence of the mechanism. The mechanism could contribute to the atypical embrittlement, but might not be the only responsible mechanism.

Segregation of impurities to carbide or precipitate interface with matrix

Thermal treatment test results indicate some potential susceptibility of VB395 to segregation of impurities such as P, potentially associated with the atypical embrittlement. However, the P-content is low and hence this mechanism cannot be considered as a single mechanism.

Loss of strength of segregation network due to atypical embrittlement of martensite

A strongly marked segregation network containing tempered martensite is present in VB395, whereas this network is much less visible and contains much less tempered martensite in D3T2. Literature shows that this type of microstructure is particularly sensitive to irradiation embrittlement due to enhanced diffusion of P in martensite. As shown above, VB395 could be susceptible to segregation of impurities.

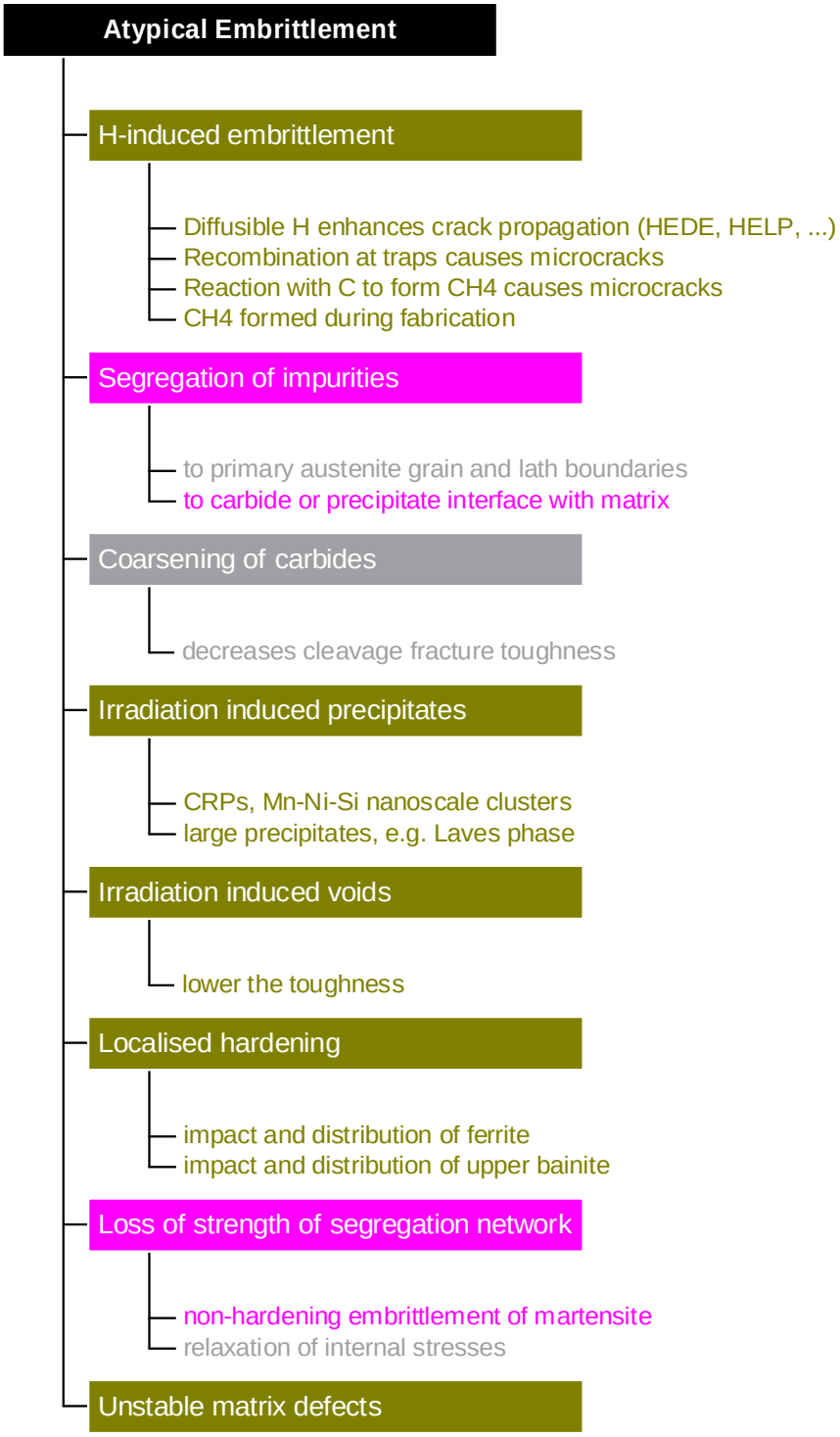

Figure 5.22: List of potential VB395 atypical embrittlement mechanisms after plausibility analysis.
(Green = excluded, Grey = unlikely, Pink = possible)

Results of the Manufacturing History Based Approach

Figure 5.23 shows the classification of the specific aspects of the manufacturing history of VB395 according to their plausibility. Possible root causes were identified in three domains: chemical composition, casting technique and thermal treatment. These causes can be linked with the possible mechanisms identified in the mechanistic approach:

- The higher amount of Cr of VB395, caused by contamination during the casting process, could have an influence on the P segregation and formation of carbides, as well as on the hardenability of the steel (contributing to a higher amount of tempered martensite). This is directly linked to both remaining possible mechanisms.
- The different casting procedure of VB395 can have an influence on the macro- and micro-segregations and the presence of a micro-segregation network. This is directly linked to the second remaining possible mechanism (loss of strength of segregation network).
- The deviating thermal treatments of VB395 can have an influence on the microstructure of the component (proportion of martensite, bainite, ferrite as well as formation, composition and coalescence of carbides). This is directly linked to both remaining possible mechanisms.

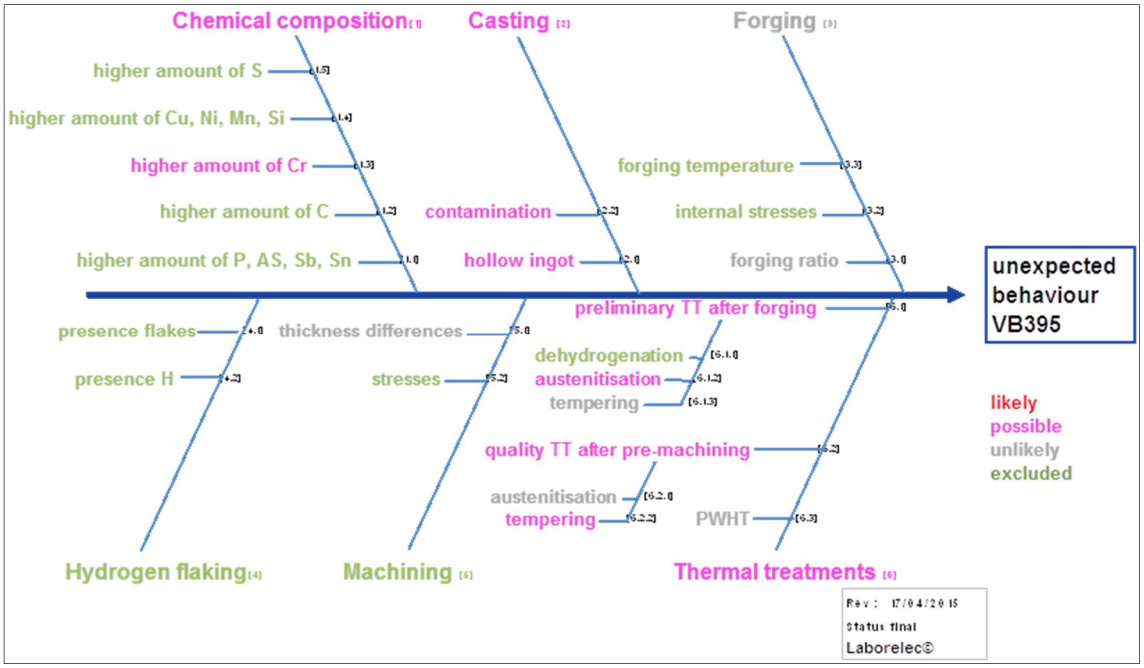

Figure 5.23: Fishbone diagram with colour-coded root causes.

Conclusion

- The root cause analysis of the atypical VB395 embrittlement concludes that several mechanisms can be excluded. In particular, hydrogen flaking or any other hydrogen related mechanism can be excluded as the cause of the unexpected behaviour. This conclusion is also further supported by the results on the German KS 02 material, which shows an important amount of hydrogen flakes and is not affected by atypical embrittlement under irradiation.
- No likely mechanisms responsible for atypical embrittlement were identified. However, two mechanisms are considered as possible: segregation of impurities to carbide or precipitate interface with matrix, and loss of strength of the segregation network due to atypical embrittlement of martensite.
- Both mechanisms might be linked to specific aspects of the manufacturing history of the rejected VB395 shell that were evaluated as being possible root causes. These aspects are related to chemical composition, casting technique and thermal treatment.
- Since the larger than predicted shift in transition temperature after irradiation of VB395 is not linked with the hydrogen flaking and since none of the above mentioned manufacturing specificities are reported for the D3T2 RPVs, it is expected the D3T2 RPV shells do not suffer from the atypical embrittlement observed on VB395.

5.5 Material Properties Considered in the SIA

Although it is very unlikely that the D3T2 RPV forgings would be more sensitive to irradiation because of the presence of hydrogen flakes, the SIA is based on the assumption that the D3T2 RPVs have an additional sensitivity to irradiation embrittlement of the same magnitude as the VB395 material. This atypical embrittlement of the VB395 is superposed in a conservative way on the commonly used RSE-M trend curve for the D3T2 RPVs, considering a conservative envelope of the macro-segregation chemical composition.

5.5.1 2012 Safety Case and Addendum

The SIA of the Tihange 2 RPV included in the 2012 Safety Case was performed on the basis of the RT_{NDT} versus fluence trend curve given in Figure 5.24. This trend curve was constructed starting from the French FIS embrittlement trend curve evaluated for the D3T2 core shell chemical composition, with an additional shift of 50°C to take into account the effects of orientation, segregation and irradiation sensitivity of the segregated zone.

$$RT_{NDT} = RT_{NDT,init} + \Delta RT_{NDT,FIS} + 50°C$$

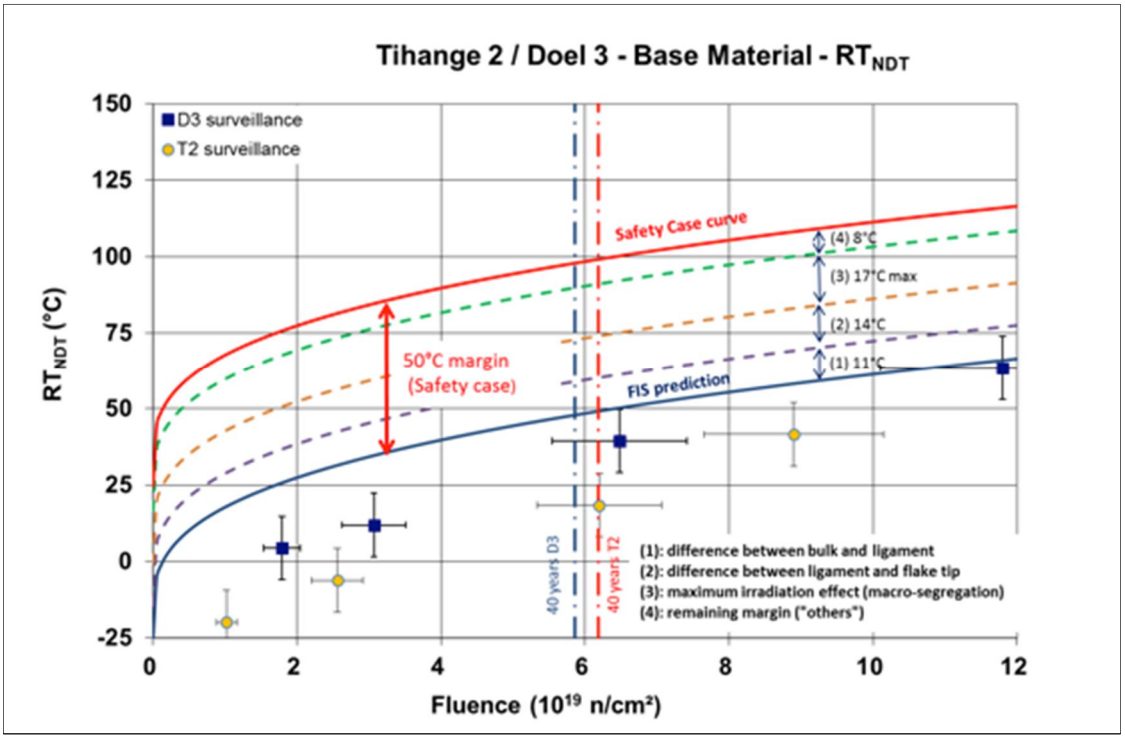

Figure 5.24: Trend curve RT_{NDT} as a function of fluence considered in 2012 Safety Case.

5.5.2 2015 Safety Case

The first mechanical tests performed on VB395 specimens under irradiated conditions indicated that the 2012 Safety Case trend curve was not enveloping the behaviour of VB395 under irradiation at high fluence values. This observation initiated the comprehensive test programme described under 5.2. On the basis of those test results modified trend curves were built.

Embrittlement trend curves

These curves were constructed as follows (Figure 5.25):

$$RT_{NDT} = RT_{NDT,init} + \Delta RT_{NDT,init,segr} + \Delta RT_{NDT,RSE\text{-}M} + \Delta RT_{NDT,VB395} + M$$

- $RT_{NDT,init}$ corresponds to the initial RT_{NDT} of the core shells as determined by Rotterdamsche Droogdok Maatschappij
- $\Delta RT_{NDT,init,segr}$ covers the potential lower fracture toughness of the material in the macro-segregated areas containing hydrogen flakes, as requested by the FANC. On the basis of material representative of the D3T2 core shells, this effect was estimated as 10°C. It should be pointed out that this additional shift is generally not considered in the international practice which addresses the effect of segregations through enrichment factors in the embrittlement trend curves (see below).
- $\Delta RT_{NDT,RSE\text{-}M}$ corresponds to the shift in RT_{NDT} as a function of fluence, as given by the French RSE-M (Ed.2010) embrittlement trend curve evaluated for the D3T2 core shell chemical composition (thereby considering enrichment factors to account for the composition of macro-segregations)
- $\Delta RT_{NDT,VB395}$ is an additional fluence dependent shift as observed on the VB395 material. It is taken as the difference between the observed atypical embrittlement of the material between hydrogen flakes and the embrittlement that can be expected for this material on the basis of the RSE-M trend curve
- M is a margin based on the uncertainties of the different terms: M equals 2 times the quadratic combination of the uncertainty on the effect of the macro-segregation (evaluated as 5°C) and the standard deviation of the RSE-M formula (9.3°C)

It should be pointed out that these trend curves are very conservative because they are based on the assumption that the D3T2 RPV core shells have an additional sensitivity to irradiation embrittlement of the same magnitude as the VB395 material, which is very unlikely taking into account the results of the test programme and the assessment of the atypical embrittlement of VB395.

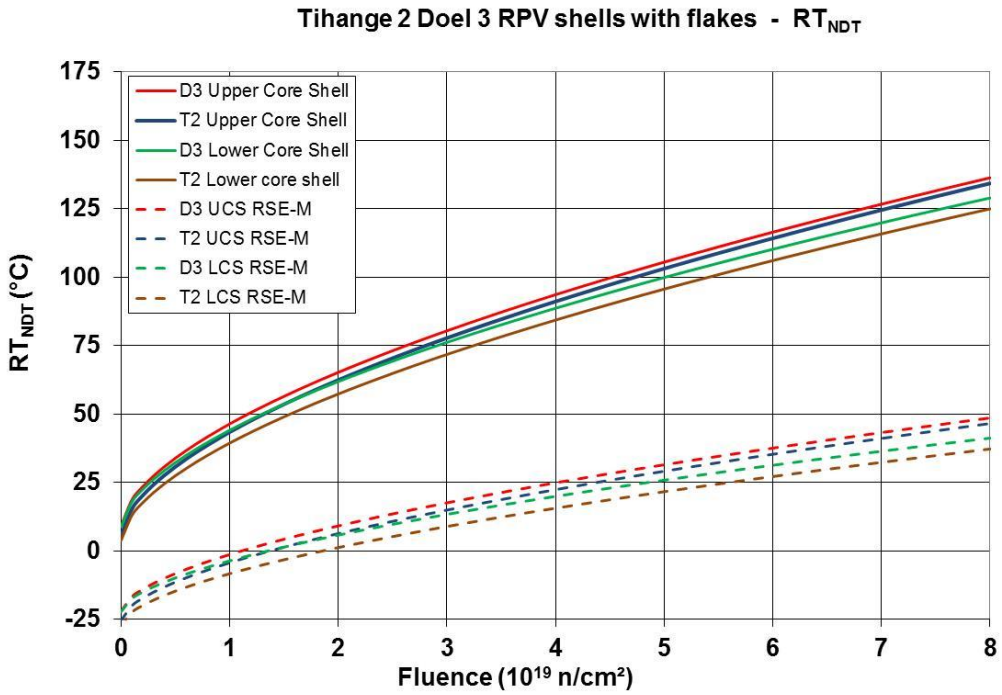

Figure 5.25: RT_{NDT} trend curves for the D3T2 core shells.

Embrittlement trend curves used in the SIA

The SIA of the D3T2 RPV core shells has actually been performed using RT_{NDT} trend curves that are slightly more conservative than the curves described above.

As an example of the curves used in the SIA, the total ΔRT_{NDT} (including the margin M) considered for the D3T2 upper core shells is given by the full blue and red curves of Figure 5.26. In this figure, a comparison is included with the trend curve considered in the 2012 Safety Case and with the results from the D3T2 RPV Surveillance Programme.

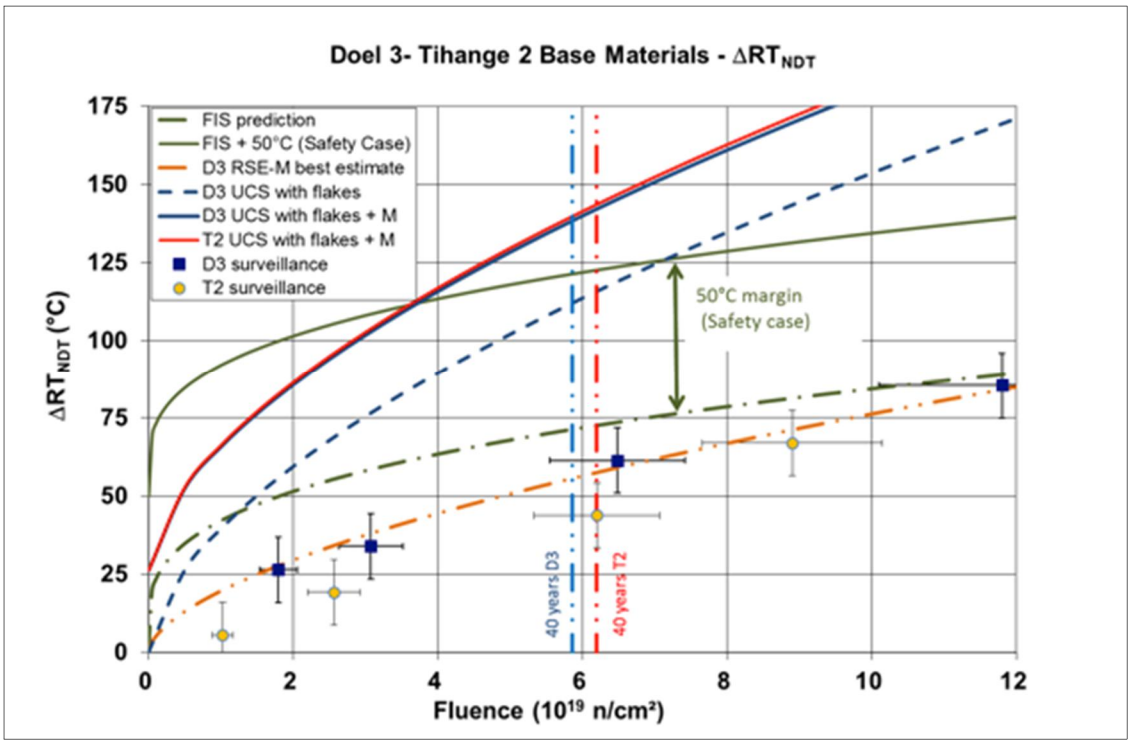

Figure 5.26: ΔRT_{NDT} for flaked D3T2 upper core shells as a function of fluence.

The final RT_{NDT} values to be considered for the four D3T2 core shells as a function of fluence are given in Figure 5.27. This figure also shows the expected maximum fluence values in the RPVs after 40 years of operation.

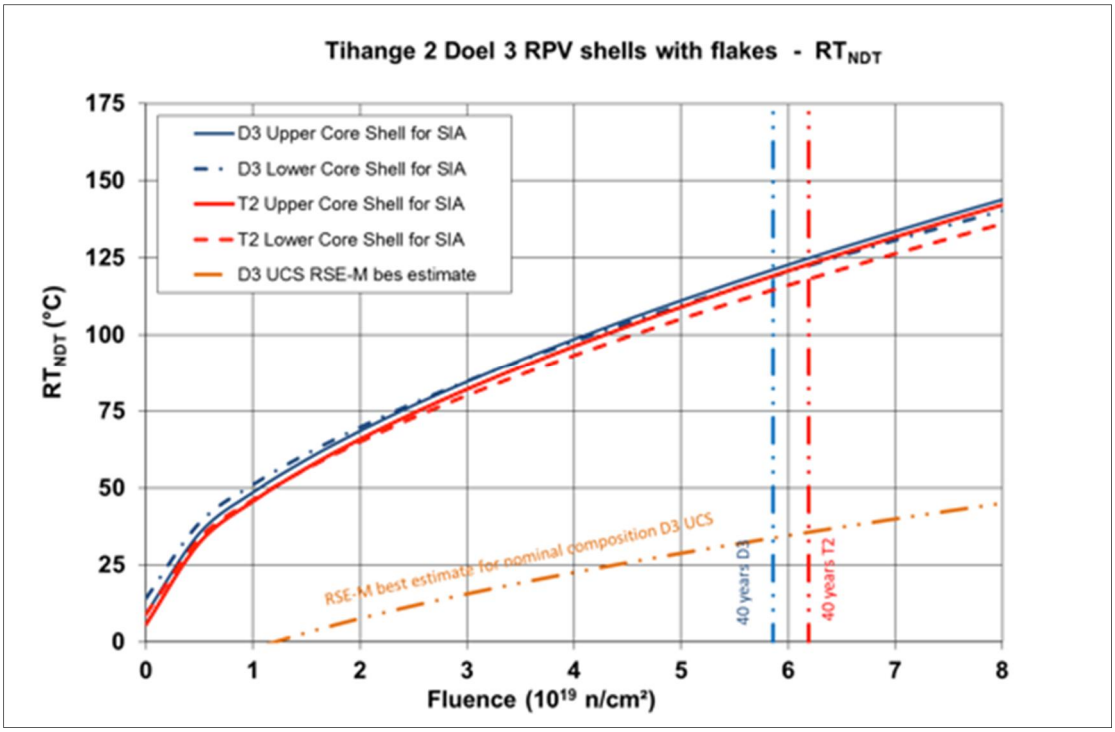

Figure 5.27: RT_{NDT} trend curves for the D3T2 core shells used in the SIA.

In addition, several alternative ways of establishing trend curves for the D3T2 core shells have been addressed in detail, such as best estimate RT_{NDT} approaches (based on Charpy shifts) and best estimate RT_{T0} approaches (based on T_0 shifts) considering different types of fits of experimental results (power law fit with 0.59 exponent, linear fit). However, it was shown that the trend curves applied in the SIA are much more conservative than all those alternatives.

6 Structural Integrity Assessment

The Structural Integrity Assessment (SIA) of the Tihange 2 RPV was performed for all relevant loading conditions according to the applicable rules of the ASME Boiler & Pressure Vessel code.

The SIA covers all indications that have been classified as hydrogen flakes as well as the indications that were classified as clad interface imperfections but that are conservatively considered as hydrogen flakes.

The Flaw Acceptability Assessment demonstrated that more than 99.70% of the flaws meet the screening criterion $2a < 0.5\ 2a_{acc}$. The remaining 0.30% meet the acceptance criterion $2a < 2a_{acc}$ by a considerable margin as demonstrated through refined analysis.

The refined analyses clearly highlighted the very low level of the crack driving forces K_{MAX} of the quasi-laminar hydrogen flakes: K_{MAX} for all flaw configurations is well below the fracture toughness lower shelf $K_{IR,lower\ shelf}$ demonstrating that the quasi-laminar hydrogen flakes are acceptable with respect to the structural integrity of the Tihange 2 RPV.

The Fatigue Crack Growth analysis showed that the maximum potential growth of the flaws in the forgings over the entire service lifetime of the RPV, assessed by a conservative methodology, is limited to 1.66% of their size. This confirms the results of the 2012 Safety Case.

The Primary Stress Re-evaluation made clear that the collapse pressure is more than 1.5 times the design pressure, confirming the criterion is met.

Context

The purpose of the SIA is to verify that the structural integrity of the RPV is maintained under all operating and accidental conditions given the presence of detected flaws. The SIA was performed for all relevant loading conditions according to the applicable rules of the ASME Boiler & Pressure Vessel code (Figure 6.1). As such, it includes:

- Assessment of the absence of crack initiation for all individual flaws with adequate safety margins
- Assessment of the stability of the flaws through fatigue crack growth evaluation
- Satisfaction of the primary stress intensity acceptance criteria

The assessment methodologies use state-of-the-art modelling and calculation techniques. They were subjected to a thorough external review and validated on the basis of experimental work. More particularly, large-scale tests were performed on samples containing flakes. These tests demonstrated that the ductility of the material in the ligament between the flakes is similar to the ductility of the material free of flakes and that the load bearing capacity is not significantly affected.

Input data

The SIA is based on the following input data:

- The RPV geometry
- The UT measurements i.e. the updated flake cartography
- The transient (p, T) loads from the design transient file
- The material properties

In the sequel of this chapter, the terms flake cartography or flaw covers both the indications that were classified as hydrogen flakes as well as the indications that were classified as clad interface imperfections but that are conservatively considered as hydrogen flakes in the Structural Integrity Analysis (Chapter 4.2.3).

Among the material properties, the RT_{NDT} curve is obtained from the conservative transposition of the properties obtained on shell VB395 (see Chapter 5.5 Material Properties considered in the SIA). The RT_{NDT} is only needed for the verification of the ASME XI acceptability criteria. The assessment of the crack driving forces is independent of the RT_{NDT} value.

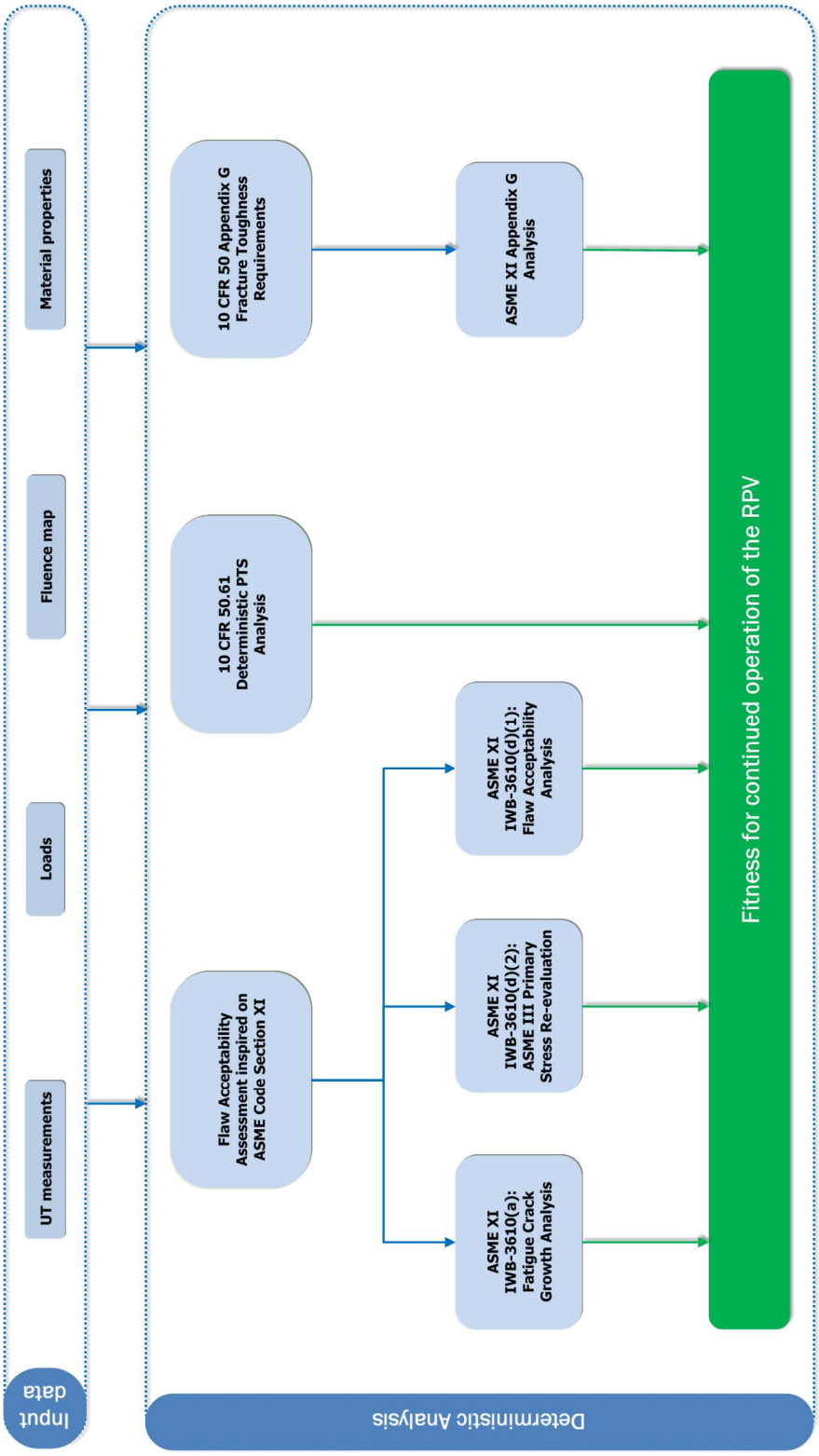

Figure 6.1: Roadmap for the SIA.

6.1 ASME XI – Flaw Acceptability Assessment

The flaw configurations – most of them – meeting the screening criterion $2a < 0.5\ 2a_{acc}$ are considered harmless. The few remaining flaw configurations that did not meet the screening criterion were subjected to a more refined analysis. This refined analysis demonstrated that all of these flaws meet the acceptance criterion with a considerable safety margin: maximum $2a/2a_{acc}$ ratio of 0.54 in the Tihange 2 RPV.

Requirement

A Flaw Acceptability Assessment was performed in accordance with 'ASME Section XI (1992) – Rules for In-service Inspection of Nuclear Power Plant Components'. The assessment was conducted on all flaws using the dimensional data gathered through ultrasound measurements and the loads from the design transients.

Approach

The general flowchart for performing this assessment is given below (Figure 6.2). Every step is then explained in greater detail.

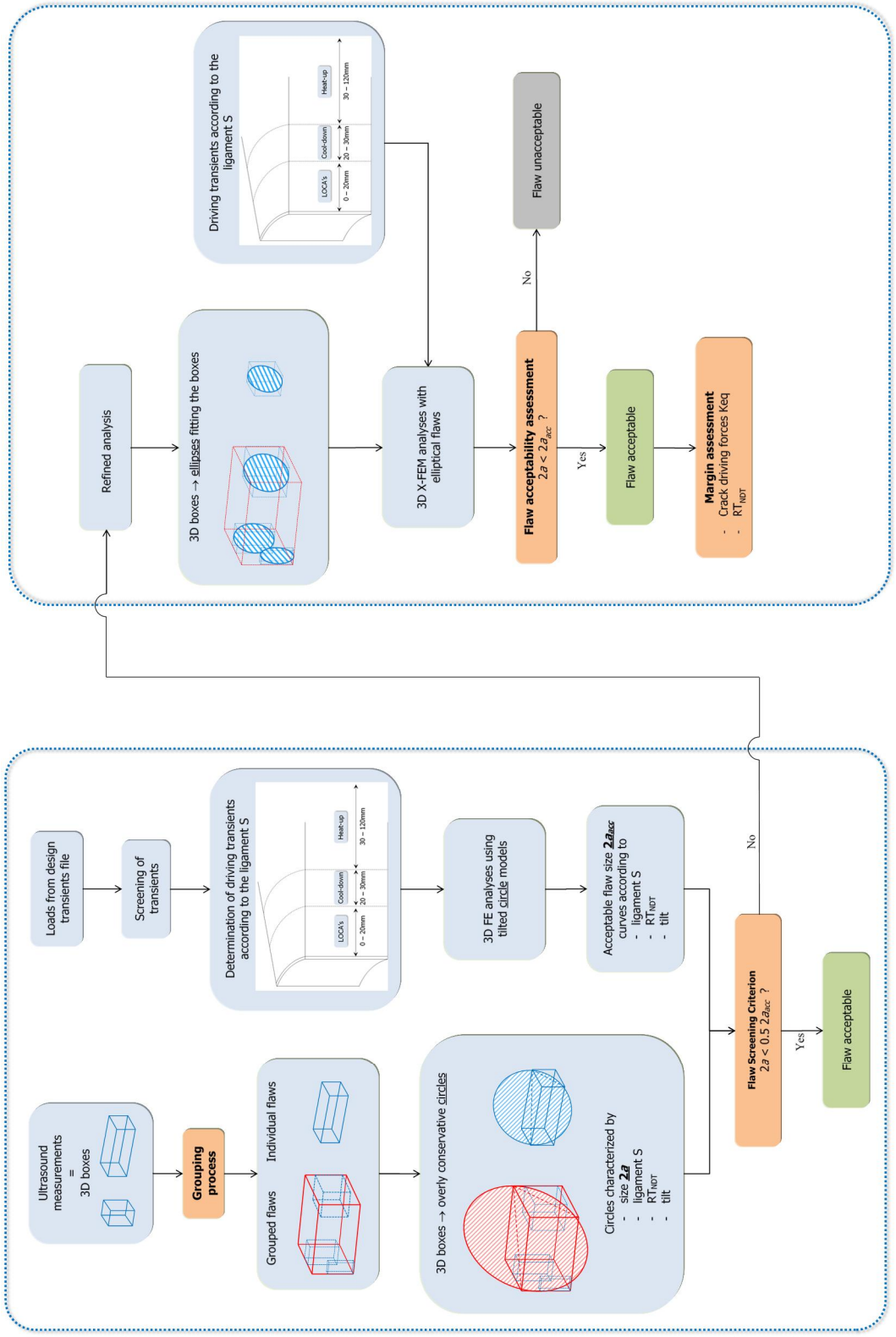

Figure 6.2: Flowchart of the Flaw Acceptability Assessment and Refined Analysis (ASME XI).

6.1.1 Flaw modelling

Each detected flaw was measured by the UT inspection equipment and characterized in terms of its position in the vessel wall and its maximum dimensions in three orthogonal directions. In doing so, each individual flaw is characterized by the 3D box enveloping the flaw (Figure 6.3).

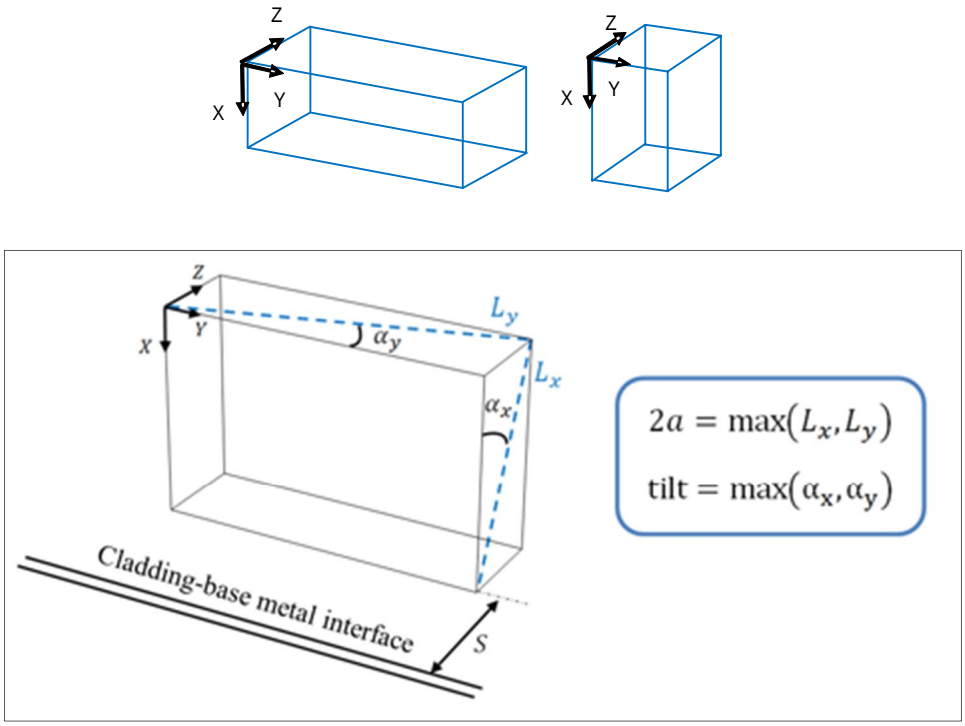

Figure 6.3: A 3D box represents each flaw.

The largest possible flaw in each corresponding 3D box is elliptical (dashed line in Figure 6.4). However, the flaw that was actually considered in the acceptability assessment is the circle (solid line in Figure 6.4) that envelops the ellipse. As depicted in Figure 6.3, the diameter 2a of this circle is taken as the largest diagonal of the box faces L_x and L_y. The tilt of the circle is taken as the highest inclination of the diagonals α_x and α_y and is limited to 20° (this value is a conservative envelope of the maximum flake inclination as shown in Chapter 3 Characterization of Hydrogen Flakes).

The circle representing an individual flaw is characterized by:

- Flaw size (2a) (diameter)
- Ligament S (shortest distance to the cladding-base metal interface, in the radial direction)
- Tilt (inclination with respect to the vessel wall surface)

The local RT_{NDT} is calculated at the flaw position, using the conservative transposition of the properties obtained on shell VB395, as detailed in Chapter 5.5 Material Properties considered in the SIA.

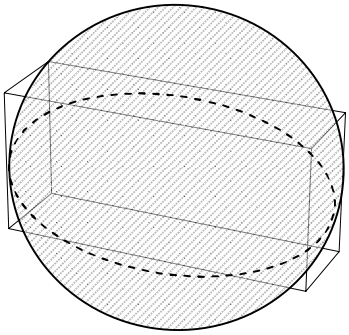

Figure 6.4: The acceptability assessment used the circle that envelops the largest possible elliptical flaw.

6.1.2 Flaw grouping

The modelling mentioned above is performed for all individual flaws. For closely spaced flaws, a specific grouping rule was developed, using 3D modelling and supported by experimental results. The grouping rule was applied to determine whether flaws should be grouped into one single combined flaw or not. This basic principle was applied to all possible pairs of flaws. The grouping rule is illustrated in the picture below for a case in which three flaws are grouped (Figure 6.5).

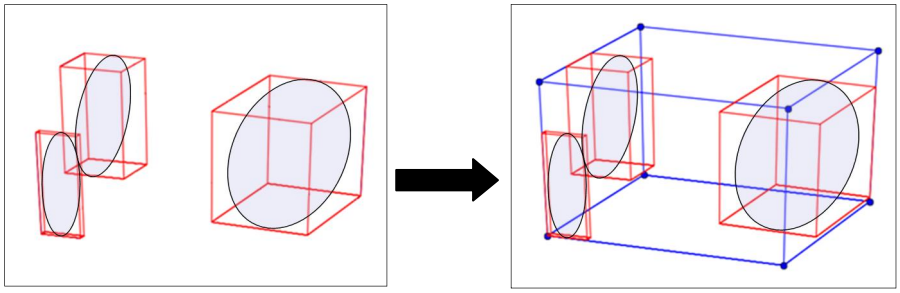

Figure 6.5: Illustration of flaw grouping.

The corresponding grouped circular flaw is defined in exactly the same manner as were the individual flaws, with the exception of the limitation of the tilt value to 20°: no tilt limitation is considered for circular grouped flaws. The starting point is the blue 3D box that envelops the red individual boxes. As a result, the flaw size considered in the assessment is much larger than the size of each of the individual flaws in the red boxes (Figure 6.6).

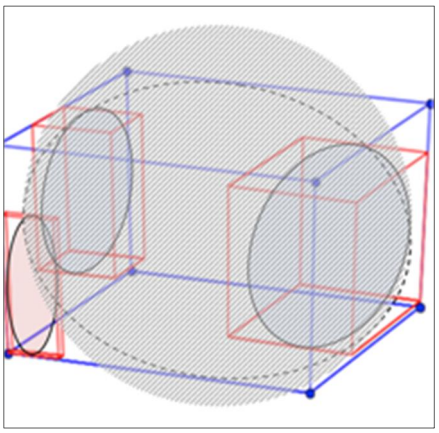

Figure 6.6: The resulting flaw to be assessed in the event of a flaw grouping.

6.1.3 Pressure and temperature loads

The transients from the Primary System design file were screened in order to determine the driving transients, i.e. the most penalizing transients with respect to brittle fracture, as a function of the position in the wall (ligament S), for the considered case of quasi-laminar flaws located in the core of the RPV shell. This screening identified the LOCAs (Loss Of Coolant Accidents) as being the driving transient for the first 20 mm from the cladding (inner side of the vessel wall), while the cool-down transients dominated in the next 10 mm and the heat-up transients in the deeper part of the wall (Figure 6.7).

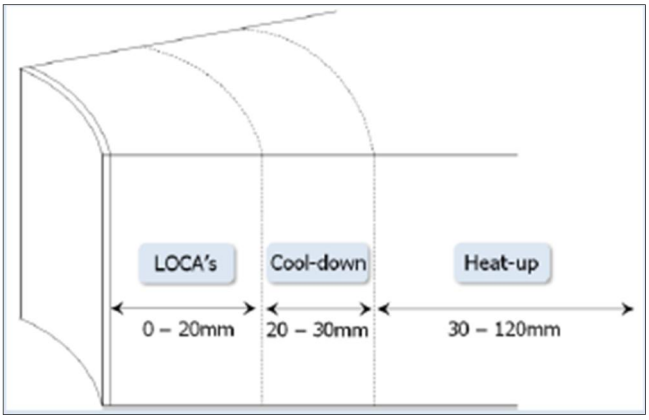

Figure 6.7: Determination of driving transients according to the ligament S.

6.1.4 Acceptable flaw size curves

The acceptable flaw size $2a_{acc}$ was determined using 3D finite element analyses based on:

- Tilted circular flaw models
- The above mentioned driving transients
- The ASME XI Code acceptance criterion $K(2a) < K_{IR}/SF$, taking into account:

For level A/B transients (Cool-down, Heat-up): $K_{IR} = K_{Ia}$; $SF = \sqrt{10}$
For level C/D transients (LOCAs): $K_{IR} = K_{IC}$; $SF = \sqrt{2}$

As a result, acceptable flaw size ($2a_{acc}$) curves were established according to flaw characterizing parameters:

- Ligament S
- RT_{NDT}
- Tilt

Fracture toughness

The fracture toughness represents the resistance of the material to crack initiation. This material property can be directly related to the solicitation of defects expressed in terms of stress intensity factor.
The ASME XI Code distinguishes between:
- K_{Ia} : crack arrest material toughness
- K_{IC} : crack initiation material toughness

Stress intensity factor

The stress intensity factor (K), or crack driving force, is a fracture mechanics concept used to characterize the stress field that exists near the tip of a crack and that is due to a remote stress field in the component.

For example, Figure 6.8 presents the acceptable flaw size curves as a function of the ligament S calculated for a 10° tilted flaw and for 6 RT_{NDT} values.

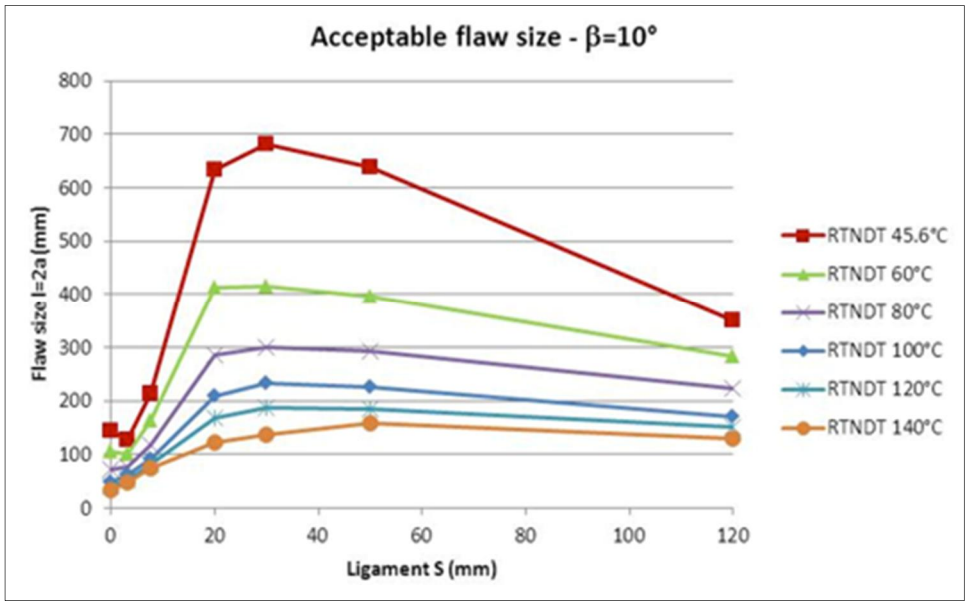

Figure 6.8: Acceptable flaw size curves for a 10° tilted flaw.

24 flaw size curves were calculated as a function of the ligament S, covering 6 RT_{NDT} values for 4 tilts (10°, 20°, 30° and 45°).

Therefore, the acceptable flaw size $2a_{acc}$ of a given flaw configuration characterized by its parameters (S, RT_{NDT} and tilt) can be calculated by interpolation using the 24 available acceptable flaw size curves.

6.1.5 Flaw Screening

Introducing the flaw characterizing parameters in the curves mentioned above, the acceptability of all flaw configurations (individual or group) was screened according to the criterion:

$$2a < 0.5\ 2a_{acc}$$

The flaw configurations meeting this screening criterion are considered harmless. As shown in Figure 6.9, most of the flaw configurations meet this screening criterion.

The few remaining flaw configurations that did not meet the screening criterion were subjected to a more refined analysis.

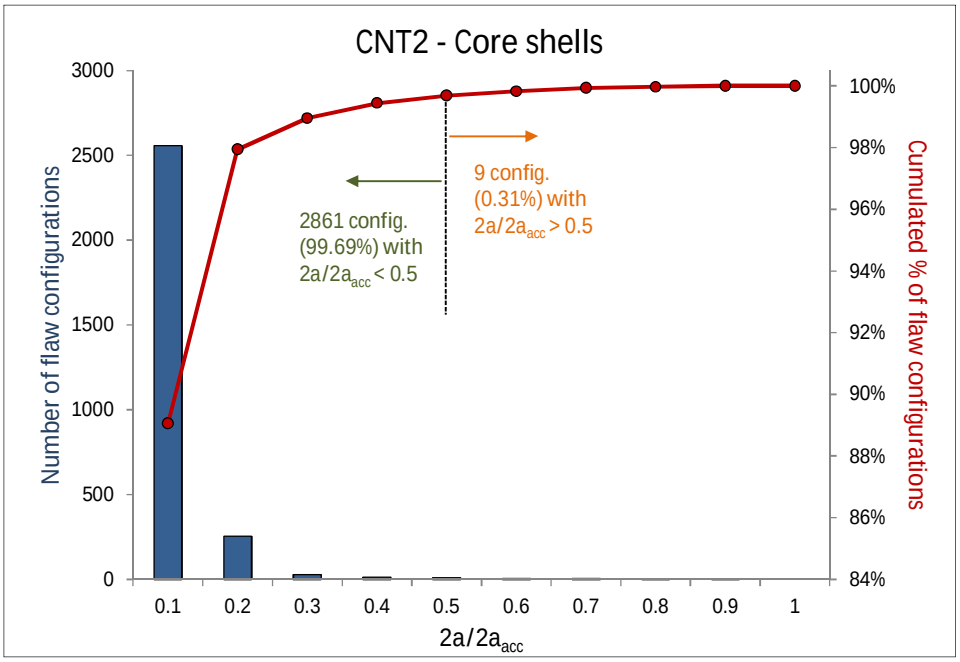

Figure 6.9: Flaw screening criterion applied to the core shells of Tihange 2-Histogram.

6.1.6 Refined Analysis

The refined analysis is similar to the flaw screening analysis in terms of input data: the UT boxes as well as the load transients are identical.

The two differences are the following:

- The flaw characterization is more realistic. Instead of considering flaws as tilted circles, flaws are modelled as ellipses fitting in the rectangular UT boxes. The ellipse has the largest size and tilts to remain included in the box delimited by the ultrasound measurements (Figure 6.10).
- The flaws belonging to a group are not replaced by a grouped flaw anymore. Each of them is modelled specifically in a multi-flaw model accounting for the potential flaw interactions.

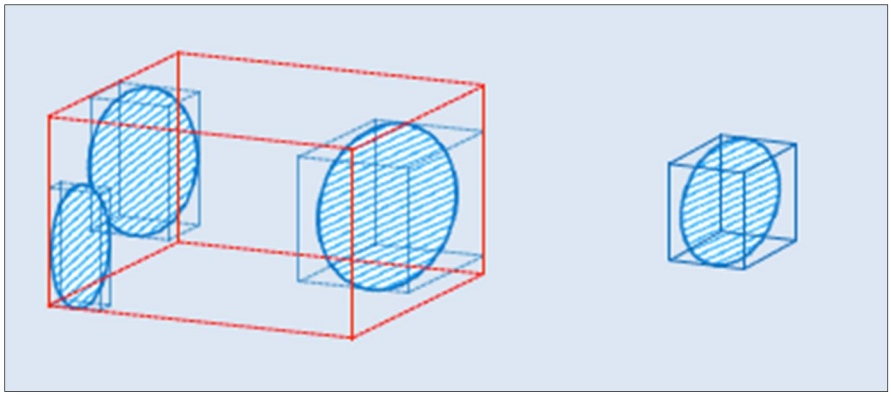

Figure 6.10: The ellipses fitting the 3D boxes.

These elliptical flaw models were then used in a 3D extended finite element fracture mechanics (XFEM) analysis, including the driving transient data (Figure 6.11).

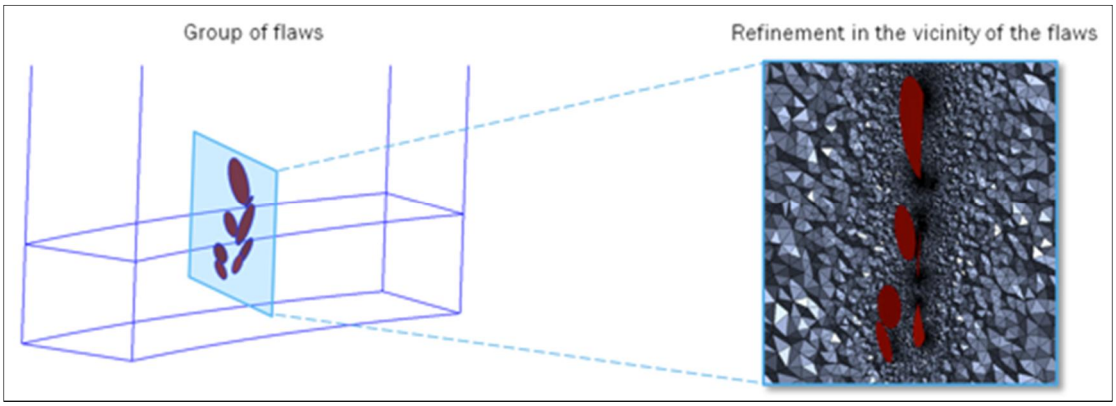

Figure 6.11: Example of the XFEM multi-flaw model.

Using the refined analysis results expressed in terms of K(2a) the flaw acceptability assessment criterion: $2a < 2a_{acc}$ was verified for each individual flaw as well as grouped flaws.

All of the flaws that were considered in the refined analysis (i.e. the few flaw configurations not satisfying the screening criterion) meet the acceptance criterion with a considerable safety margin: maximum $2a/2a_{acc}$ ratio of 0.54 in the Tihange 2 RPV (Figure 6.12).

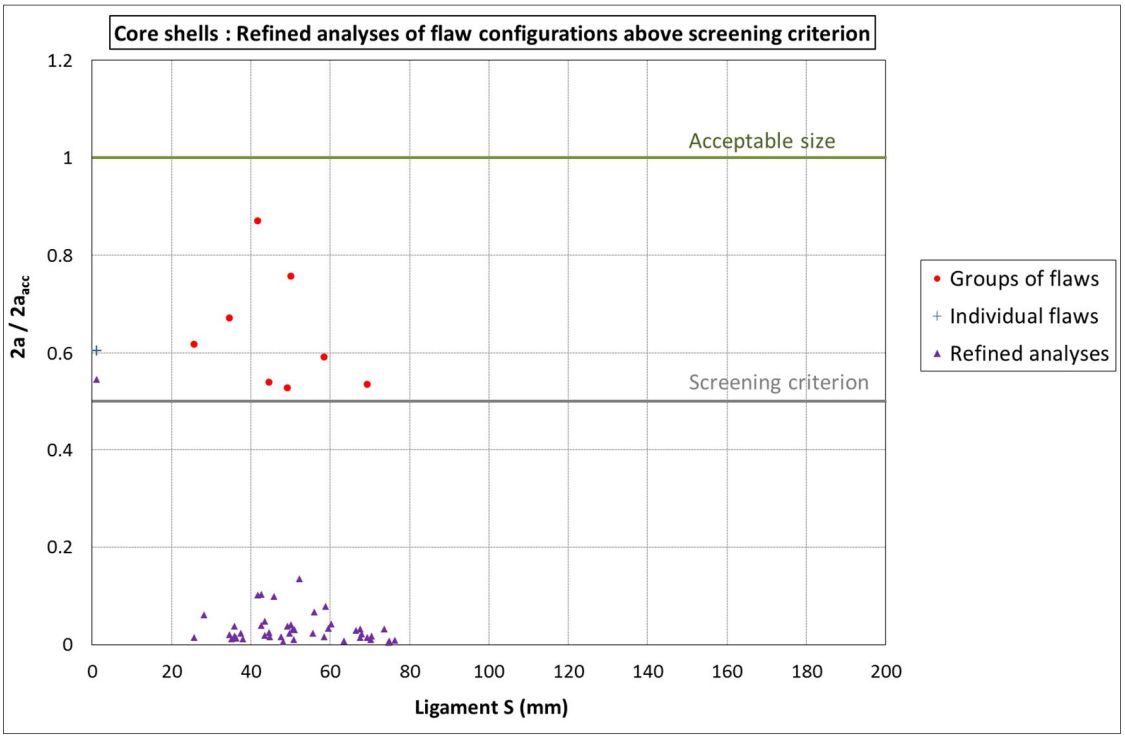

Figure 6.12: Comparison of core shell flaw configurations of Tihange 2 to acceptable size as a function of ligament after 3D refined analyses.

6.1.7 Crack driving forces

The results of the refined XFEM analyses made it possible to assess the severity of the crack driving forces K (value of the stress intensity factor at any point of the crack tip during the driving transient), as well as the margins to the applicable fracture toughness curve.

A screening was performed to select additional bounding flaw configurations in terms of crack driving force among individual flaws. The screening focused on flaw parameters leading to the maximisation of the crack driving forces (tilt, size, etc.).

The crack driving forces were compared to the fracture toughness lower shelf $K_{IR,lower\ shelf}$ and to the fracture toughness lower shelf including the margin $K_{IR,lower\ shelf}/SF$. The value of the lower shelf is defined by the fracture toughness curve of the ASME code.

When the crack driving force is lower than the lower shelf (with safety factor), the flaw acceptability is independent from the RT_{NDT} of the material.

Fracture toughness lower shelf

The fracture toughness K_{IR} is a function of temperature T and RT_{NDT}. For temperatures lower than RT_{NDT}, the K_{IR} curve according to T tends to a lower shelf:

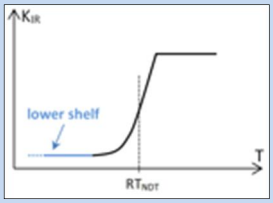

Therefore, when the crack driving force K of a flaw is lower than the toughness lower shelf, no crack initiation is expected to occur regardless of T and RT_{NDT} values.

When the crack driving force is higher than the lower shelf (with safety factor), the temperature dependence of the material toughness K_{Ia} or K_{IC} (noted K_{IR}) with safety factor SF is taken into account and illustrated in a K vs. T graph together with the crack driving force K. The margin in terms of RT_{NDT} is calculated by shifting the K_{IR}/SF curve to reach the K curve (Figure 6.13).

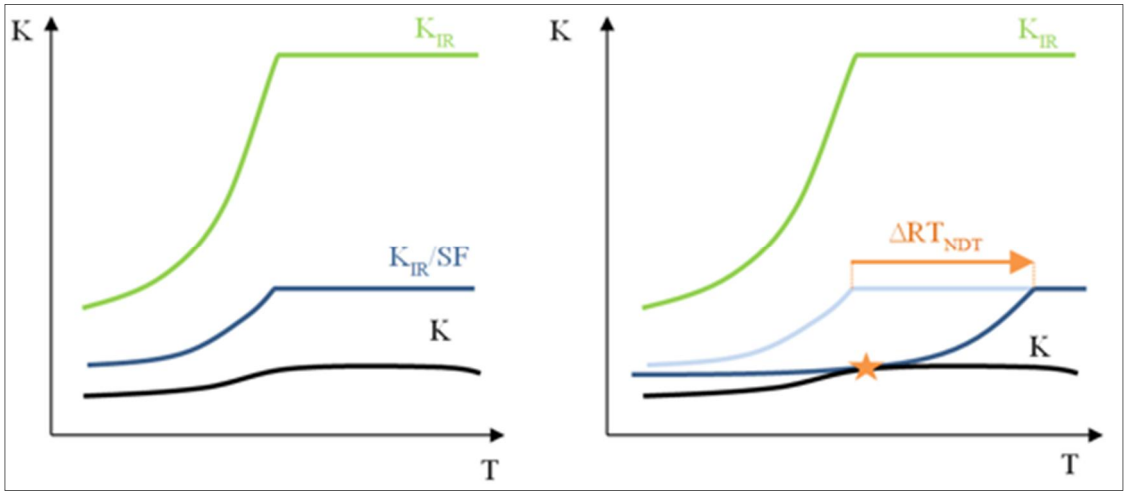

Figure 6.13: Example of determination of margin in terms of RT_{NDT}.

Figure 6.14 and 6.15 compare, for all the analysed flaws, the maximum value of the crack driving force K_{MAX} during the transients to $K_{IR,lower\ shelf}$ and to $K_{IR,lower\ shelf}/SF$.

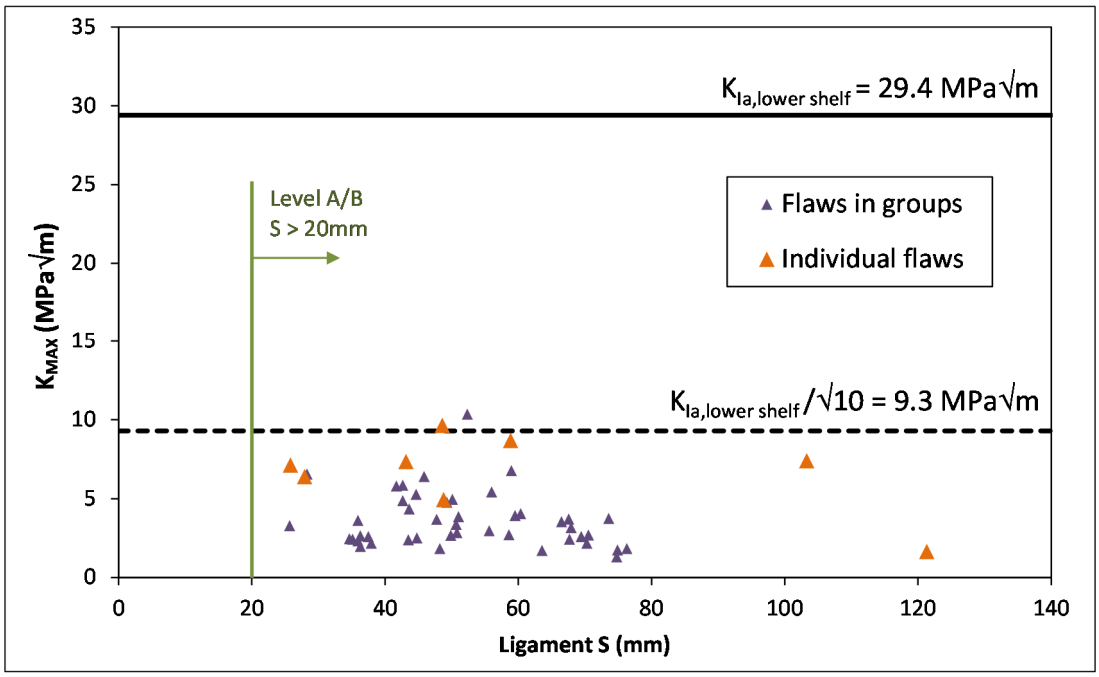

Figure 6.14: K_{MAX} values compared to lower shelf toughness for flaws far from the cladding-base metal interface (Tihange 2 RPV).

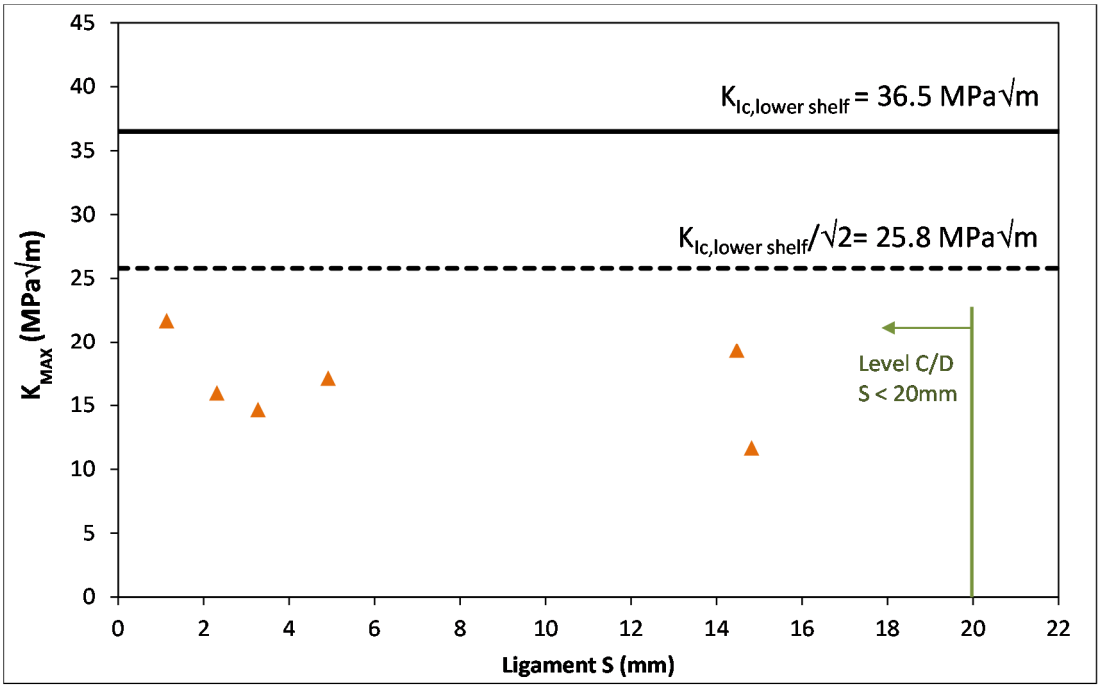

Figure 6.15: K_{MAX} values compared to lower shelf toughness for flaws close to the cladding-base metal interface (Tihange 2 RPV).

The vast majority of the flaws have a K_{MAX} value below the $K_{IR,lower\ shelf}$/SF which means that their acceptability is independent of the RT_{NDT}. For the Tihange 2 RPV, there are only two flaws far from the cladding for which K_{MAX} exceeds $K_{Ia,lower\ shelf}/\sqrt{10}$.

For these 2 configurations, the margin in terms of RT_{NDT} calculated considering the temperature dependence of K and K_{Ic}, is presented in Table 6.16. This RT_{NDT} margin is very large (110°C or more).

N°év	Group	S (mm)	K_{MAX} ($MPa\sqrt{m}$)	For transient	RT_{NDT} (°C)	RT_{NDT} margin (°C)
135	Indiv.	48.58	9.64	Cool-down	73.5	130
1817	GP0125	52.35	10.35	Cool-down	75.0	110

Table 6.16: Configurations above the lower shelf toughness, margin included (Tihange 2 RPV).

6.2 Fatigue Crack Growth Analysis

The fatigue crack growth analysis was updated using all of the reported indications from the qualified UT inspection that was performed during the 2014 outage. The calculated fatigue crack growth is limited, confirming that it is not a concern.

Requirement

As requested by ASME XI IWB-3610(a), fatigue crack growth is evaluated by the analytical procedures described in ASME XI Appendix A 'Analysis of Flaws', based on linear elastic fracture mechanics. The objective is to calculate the growth of the nearly laminar flaws until the end-of-service lifetime of the Tihange 2 RPV.

Approach

As requested by ASME XI IWB-3610(a), the Fatigue Crack Growth was evaluated by the analytical procedures described in ASME XI Appendix A 'Analysis of Flaws', based on linear elastic fracture mechanics. The objective was to assess the stability of the flakes, i.e. the possible growth of the quasi-laminar flaws until the end of service lifetime.

A conservative approach was applied for the fatigue crack growth assessment, in three steps:

1	The flaw configurations obtained after grouping were distributed in subcategories according to their tilt: • Tilt ≤ 10° • 10° < tilt ≤ 15° • 15° < tilt ≤ 20° • Tilt > 20°
2	Reference flaws were determined for each subcategory, in order to cover the maximum sizes of all flaws and groups of flaws with a minimum ligament. 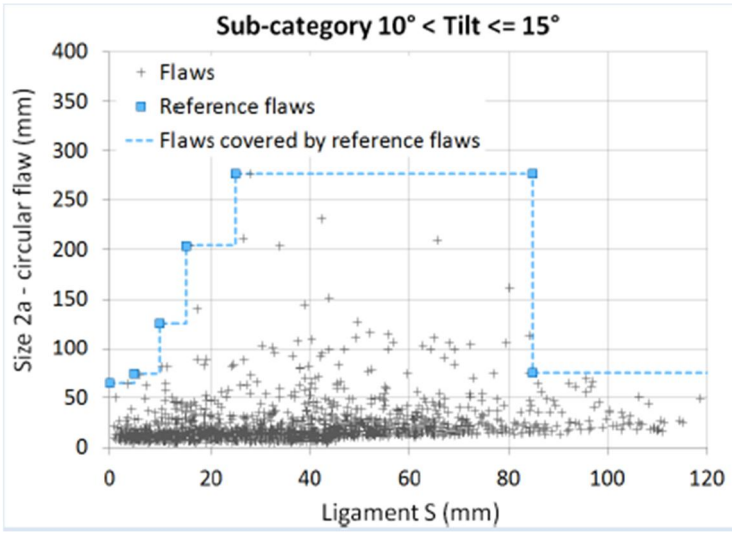

3	The reference flaws were then projected onto an axial plane. 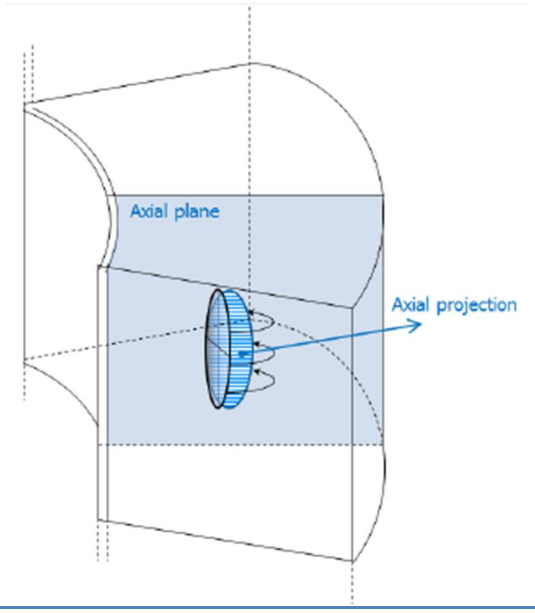

This approach resulted in:

- Calculations of the ΔK_I according to the ASME XI Appendix A deriving conservative solutions for elliptical flaws in plates based on the loads from the design transients file
- A fatigue crack growth rate curve from ASME XI Appendix A—the threshold $\Delta K_{I,th}$ is set to 0
- A fatigue crack growth calculation formula: $2a \rightarrow 2a + \Delta a$ considering the transient occurrences from the design transients file (Figure 6.17)

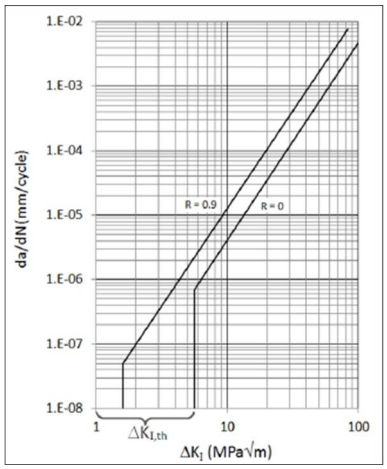

Figure 6.17: Fatigue Crack Growth Rate Curves (ASME XI Appendix A).

Conclusion

The Fatigue Crack Growth analysis shows that the maximum potential growth of the flaws in the forgings over the RPV's entire service lifetime, assessed by a conservative methodology, is limited to 1.66% of their size in the Tihange 2 RPV. This confirms the results of the Safety Case. Fatigue crack growth is not a concern and does not need to be considered further in the Flaw Acceptability Analysis.

6.3 ASME III – Primary Stress Re-evaluation

The elasto-plastic analysis was updated using all of the reported indications from the qualified UT inspection that was performed during the 2014 outage. The results confirmed that the collapse load for the most penalizing flaw configuration meets the ASME III NB-3228.3 acceptance criterion.

Requirement

A Primary Stress Re-evaluation was performed in accordance with 'ASME, Section III – Rules for Construction of Nuclear Facility Components'. This evaluation takes into account the presence of flaws in the Tihange 2 RPV shells. The re-evaluation was performed on all flaws using the dimensional data gathered through ultrasound measurements and starting from the flaw modelling as in ASME XI. The acceptance criterion that needed to be verified is that the calculated collapse pressure should be more than 1.5 times the design pressure.

Approach

The general flowchart for performing this assessment is given in Figure 6.18. Every step is then explained in more detail.

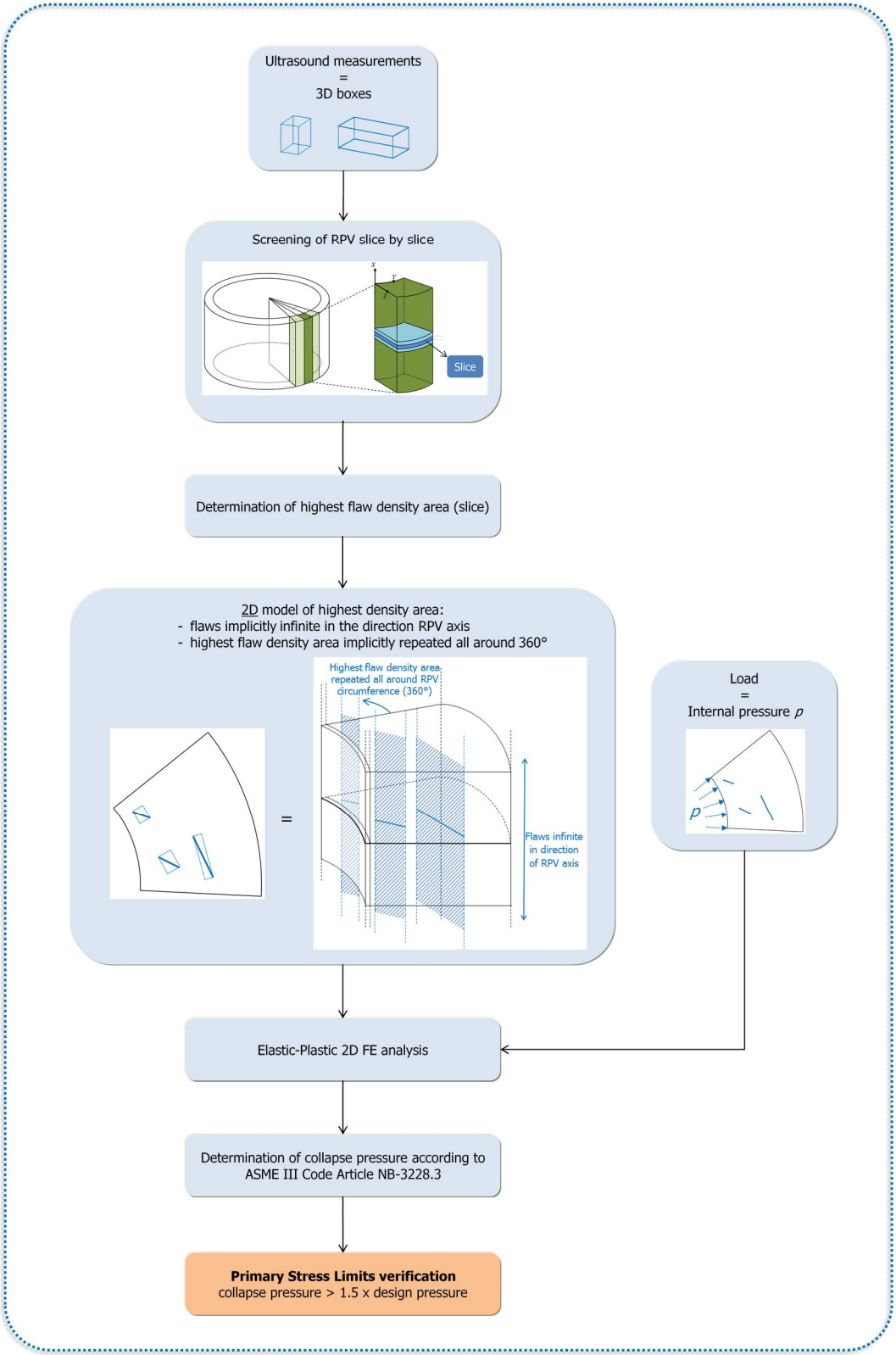

Figure 6.18: Flowchart of the Primary Stress Re-Evaluation (ASME III).

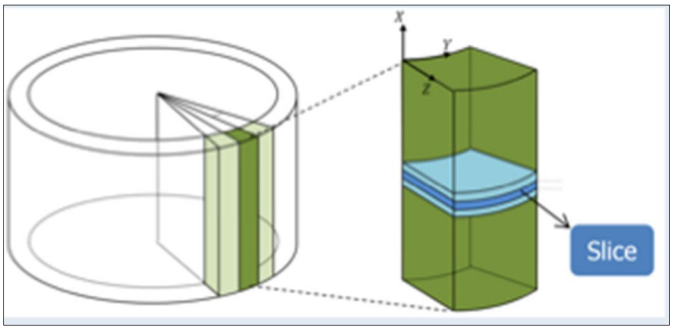

Figure 6.18bis: Screening of the RPV, slice by slice.

2D modelling

The re-evaluation was performed step by step. First, the RPV wall was screened slice by slice in search of the area with the highest flaw density. Once this area was localized, it was reconstructed as a 2D model (Figure 6.19).

As part of this approach, all the flaws are implicitly infinite in the direction of the RPV axis, and the highest flaw density area is repeated around the entire RPV circumference, i.e. 360°.

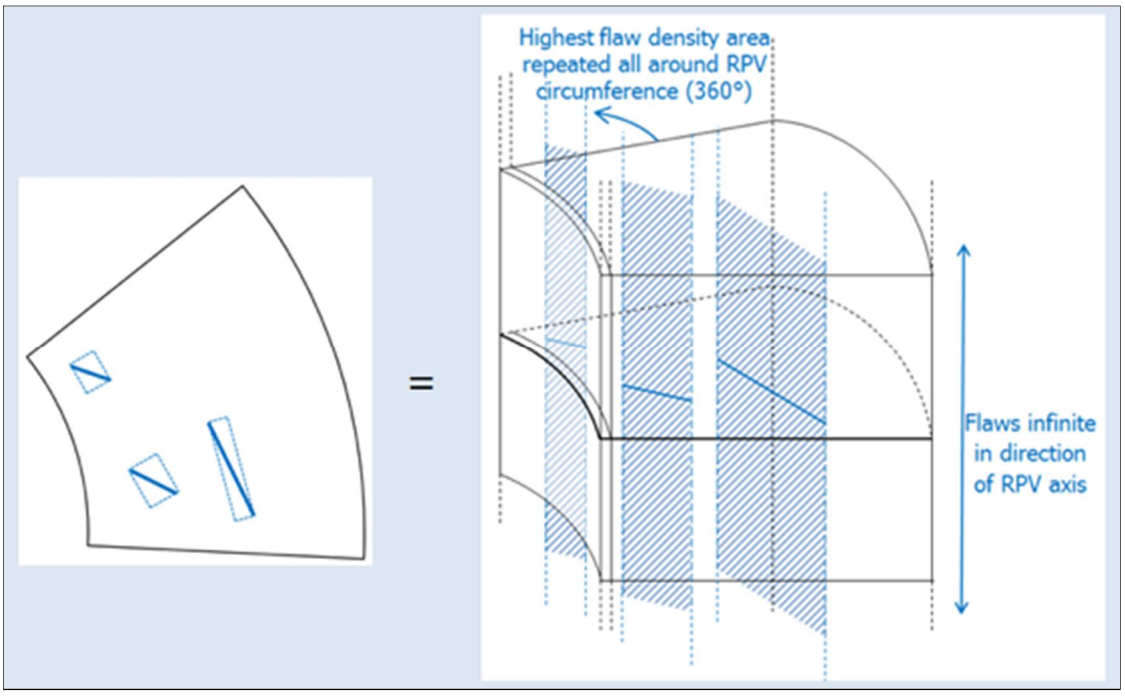

Figure 6.19: The highest density area made into a 2D model.

An elasto-plastic 2D FE analysis was made based on this model. This led to the determination of the collapse pressure according to ASME III Code Article NB-3228.3 and the verification of the primary stress limits. The collapse pressure is more than 1.5 times the design pressure, confirming the criterion is met.

6.4 10CFR50 Appendix G and PTS Analyses

The p-T curves integrated into the plant's Technical Specifications in the framework of the 2012 Safety Case remain valid and do not have to be updated.

The Deterministic PTS Analysis of the RPV core shells shows that the RT_{NDT} of the base metal will remain below 132°C at the end of its service lifetime.

6.4.1 10CFR50 Appendix G – Fracture Toughness Requirements

Appendix G of 10CFR50, which is applicable to the Tihange 2 RPV, defines the fracture toughness requirements for ferritic materials of pressure-retaining components of the reactor coolant pressure boundary of light water nuclear power reactors. The goal is to provide sufficient safety margins in any conditions of normal operation, as well as anticipated transient and accident conditions, to which the pressure boundary may be subjected over its service lifetime. As such, 10CFR50 Appendix G refers to the analysis method included in ASME XI Appendix G, which covers the requirements regarding Pressure-Temperature Operating Limits and Low-Temperature Overpressure Protection.

Pressure-Temperature Operating Limits

The pressure-temperature domain, in which the reactor can be operated safely, is characterized by the pressure-temperature operating limits given in the form of pressure-temperature (p-T) curves.

In the framework of the 2012 Safety Case, the p-T curves were updated based on the RT_{NDT} embrittlement curve considering the absolute additional shift in RT_{NDT} of 50°C (Chapter 5.5.1). The updated p-T curves were integrated into the plant's Technical Specifications.

It was shown that the RT_{NDT} value used for the calculation of the p-T curves and issued from to the RT_{NDT} curves of the present Safety Case (Chapter 5.5.2.) are lower than those issued from the absolute additional shift in RT_{NDT} of 50°C as considered in the 2012 Safety Case.

The p-T curves updated in the framework of the 2012 Safety Case are therefore more restrictive than an update performed with the current RT_{NDT}.

The p-T curves integrated into the plant's Technical Specifications remain valid and do not have to be updated.

Low-Temperature Overpressure Protection

As the p-T curves remain unchanged, the same goes for the low-temperature overpressure protection.

6.4.2 Deterministic PTS Analysis

The assessment prescribed in 10CFR50.61 'Fracture Toughness Requirements for Protection Against Pressurized Thermal Shock Events' aims to verify that the (irradiated) RT_{NDT} of the base metal of the Tihange 2 RPV forged components will remain below 132 °C (270°F) at the end of its service lifetime, and that the RT_{NDT} of the circumferential welds at the end of the RPV's service lifetime will remain below 149 °C (300 °F). This assessment was performed only for the two core shells, as they are the only forgings exposed to neutron irradiation.

The RT_{NDT} of the core shells at the end of the RPV's service lifetime was calculated according to the RT_{NDT} curve obtained from the conservative transposition of the properties obtained on shell VB395, as detailed in Chapter 5.5 Material Properties considered in SIA. The maximum RT_{NDT} obtained is 116.3°C in the upper core shell, which is still below the acceptable value of 132°C.

For the circumferential weld material of the Tihange 2 RPV, there was no additional shift of RT_{NDT} due to macro-segregations to be considered. Hence, the RT_{NDT} at the end of the RPV's service lifetime evaluated in the framework of the Tihange 2 RPV Surveillance Programme (46.5°C) remains valid. This temperature is well below the allowable value of 149°C.

6.5 Conservativeness

This paragraph presents the conservativeness present at each step of the SIA of the Tihange 2 RPV. Besides the conservative approaches inherent to and part of applicable codes, norms and common penalizing assumptions, conservativeness of the SIA exist within the:

- Definition of the input data: UT examination technique and load transients
- Methodology of the Flaw Acceptability Analysis: grouping process, flaw characterization and acceptable size calculation
- Methodology of the Fatigue Crack Growth Analysis
- Methodology of the ASME III – Primary Stress Re-evaluation

The conservativeness related to these assessments are exposed in the following paragraphs.

The main conservativeness related to the Flaw Acceptability Analysis (numbered C1 to C14) is also highlighted in Figure 6.20.

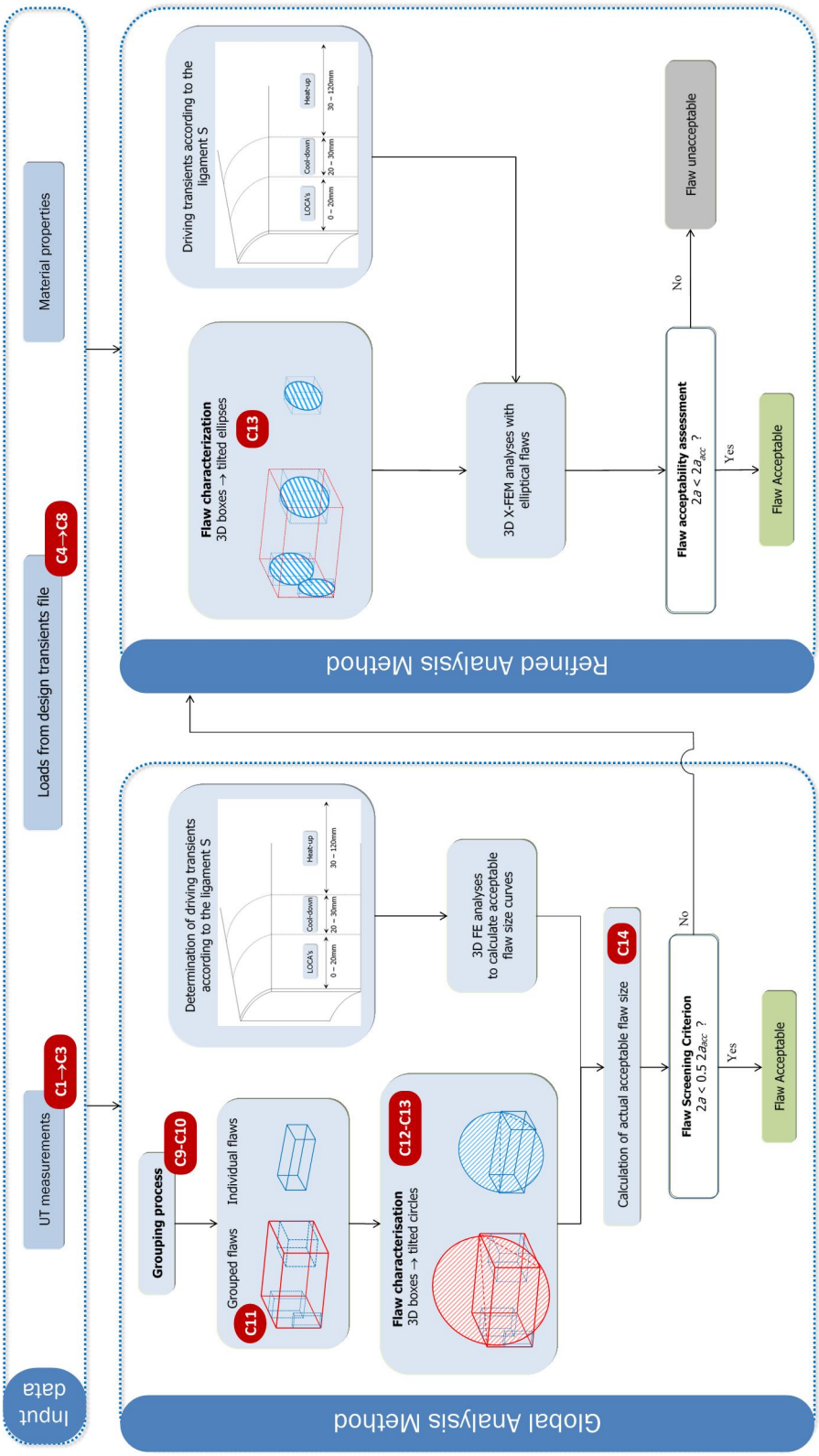

Figure 6.20: Flaw acceptability assessment (ASME XI).

6.5.1 Conservativeness regarding the input data

6.5.1.1 UT examination technique

The overall tendency of the flaw sizing procedure is to overestimate actual flaw dimensions. This has been highlighted during the UT qualification exercise with flakes cut from block VB395/2A and subjected to detailed destructive examination (C1). Moreover, the size of small flakes is increased up to the beam size, before proceeding to structural integrity calculations (C2). Consequently, oversizing neighbouring flaws leads to undersize the sound metal distance between them (Figure 6.21), or, should the flaws lie too close to be possibly discriminated, to report them as a single large indication (C3).

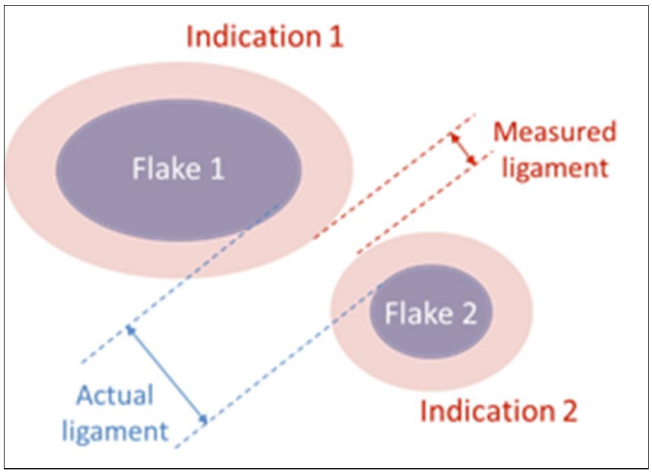

Figure 6.21: Undersizing the sound metal ligament between two oversized neighbouring flaws.

6.5.1.2 Load transients

The transients considered in the SIA were taken from the design transient file and are divided into two categories: Level A/B and Level C/D conditions. Both categories include conservative hypotheses which penalize the subsequent flaw acceptability analysis.

Level A/B conditions

In the considered level A/B heat-up and cool-down transients, the applied evolution of the primary pressure is significantly higher than the evolution which would occur when following the normal plant procedures and more specifically the operating limits diagram (C4). The pressure evolution considered in the Safety Case is thus enveloping. From a structural integrity point of view, this hypothesis leads to an overestimation (by about 10%) of the crack driving force related to the cool-down transient.

The assumed heat-up/cool-down rates are the values documented in the Technical Specifications. However, at the Doel 3 NPP the normal plant procedures for heat-up/cooldown of the plant instruct the operators to heat-up/cool-down at significantly lower rates than assumed in the Safety Case (C5). This leads to a reduction of the thermal stresses and hence of the thermal contribution to the maximum crack driving force by a few percent.

Level C/D conditions

The most stringent level C/D transient regarding the RPV structural integrity is the small break LOCA. In the Safety Case analysis of this transient, a constant High-Pressure Safety Injection (HPSI) flow rate is considered. This constant flow rate is equal to the run-out flow rate of the HPSI pump, i.e. the flow rate corresponding to a counterpressure of 1 bar abs (cf. Figure 6.22). This assumption is conservative as it does not account for the actual counterpressure during the transient (C6). Accounting for the actual counterpressure leads to a lower SI flow rate and thus to a lower downcomer cool-down rate and final temperature. In terms of structural integrity, this conservativeness is assessed on selected flaws from the Doel 3 RPV (with maximal $2a/2a_{acc}$ and with the highest crack driving force) and leads to an overestimation of:

- The ratio to acceptable flaw size by 5% (for the highest $2a/2a_{acc}$ flaw).
- The maximum crack driving force by 7% (for the highest $K_{J,MAX}$ flaw).

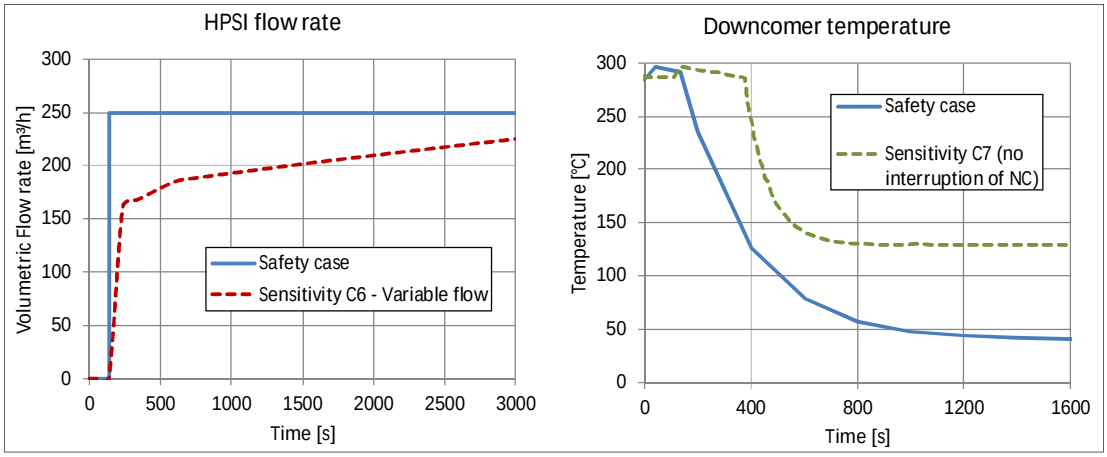

Figure 6.22: Conservative hypotheses C6 and C7 in the definition of Small Break LOCA transient.

On the other hand, a complete interruption of the circulation flow rate (be it forced or natural) in the primary loops is considered during the entire small break LOCA transient (C7). As a consequence no mixing occurs between the relatively hot water coming from the SGs and the relatively cold SI flow. The temperature of the water reaching the RPV downcomer is thus conservatively assumed to be equal to the relatively low SI temperature and this during the entire transient. This results in a high cool-down rate of the RPV downcomer wall leading to an overestimation (based on the same selected flaws from the Doel 3 RPV) of:

- The ratio to acceptable flaw size up to 18% (for the highest $2a/2a_{acc}$ flaw).
- The maximum crack driving force up to 41% (for the highest $K_{J,MAX}$ flaw).

The small break LOCA is defined with a minimum SI temperature of 7°C at Tihange 2 (C8). However, when considering best-estimate temperatures (15°C at Tihange 2), calculations based on the flaws with maximal $2a/2_{acc}$ and with the highest crack driving force (from the Doel 3 and Tihange 2 RPVs) have shown additional margins:

- 7% on the ratio to acceptable flaw size (for the highest $2a/2a_{acc}$ flaw).
- 4% on the maximum crack driving force (for the highest $K_{J,MAX}$ flaw).

The conservativeness is illustrated in Figure 6.23 for an individual flaw close to the cladding-base metal interface.

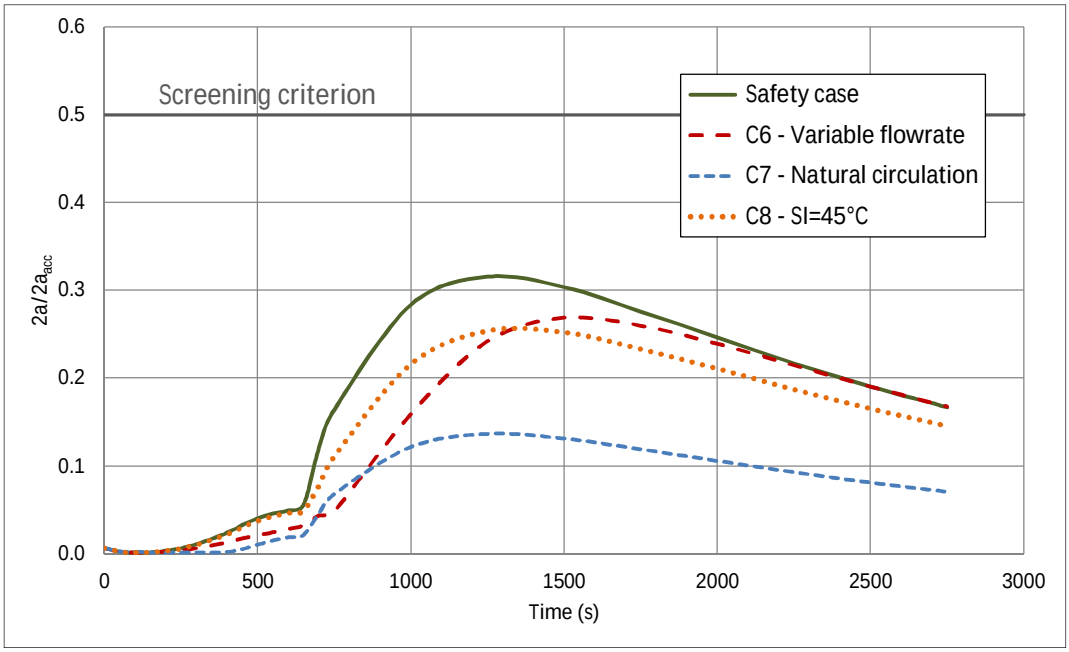

Figure 6.23: Time evolution of the ratio to acceptable size of a flaw close to the cladding-base metal interface, for the different sensitivity analyses on the Small Break LOCA transient.

6.5.2 Conservativeness regarding the Flaw Acceptability Assessment

Grouping process

The following conservativeness results from the definition of the proximity rules that are suitable for quasi-laminar flaws.

- The reference configuration of flaws used to determine the proximity criteria has been defined to maximize the flaw interaction (C9), enveloping all possible flaw configurations.
- The interaction domain has been enlarged with an additional arbitrary margin of 20% (C10). This means that one considers that two flaws interact when the distance between them is larger than it should.

Both conservativeness lead to a higher grouping rate and to groups containing more flaws, which gives additional confidence that absolutely all interacting flaws have been detected and included in a group. Moreover, when flaws have to be grouped, the resulting combined flaw is conservatively sized by the minimum bounding box that contains the individual boxes (C11).

Flaw characterization

As depicted above, the 3D boxes of individual or grouped flaws are replaced by circles with conservative diameter and tilt (C12) for the structural integrity calculations. Besides, the calculated tilt of individual flaws is saturated to 20° instead of 16°, this latter value is a conservative envelope of the maximum flakes inclination. (C13). Consequently, all individual flaws having a calculated tilt higher than 16° include some conservativeness.

Acceptable size calculation

The application of acceptable size curves to actual flaws includes two conservativeness (C14):

- The flaw configurations associated with a RT_{NDT} lower than 45.6°C (6% of the flaw configurations in Tihange 2) are conservatively considered to have an acceptable size corresponding to a RT_{NDT} of 45.6°C.
- The flaw configurations with an inclination lower than 10° (76% of the flaw configurations in Tihange 2) are conservatively considered to have an acceptable size corresponding to an inclination of 10°.

6.5.3 Conservativeness highlighted by refined analyses

While the refined analyses have demonstrated the flaw acceptability with significant remaining margins, they can also be used to highlight the previously defined conservativeness.

The conservativeness linked to the proximity rules (C9 and C10), to the grouped flaw definition (C11 and C12) and to the acceptable size calculation (C14) are together illustrated in Figure 6.24. This figure compares the ratio to acceptability before (grouped flaw) and after (multi-flaw) refined analysis.

For Tihange 2, the ratio $2a/2a_{acc}$ of the grouped flaw is between 4 times and 18 times higher than the ratio $2a/2a_{acc}$ calculated with refined analyses.

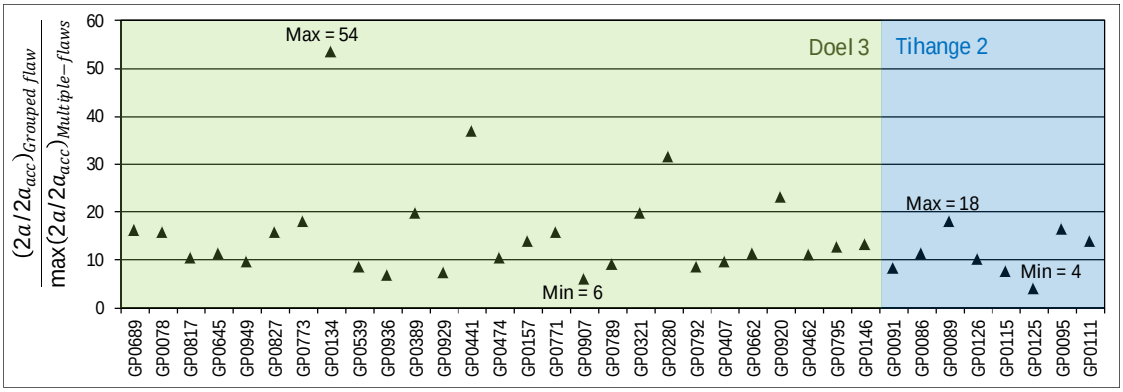

Figure 6.24: Impact of multiple-flaws analyses on $2a/2a_{acc}$ for Doel 3 and Tihange 2 core shells.

On the other hand, the conservativeness linked to the characterization of individual flaws (C12) and to the acceptable size calculation (C14) are highlighted by the refined analysis of the highest $2a/2a_{acc}$ individual flaw, the ratio to acceptable size dropping from 0.60 to 0.54.

6.5.4 Conservativeness of Fatigue Crack Growth Analysis

While the fatigue crack growth turned out not to be a concern, the Fatigue Crack Growth Analysis nonetheless includes many conservativeness at each step of its process (as defined in Chapter 6.2 Fatigue Crack Growth Analysis).

The conservativeness related to the input data used in the fatigue analysis are similar to the ones of the Flaw Acceptability Analysis (at least for the UT measurements and transient load definition). Moreover, a conservative heat transfer coefficient between the primary coolant and the vessel wall is considered whatever the level A/B transient. As far as the transient occurrence is concerned, the considered number of transients is greater than the actual one, leading to a higher calculated crack growth.

Regarding the calculation methodology, the main conservativeness are related to:

- The application of the conservative grouping process, and the resulting flaw characterization, just as in the Flaw Acceptability Analysis.
- The use of conservative reference flaws which envelope the whole population of flaw configurations present in the RPVs.
- The consideration of the axial projection of these reference flaws to assess the stress intensity factors, leading to overestimate the crack growth $\Delta 2a$ by more than a factor 13 compared to the actual quasi-laminar flaw configuration.

6.5.5 Conservativeness of ASME III – Primary Stress Re-evaluation

The ASME III analysis relies on the same conservativeness regarding the UT measurements as the Flaw Acceptability Analysis. Moreover, as detailed in Chapter 6.3 ASME III—Primary Stress Re-evaluation, the replication of the highest flaw density area as well as the use of a 2D model with infinite flaws make the applied methodology overly conservative.

6.6 Conclusions of the SIA

The SIA of the Tihange 2 RPV was performed considering all indications that were revealed by the qualified UT inspection procedure. As such, it covers the indications that were classified as hydrogen flakes as well as the indications that were classified as clad interface imperfections but that are conservatively considered and treated as hydrogen flakes.

The Flaw Acceptability Assessment with its refined analysis was based on conservative data and calculation methodologies. For Tihange 2, more than 99.69% of the flaw configurations meet the screening criterion $2a < 0.5\ 2a_{acc}$. This means that most of the flaws affecting the Tihange 2 RPV shells are harmless in the event of a transient. This is a consequence of their quasi-laminar character.

The remaining 0.31% of the flaw configurations that were subjected to a refined 3D XFEM analysis meet the acceptance criterion $2a < 2a_{acc}$ by a considerable margin (maximum ratio of 0.54 in the Tihange 2 RPV).

The refined analyses clearly highlighted the very low level of the crack driving forces K_{MAX} of the quasi-laminar hydrogen flakes: K_{MAX} for all flaw configurations is well below the fracture toughness lower shelf $K_{IR,lower\ shelf}$ demonstrating that the quasi-laminar hydrogen flakes are acceptable with respect to the structural integrity of the Tihange 2 RPV.

The majority of the flaws even have a K_{MAX} value below the lower shelf considering the safety factor $K_{IR,lower\ shelf}/SF$ which means that their acceptability is independent from the RT_{NDT}.

For the few flaws of which K_{MAX} exceeds $K_{IR,lower\ shelf}/SF$, the margin in terms of RT_{NDT} is calculated based on the conservative transposition of the VB395 properties. The calculated margin is very large (110°C or more).

The Fatigue Crack Growth analysis shows that the maximum potential growth of the flaws in the forgings over the entire service lifetime of the RPV, assessed by a conservative methodology, is limited to 1.66% of their size in the Tihange 2 RPV. This confirms the results of the Safety Case. Fatigue crack growth is not a concern and does not need to be considered further in the Flaw Acceptability Analysis.

The Primary Stress Re-evaluation was performed using 2D modelling of the highest flaw density area. The re-evaluation made clear that the collapse pressure is more than 1.5 times the design pressure, confirming the criterion is met.

7 Sensitivity Studies

The project team performed several sensitivity studies in order to assess the robustness of the Safety Case with respect to variations of some parameters of the methodologies or input data. These studies concern the different key elements of the roadmap: UT inspection, material properties and Structural Integrity Assessment (SIA). The following sensitivity studies were performed:

- UT inspection: consideration of an alternative DZ sizing procedure for the indications
- Material properties: impact of the KS 02-based RT_{NDT} curve on the margins of the SIA
- SIA: SIA Analysis with 2012 Methodology

7.1 Consideration of an Alternative DZ Sizing Procedure

The DZ sizing procedure, based on a 6 dB drop from the maximum amplitude of the indication, shows that the structural integrity is not impacted by the variation of the Z coordinates of indications larger than 20 mm in the DX and DY dimensions.

An alternative methodology has been used to evaluate the sensitivity of the SIA results to the sizing along the Z-axis (radial) for the large indications and groups of indications. The sizing method for DZ as implemented in the examination procedure (DZ sizing procedure) is based on a 6 dB drop from the maximum amplitude of the indication. This sizing is performed by an automatic measurement on the UT contour.

The alternative DZ sizing method that was used for the present evaluation is based on a -6 dB drop performed manually on each of the different maxima of a given indication.

Results for the qualification blocks

The qualification is based on the correlation between UT and destructive tests on a large number of cut flaws. It shows that the DZ sizing procedure generally leads to overestimate the DZ value.

The comparison shows that the DZ sizing procedure has a level of performance equivalent or very close to the alternative DZ sizing. The conclusion is applicable to the numerous cut indications used in the qualification and also to the six clusters of indications (total 23 indications) examined by destructive testing.

Results for Tihange 2 core shells

The objective was to compare UT dimensions obtained by two different sizing methods and to highlight the differences between them.

It appears that the DX or DY dimension of 20 mm is a limit beyond which the DZ sizing procedure and alternative DZ sizing may lead to different results.

Sensitivity study for SIA

In order to illustrate that the alternative DZ sizing method has no impact on the structural integrity of the RPV shells, a sensitivity study was performed for all indications larger than 20 mm in the DX or DY dimension, based on the alternative DZ values. In this study, the grouping and screening steps of the SIA methodology were applied on another data set of indications dimensions, where the DZ sizing procedure value was replaced for each concerned indication by the alternative DZ value. The results were then compared for each vessel shell and showed that very similar results were obtained in terms of $2a/2a_{acc}$ values.

Conclusion

The sensitivity study shows that the structural integrity is not impacted by the variation of the Z coordinates of indications larger than 20 mm.

7.2 Impact of the KS 02-based RT_{NDT} Curve on the Margins of the SIA

The impact of considering the KS 02-based RT_{NDT} embrittlement curve (an overestimation of what can be expected in the D3T2 RPV forgings) on the margins of the SIA has been assessed. As all of the considered flaw configurations are in the low fluence range, applying the KS 02-based approach is more conservative as compared to the VB395-based curve used in the SIA. However, the KS 02-based RT_{NDT} margins still remain very large: above 70°C (instead of 80°C with VB395 based RT_{NDT} curve).

The fracture toughness curve used in the SIA is based on the conservative transfer of VB395's atypical embrittlement to the D3T2 RPV shells. A sensitivity study was performed to evaluate an alternative approach based on the German KS 02 material.

The principle of the KS 02-based approach is to consider that the irradiation embrittlement is normal and well-predicted by the RSE-M formula for the D3T2 RPVs (evaluated for the D3T2 core shell's chemical composition thereby considering conservative enrichment factors to account for the composition of macro-segregations), but that a fixed penalty should be considered in the entire fluence range, to take into account the potential difference in properties between the surveillance specimens' sampling location (out of the segregation) and the zone affected by flaking (in the macro-segregation). This penalty is taken as the maximum difference observed between the segregated and non-segregated zones in the KS 02 material: 47°C. As explained in §5.2.2., this difference is larger than the difference observed on the D3T2 nozzle shell cut-outs and it is an overestimation of what can be expected in the D3T2 RPV forgings for the following reasons:

- In the D3T2 RPV forgings a large part of the segregated zone was removed by the piercing of the ingots. In the KS 02 component, no piercing was performed and hence the whole segregated zone is maintained.
- The difference of 47°C is read from the Charpy curves inside and outside the segregated zone at the 41J level. This difference cannot be interpreted as a difference in RT_{NDT} in unirradiated conditions as the latter is defined by a combination of Pellini drop weight and Charpy impact tests. For the KS 02 material, this leads to a difference in RT_{NDT} in unirradiated conditions of only 3°C instead of 47°C.

- The set of Charpy specimens from the non-segregated zone are located in a zone that was significantly affected by the quenching, leading to better mechanical properties (i.e. lower transition temperature) as compared to the central part of the component.

The curve of RT_{NDT} as a function of fluence considered in this alternative KS 02-based approach is the following:

$$RT_{NDT} = RT_{NDT,init} + \Delta RT_{NDT,RSE\text{-}M} + \Delta RT_{NDT,KS\ 02} + 2\sigma_{RSE\text{-}M}$$

$2\sigma_{RSE\text{-}M}$ is twice the standard deviation of the RSE-M trend curve for forgings ($\sigma_{RSE\text{-}M}$ = 9.3°C).

The curve of RT_{NDT} evolution vs. fluence for the KS 02-based approach for the upper core shell of Tihange 2 is compared in Figure 7.1 to the curve used in the SIAs in 2014-2015 as well as to the curve used in the initial Safety Case of 2012. The KS 02-based approach is close to the one of the 2012 Safety Case in the fluence range of interest (up to 6 10^{19} n/cm^2). It is more conservative than the VB395-based approach in the low fluence range (up to approximately 3.4 10^{19} n/cm^2) and less conservative above this value.

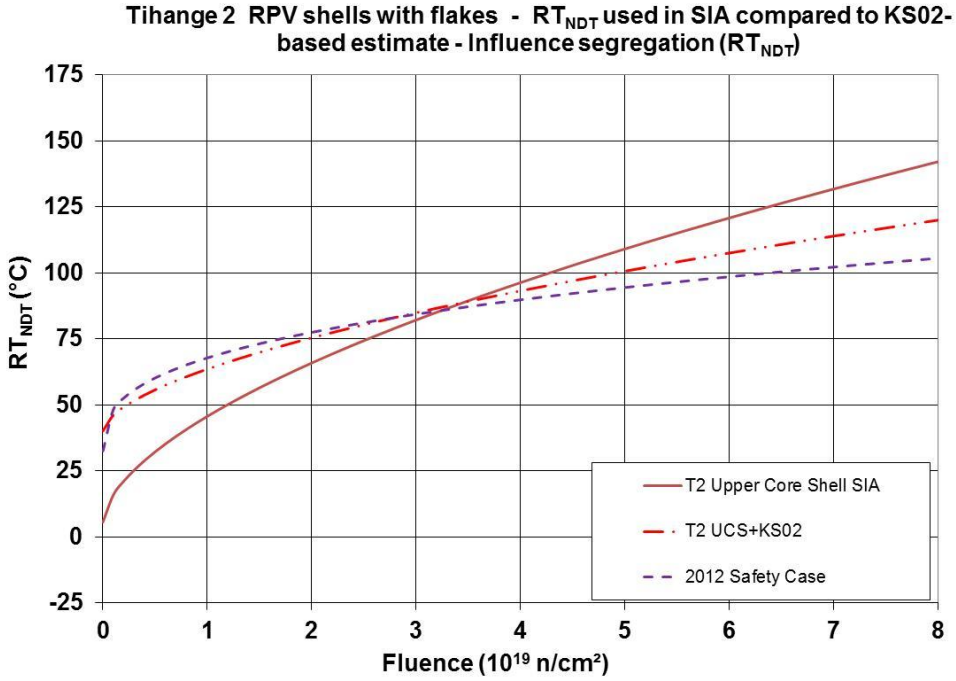

Figure 7.1: RT_{NDT} evolution with fluence considered in the 2014-2015 SIA compared to the curve of the initial Safety Case and to the alternative KS 02 based approach.

Specific curves are available for each of the four core shells, based on the specific initial RT_{NDT} and chemical composition.

The impact of considering the KS 02-based RT_{NDT} embrittlement curve on the margins of the SIA has been assessed. For that purpose, flaw configurations with the lowest margins for flaw acceptability have been selected in the Tihange 2 core shells.

Based on the specific end-of-life fluence at the flaw location, a new RT_{NDT} value has been calculated for each selected flaw, considering the KS 02-based approach in terms of RT_{NDT}.

As all of the considered flaw configurations are in the low fluence range (less than 3.4 10^{19} n/cm2), applying the KS 02-based approach is more conservative than the VB395-based curve used in the SIA. However, the KS 02-based RT_{NDT} margins still remain very large: above 100°C (instead of 110°C with VB395-based curve).

7.3 SIA Analysis with 2012 Methodology

The acceptability of all 2014 UT reported flaws in the Tihange 2 core shells is demonstrated even when applying the analysis method and the input parameters of the 2012 Safety Case. This confirms that the structural integrity of the RPV has always been guaranteed.

Scope

The aim of this sensitivity analysis is to demonstrate the acceptability of all 2014 UT reported flaws in the Tihange 2 core shells even when applying the assumptions used in the 2012 Safety Case for performing the SIA of the RPV in presence of flaws.

Changes in the assumptions

Changes between the SIA of the 2012 Safety Case and its 2014 update are related to analysis methods on the one hand and input parameters on the other hand.

Changes in analysis methods:

- Grouping process: update of grouping rules of flaws based on 3D supporting calculations (2014) instead of 2D calculations (2012).

Changes in input parameters (2014 vs. 2012):

- Fluence map: update of the reactor pressure vessel fluence after 40 years of operation, taking extra downtime in 2014 and 2015 into account, and consideration of the fluence decrease in the lower part of the core shells
- Embrittlement law (2014 vs 2012): reassessment of the RT_{NDT} shift of the core shell material from the transposition of the properties obtained on shell VB395 (addition of a variable margin on top of the RSE-M formula), instead of the consideration of a fixed margin 50°C on top of the FIS formula.

Results

The SIA (screening and refined analysis) of the Tihange 2 core shells was performed for the updated cartography of the 2014 UT reported flaws, with application of the same analysis method and input parameters as in the 2012 Safety Case. This showed that all 2014 UT reported flaws are acceptable even when applying the analysis method and input parameters of the 2012 Safety Case.

This sensitivity analysis also highlights the robustness of the set up methodology and the soundness of the assumptions update compared to the 2012 Safety Case.

7.4 Conclusions

The sensitivity studies performed on three key elements of the roadmap have demonstrated the robustness of the approach that is applied in the Safety Case.

The sensitivity study based on an alternative sizing procedure shows that the structural integrity is not impacted by the variation of the Z coordinates of indications larger than 20 mm.

The use of alternate fracture toughness properties based on the transfer of tests results obtained on the KS 02 component, instead of the VB395 shell, has a very limited effect on the evolution of the RT_{NDT} with fluence and hence on the results of the SIA.

The application of the methodology used in 2012 for SIA, even when based on assumptions that have been updated in the meantime, to the indications cartography obtained in 2014 with application of the qualified inspection procedure, has confirmed that the severity of the loading is marginally affected and that the acceptance criteria were always satisfied at any time in the life of the RPV.

8 Conclusions

Through this Safety Case Report Electrabel is convinced of having demonstrated that the structural integrity of the Tihange 2 RPV is fully maintained, with considerable margins, under all operating and accidental conditions. The Structural Integrity Assessment (SIA) has provided evidence of the harmless character of all detected flaws in the RPV. This allows for a safe restart and operation of the Tihange 2 NPP.

8.1 Detailed Conclusions from the Safety Case Roadmap

To demonstrate the integrity of the reactor pressure vessel under all conditions, the Safety Case roadmap specified an extensive phase of studies and material tests. This led to the following results and conclusions.

Hydrogen flaking is fully characterized

The Safety Cases of 2012 and 2013 confirmed the diagnosis of flaking, caused during fabrication. . Flaking is not correlated to the chemical enrichment level of the segregation in the material, as both mechanisms are explained by independent factors. Further examination demonstrated the facetted appearance of the flakes and their nearly laminar character, with a maximum possible inclination of 15° towards the inner surface of the reactor pressure wall.

Qualified UT inspection procedure achieves high performance in detection and sizing

The formal qualification process has led to an inspection procedure with a very high level of confidence for the detection, localization and sizing of the flakes. The qualification process resulted in upgrading the inspection procedure to ensure its compliance with inspection objectives in terms of flaw detection and characterization. A very high confidence level is achieved for detecting flakes. The flake sizing was shown to be conservative. The applied straight beam technique (2012 and 2013) has proven to be adequate in detecting the presence, if any, of hydrogen flaking in the RPV shells.

Re-inspection of the vessel shells delivers a complete cartography of the indications and confirms that the flakes are stable

The inspection of 2014 confirmed that the flakes are stable (there has been no growth), that they have a quasi-laminar character, and that there is no radial connection between them. By applying the improved settings of the qualified inspection procedure, the number of reported indications proved to be significantly higher than in 2012 though the affected volume remained unchanged. The conservativeness introduced by the updated flaw sizing procedure and the non-discrimination of clustered flakes have led to the reporting of larger average dimensions and much larger maximum dimensions. The new and complete cartography, that integrated the clad interface imperfections further treated as hydrogen flakes, has entirely been taken over as input for the SIA. The clustered flakes have been considered as single flaws.

Conservative material properties are derived for use in the SIA

The extended and comprehensive material test programme has shown that the microstructure of the Doel 3 and Tihange 2 forgings is identical, and that these forgings – such as the German KS 02 – behave as expected under irradiated conditions. The tests on the flaked material have also shown that the presence of hydrogen flakes does not have any effect on the evolution of the fracture toughness under irradiation.

The mechanical tests and the assessment of atypical embrittlement of the VB395 shell have made clear that it is very unlikely that the Tihange 2 RPV core shell forging would be more sensitive to irradiation because of the presence of hydrogen flakes. However, as a conservative measure, it has been postulated that the Tihange 2 RPV core shells have an additional sensitivity to irradiation embrittlement of the same magnitude as the VB395 material.

In general, the RT_{NDT} trend curves built for use in the SIA include considerable margins and are conservative.

Structural integrity of the RPV is demonstrated with large safety margins, and has never been a concern during the whole operation of the plant since commissioning

Given the presence of the detected flaws, the goal of the SIA is to demonstrate that the structural integrity of the RPV is maintained under all operating and accidental conditions. Therefore it addressed the following in a very comprehensive way:

- Assessment of the absence of crack initiation for all individual flaws
- Assessment of the stability of the flaws through fatigue crack growth evaluation
- Satisfaction of the primary stress intensity acceptance criteria

The SIA has provided evidence of the harmless character of all detected flaws. It concludes that the driving forces K_{max} are very low, even below the lower shelf of fracture toughness. Given the presence of the detected flaws, the structural integrity of the Tihange 2 RPV is fully maintained, with considerable margins, under all operating and accidental conditions.

The application of the methodology used in 2012 for SIA to the indications cartography obtained in 2014 has confirmed that the severity of the loading is marginally affected and that the acceptance criteria were always satisfied at any time in the life of the RPV.

8.2 Conservativeness and Sensitivity Studies

To ensure a high confidence in its conclusions, each step of the Safety Case was taken from a very conservative approach. This conservativeness had led to the existence of additional margins between the assessments and reality. Some of those margins have been quantified, others have been assessed through sensitivity studies or remain qualitative. The overall conservative approach is present through every step of the assessment:

- The ultrasonic examination technique
- The deterministic SIA
- The material properties for use in the SIA

This conservativeness is associated with both the input data and the applied methodology. The conservative approach is also inherent to and part of the applicable codes, standards, and common penalizing assumptions.

Sensitivity studies have been performed on three key elements of the roadmap. They have demonstrated the robustness of the applied approach in the Safety Case.

8.3 General Conclusion

The current Safety Case takes into account the operational p-T limits that were adapted in 2013.

This Safety Case Report demonstrates that all studies and calculations are solid, and that all safety criteria in the SIA of the reactor pressure vessel are met with considerable margins and for each detected flaw. Consequently, no further action needs to be implemented.

All studies and calculations have been subjected to a rigid review process and validated by external experts.

Having thoroughly assessed the roadmap results, Electrabel is convinced that the integrity of the reactor vessel has been demonstrated, allowing for a safe restart and operation of the Tihange 2 NPP.

At the end of the next fuel cycle a follow-up inspection of the RPV will be performed with the qualified UT inspection procedure.

9 List of Abbreviations

AE	Acoustic Emission
AIA	Authorized Inspection Agency (AIB Vinçotte)
ASME	American Society for Mechanical Engineers
BF	Material between flakes
CEA	Commissariat à l'Energie Atomique et aux Energies Alternatives
CT	Compact Tension
D3	Doel 3
D3H1	Doel 3 nozzle shell cut-out H1
EAR	Examen d'Accrochage du revêtement (specific straight beam transducer)
Ev	Label for individual flaw
FANC	(Belgian) Federal Agency for Nuclear Control
FE	Finite Element
FKS	Forschungsvorhaben Komponenten Sicherheit
GP	Label for grouped flaw
IAEA	International Atomic Energy Agency
IRB	International Review Board
K_{Ia}	Crack arrest material toughness
K_{IC}	Crack initiation material toughness
LCS	Lower Core Shell
LOCA	Loss-Of-Coolant-Accident
MER	Mesure d'Epaisseur du Revêtement (ultrasonic transducer)
MIS-B	Machine d'Inspection en Service Belge
NPP	Nuclear Power Plant
OF	Material outside the flaked area
PCCV	Pre-Cracked Charpy-V specimen (Charpy-size fracture mechanics specimen tested in three-point bending)
ppm	Parts per million
PTS	Pressurized Thermal Shock
RPV	Reactor Pressure Vessel
RSE-M	Règles de Surveillance en Exploitation des Matériels Mécaniques
RT_{NDT}	Reference Temperature for Nil Ductility Transition
SEM	Scanning Electron Microscope
SF	Safety Factor
SI	Safety Injection System
SIA	Structural Integrity Assessment
SINTAP	Structural Integrity Assessment Procedures for European Industry
T2	Tihange 2
T2H2	Tihange 2 nozzle shell cut-out H2
TEM	Transmission Electron Microscope
UCS	Upper Core Shell
UT	Ultrasonic Testing
XFEM	Extended Finite Element Modelling